Corrosion Assessment for Failed Bridge Deck Closure Pour

Ebrahim K. Abbas

Thesis submitted to the faculty of the Virginia Polytechnic Institute and State University
in partial fulfillment of the requirements for the degree of

Master of Science
In
Civil and Environmental Engineering

William J. Wright, Chair
Richard E. Weyers, Co-Chair
Carin L. Robert-Wollmann

December 2, 2011
Blacksburg, VA

Keywords: Corrosion, Epoxy Coated Reinforcement (ECR), Unrestrained Shrinkage, Restrained Shrinkage, Bridge Deck, Prediction Models

Corrosion Assessment for Failed Bridge Deck Closure Pour

Ebrahim K. Abbas

ABSTRACT

Corrosion of reinforcing steel in concrete is a significant problem around the world. In the United States, there are approximately 600,000 bridges. From those bridges 24% are considered structurally deficient or functionally obsolete based on the latest, December 2010, statistic from the Federal Highway Administration (FHWA). Mainly, this is due to chloride attack present in deicing salts which causes the reinforcing steel to corrode. Different solutions have been developed and used in practice to delay and prevent corrosion initiation.

The purpose of this research is to investigate the influence of corrosion on the failure mechanism that occurred on an Interstate 81 bridge deck. After 17 years in service, a 3ft x3ft closure pour section punched through. It was part of the left wheel path of the south bound right lane of the bridge deck. The bridge deck was replaced in 1992 as part of a bridge rehabilitation project, epoxy coated reinforcement were used as the reinforcing steel. Four slabs from the bridge deck, containing the closure, were removed and transported to the Virginia Tech Structures and Materials Research Laboratory for further evaluation. Also, three lab cast slabs were fabricated as part of the assessment program.

Corrosion evaluation and concrete shrinkage characterization were conducted in this research. The corrosion evaluation study included visual observation, clear concrete cover depth, concrete resistivity using single point resistivity, half-cell potential, and linear polarization using the 3LP device. Shrinkage characteristics were conducted on the lab cast slabs only, which consisted of monitoring shrinkage behavior of the specimens for 180 days and comparison of the data with five different shrinkage models. Based on the research results, guidance for assessment of other bridge decks with similar conditions will be constructed to avoid similar types of failures in the future.

ACKNOWLEDGEMENTS

First, I would like to take this opportunity and thank my committee members Dr. Richard E. Weyers, Dr. Carin L. Robert-Wollmann, and Dr. William J. Wright for giving me their trust and continuous support from the first day on this research. Their doors were always open for any guidance, assistance, questions, and concerns.

I would like to thank Elias Rivera for being a great help and support throughout this project. Also, I would to express my thanks for all others who contributed and helped on this project.

I would like to acknowledge and thank Kuwait University for funding and giving me this valuable opportunity to finish my graduate studies in one of the top respected schools.

Finally, I would like to thank and dedicate this work for my parents, Khaleel Abbas and Wafaa Al-Sabaghah, and my wife, Noha Mohamed, and our children, Mohammad and Dana. Their continuous support, care, and prayers were a strong motivation throughout my life and career.

TABLE OF CONTENTS

LIST OF FIGURES

LIST OF TABLES

CHAPTER 1: INTRODUCTION

1.1 General Introduction

Corrosion is one of the most significant problems around the world, in the United States the cost of all corrosion is $276 billion/year (Koch, Brongers et al. 2002). There are approximately 600,000 bridges in the United States according to the Federal Highway Administration (FHWA), and 24% (146,633 bridges) are considered structurally deficient or functionally obsolete based on the latest FHWA statistics dated December 2010 (FHWA 2010). Most deficiencies are due to the corrosion of the reinforcing steel from deicing salt exposure. In the state of Virginia there are 13,522 bridges, and 25% (3,429 bridges) are considered structurally deficient or functionally obsolete, reflecting the amount of bridge repair and rehabilitation work required to maintain Virginia bridges. Typically, the first bridge component that needs to be repaired and rehabilitated is the concrete bridge deck, mainly due to chloride-laden environment (deicing salts) which cause chloride-induced corrosion of the reinforcing steel imbedded in the concrete decks. The result is premature rehabilitation before the concrete bridge decks reach their designed service life.

There are many methods are used to delay premature rehabilitation work due to chloride induced corrosion of the reinforcing steel. Methods include decreasing the concrete permeability by decreasing the water to cement ratios (w/c), using cementitious materials (flyash, slag, and silica fume), increasing the clear concrete cover depth for the reinforcing steel, using alternative types of reinforcing steel which have higher resistance to corrosion, the use of concrete surface sealers and membranes, and improving the deck drainage system. Concrete quality and cover depth are mainly influenced by construction method and procedures. All of these methods have a positive degree of increasing the service life of the bridge deck.

For chloride-induced corrosion of the reinforcing steel, an electrochemical process, the concrete void structure properties such as size, size distribution, connectivity, and degree of saturation are controlling factors for the initiation of corrosion and the subsequent cracking and spalling of the cover concrete (Weyers, Pyc et al. 2003).

Generally, the first step in bridge deck rehabilitation consists of patching spalled and delaminated areas. Followed by overlaying the deck with a low-slump dense concrete (LSDC), latex-modified concrete (LMC), rapid set latex-modified concrete (RSLMC), or hot-mix asphaltic concrete with a performed membrane (HMAM). The overlay dead load increase decreases the live load capacity. Typically, the overlay dead load increase is included in the deck design.

Economical factors need to be considered for any overlay. In some cases it is more economical to remove the contaminated concrete below the top reinforcing steel rather than repair overlay because of the high risk of chloride attack for the bottom reinforcing steel. The chloride content must be low enough that it does not diffuse and initiate the corrosion to the bottom reinforcing steel. This method is influenced by environmental exposure conditions, mainly chloride concentration and temperature. In addition to that, the service life of an overlay depends on the type of overlay used also (Weyers, Powell et al. 1993).

Deck replacement can be performed either by fully or partial replacement depending on the severity of damage and other economic factors, and it requires a partial or full closure for traffic which leads to traffic diversion to other lanes or the other side of the bridge. Cast-in-place or pre-cast reinforced concrete bridge decks are most commonly used.

1.2 Interstate 81 Closure Pour Failure

After 17 years in service, a 3ft x3ft closure pour section punched through, as shown in Figure 1.2. It was part of the left wheel path of the south bound right lane of the bridge deck. The bridge deck was replaced in 1992 as part of a bridge rehabilitation project, epoxy coated reinforcement were used as the reinforcing steel. A transverse section of the bridge deck with the closure pour is shown in Figure 1.1.

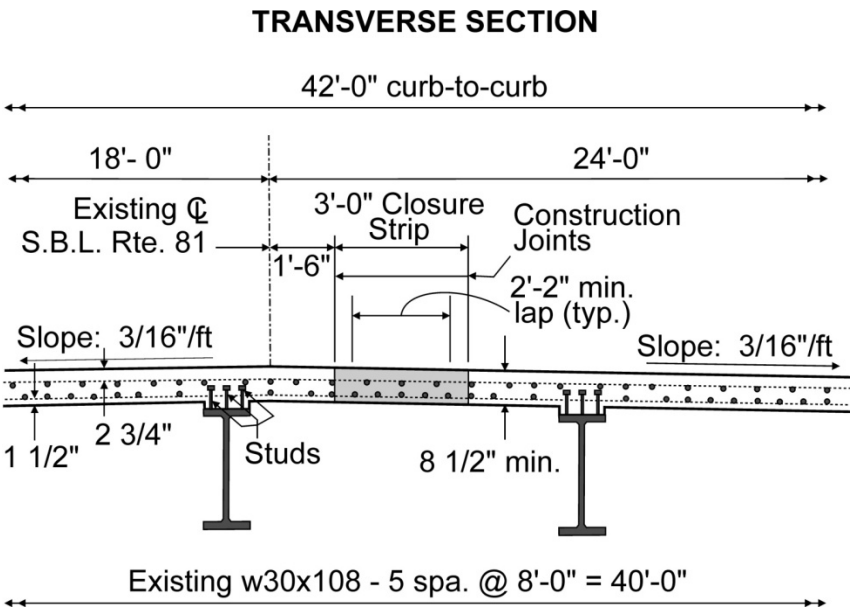

Figure 1.1 Transverse Section of the Bridge Deck with the Closure Pour

The purpose of this research is to investigate corrosion influence on the failure mechanism that occurred on an Interstate 81 bridge deck slab. Based on the research results, guidance for assessment of other bridge decks with similar conditions will be constructed to avoid similar failures in the future.

Figure 1.2 Failed Section of Closure Pour

Four slabs have been removed from the failed bridge deck to perform a series of tests. Those tests are performed to determine the corrosion severity and find a relation between fatigue and corrosion of the reinforcing steel. Three lab cast slabs were fabricated identically to the slabs removed from the actual bridge deck. This was done to understand the behavior and impact of shrinkage on the closure pour. Also, the lab cast slabs provide an undamaged baseline for comparison to the slabs removed from the bridge deck.

The testing may be separated in three parts, corrosion evaluation, fatigue and strength, and shrinkage characteristics. The two parts that are the focus of this thesis are corrosion evaluation and shrinkage characteristics. Corrosion evaluation tests included visual observation, cover depth measurements, concrete resistivity using single point resistivity, half-cell potential, linear polarization using 3LP device. Fatigue and strength testing included cycling both I81 slabs and lab cast slabs. Shrinkage characteristics were evaluated on lab cast slabs only. Shrinkage specimens were monitored for 180 days and compared with predictive shrinkage model results.

CHAPTER 2: LITERATURE REVIEW

2.1 Corrosion of Reinforcing Steel

Corrosion of reinforcing steel inside concrete is an electrochemical process. The reaction at the anode and cathode site must take place at the same rate for $FeO.(H_2O)_x$, which is also known as rust, to occur. If a large cathode to anode area ratio is present, it will result in a rapid rate of corrosion, due to the requirement of equal rates of reaction at the anode and cathode. Corrosion is also affected by the distance between the cathode and anode, usually greater near the junction and decreasing with increasing the distance between them. A lower corrosion rate can be achieved by increasing the resistance to ion flow.

In concrete, the reinforcing steel acts as the electronic conductor, and the concrete pore water acts as the ionic conductor (Bentur, Diamond et al. 1997). These contribute to the two main factors that induce the generation of the corrosion cells (Mehta and Monteiro 2006):

$Fe \rightarrow Fe^{++} + 2e^-$ (anode)

$H_2O + ½O_2 + 2e^- \rightarrow 2OH^-$ (cathode)

In the concrete the moisture content is generally greater than 80%, and the relative humidity (RH) is generally greater than 70%. The pH of the concrete pore water ranges from 12.5 – 13.5 which is in the alkaline range. The pore contains sodium (Na^+), potassium (K^+), calcium (Ca^{++}), and hydroxide (OH^-) ions, amount others. Also, oxygen is dissolved in the concrete pore water at the corrosion (bar) site. A passivation layer of ferric oxide (Fe_2O_3) and ferrous oxide (Fe_3O_4) forms on the reinforcing steel. Ferric oxide (iron (III) oxide) has a reddish brown color which we refer to as red rust, while ferrous oxide (iron (II) oxide) has a black color. This passive diffusion-barrier oxide layer reduces the corrosion rate to almost zero for the reinforcing steel in the concrete.

Oxygen in the atmosphere migrates through the concrete to the rebar surface. This migration mainly depends on the concrete saturation and the void percentage. For

conditions where the void percentage is relatively constant and the concrete moisture content varies as follows:

- Saturated concrete: Oxygen migration is extremely slow since it has to diffuse through the concrete pore solution. The corrosion rate is low since there is high resistance for the oxygen to penetrate the concrete reaching the cathode sites on the reinforcing steel.
- Partially saturated concrete: Oxygen migration is slow, but oxygen gas diffuses through the empty pores and dissolves in the pore water. It continues to diffuse until it reaches the cathode site. The corrosion rate is high since there is less resistance for the oxygen to diffuse in the empty voids.
- Dry concrete: Oxygen migration is rapid but water is absent. The corrosion rate is low since there is high ionic resistance due to the absence of water which acts as an electrolyte for ionic conduction.

Based on the three cases mentioned above, partially saturated concrete is at higher risk in having higher corrosion rates compared to saturated and dry concrete. The change in temperature is another environmental factor which has a strong impact on the corrosion rate. As the temperature increases the corrosion rate increases, providing there is a maintenance electrolyte (pore water).

Decreasing the concrete permeability is one of the major and first precautions that can be controlled during construction methods against steel aggressors. This can be done by decreasing the water to cement ratio (w/c), or by using mineral additives like silica fumes, fly ash, ground granulated blast furnace slag or metakaolin (Böhni 2005). Another mean of defense against steel aggressors is increasing the cover depth which will delay their penetration through the concrete to reach the reinforcing steel. In combinations these methods are considered the most economical solution but in some cases they are not enough to rely on because of the severity of environmental exposure conditions and construction practices (Böhni 2005).

There are certain conditions which destroy the passive layer formed on the reinforcing steel embedded inside the concrete. When the pH decreases below about 10 the

reinforcing steel will start to corrode. This occurs when the concrete is exposed to an acidic environment, which can occur when carbon dioxide (CO_2) dissolves in water (H_2O) to form carbonic acid (H_2CO_3) which reacts with calcium hydroxide ($Ca(OH)_2$). Also, humic acid is an organic acid formed by the biodegradation of dead organic matter such as the decay of vegetation. Sulphuric acid (H_2SO_4) is common in industrial operations and sewage treatment facilities. Acids will interfere and reduce the alkalinity of the concrete which initiates severe corrosion of the reinforcing steel. They will also cause dissolution of hardened cement. Another factor which initiates severe corrosion is chloride since they destroy the passive layer formed on the reinforcing steel. Soluble chloride can be found in aggregates or added intentionally as admixtures during the mixing process. They can also penetrate the concrete from an external source such as deicing salts or seawater. Both conditions lead to severe corrosion in the reinforcing steel. It starts by the initiation of corrosion of the reinforcing steel and continues until the corrosion products create sufficient internal pressure to crack and spall the concrete cover. The stains of rust can be seen from the exterior, which are due to the expansive reaction of iron to iron oxide (Lambert 1998). Spalling usually takes place in locations where the concrete has the lowest cover depth and continues to move throughout the structure.

There are other means to delay the corrosion occurrence in the reinforcing. This can be achieved by using different types of materials which have higher corrosion resistance compared to using bare bars. Some of those means are epoxy coated bars (ECR), zinc coated bars, or stainless steel bars (A955 & A1035). The most promising measure amongst reinforcing steel corrosion is the use of stainless steel. It has a higher corrosion resistance and also higher material pricing compared to other reinforcing solutions, but in a long term study it can be the least cost option to choose since it requires less rehabilitation work due to the corrosion of the reinforcing steel (Brown, M.C. el al 2002).

2.2 Corrosion of Epoxy Coated Reinforcement (ECR)

2.2.1 History of ECR

It was observed in the mid 1960's that the corrosion of reinforcing steel caused premature deterioration of bridge decks in the United States in some cases less than five years. The cause was related to increased deicing salt usage, low clear concrete cover depths, relatively high concrete permeability (high w/c), and poor deck drainage. A research study was funded by the Federal Highway Administration (FHWA) at the National Bureau of Standards (currently the National Institute for Standards and Technology) in the early 1970's on epoxy coated reinforcement as an effective protection method for bridge decks. The coating was adapted from the petroleum industry and utility companies. Since a dry epoxy coating is dielectric, it averts charged chloride to penetrate it (Broomfield 2007). In 1973, the first ECR was used in a bridge deck in Philadelphia to achieve better service life (Manning 1996).

In 1986, severe corrosion was noticed in some bridges in the Florida Keys after five to seven years of service life (Sagüés 1994). Some of the ECR were examined and the result were that the epoxy coating disbonded, and corrosion had taken place underneath the coating in an acidic environment with a pH of 5 (Manning 1996). This was the first serious incident which showed the lack of efficiency of ECR in corrosive environment.

2.2.2 Manufacturing Process of ECR

Reinforcing bars are blasted with grit to remove rust, mill scale and contaminates. They are then heated in an induction furnace to approximately 450°F and sprayed with an electrostatic spray that applies fine epoxy powder. This causes the epoxy powder to melt, flow and a cure to form complex link-polymer. Water quench is usually used to cool the epoxy coated bars (Manning 1996; Pyc, Weyers et al. 2000; Broomfield 2007).

Testing is conducted during manufacturing to check the integrity and quality of the epoxy coating. Tests include film thickness, holidays, coating flexibility, adhesion, chloride

permeability, abrasion resistance, and impact resistance. They are presented in detail in ASTM Standard A 775/A 775M, the standard specifications for epoxy-coated steel reinforcing bars.

2.2.3 Corrosion of ECR

The purpose of the epoxy coating on the reinforcing steel is to act as a protective barrier from the surrounding corrosive environment. Since epoxy is a dielectric nonconductive material it also protects the reinforcing steel from any electrical transfers (prevents electrolyte penetration) (Dickie, Hammond et al. 1981). Even if an assumption of undefected coating is present, at some level organic coatings are permeable to water and oxygen (Clear, Hartt et al. 1995).

Corrosion initiation can occur under the epoxy coating and the reinforcing steel when the epoxy debonds from the reinforcing steel which is generally not visible unless the coating is peeled (Sagues and Powers 1996; Liu and Weyers 1998). In some cases the debonding can occur before the chlorides attack the ECR which will add insignificant or no additional service life to the reinforcing steel (Pyc 1998). Some studies conducted by Sagues and Zayed (1989) concluded that the potential of corrosion occurrence in bent areas is higher due to the epoxy debondement (Sagues and Zayed 1989). Continuous water exposure can cause water to be trapped between the epoxy coating and the reinforcing steel resulting in adhesion loss (Nguyen, Byrd et al. 1996).

The corrosion of ECR is similar to the corrosion of bare bars. However, the corrosion rate is faster underneath the epoxy coating of the ECR compared to bare bars corrosion rate (Pyc 1998). Crevice corrosion usually occurs in ECR, while pitting corrosion dominates on bare bars. The main difference between the corrosion process in ECR and bare bars occurs on the cathode side. For ECR, hydrogen is reduced at the cathode side resulting in acidic environment under the coating, while for bare bars oxygen is reduced at the cathode side.

A conclusion can be build that the possibility of epoxy coating to be damaged during manufacturing process, transporting or storage cannot be avoided. This will result in an adhesion loss between the epoxy and the reinforcing steel, with the influence of other factors mentioned previously, in a relatively short period of time, as little as four years. Based on research results, whenever adhesion loss occurs, the risk of corrosion taking place under the coating increases.

2.3 Corrosion Assessment Methods

2.3.1 Introduction

Before performing any repair on a structure, a proper understanding of the causes and severity of deterioration is needed. A full evaluation must be performed on the structure so the type and level of rehabilitation can be quantified. Otherwise, unnecessary work will be performed which will cost more time, money and delay. Also, the root cause of the problem must be fully diagnosed or it will be useless doing the expensive repairs (Broomfield 2007). As Broomfield (2007) described, "It is easy to generate large amounts of test data and fail to come to a conclusion about the cause and extent of damage and the best options for repair."

"A minimum requirement would usually be a visual survey, a delamination survey, carbonation and chloride measurements, and cover depth measurements (Broomfield 2007)."

There are many deterioration mechanisms which occur in structures. Only the assessment methods to monitor and determine corrosion potentials and rates will be discussed in details.

2.3.2 Visual Observation

Visual observation is the first step to know how extensive the damage is when investigating any structure. It requires a close look at the structure and noting the type of visual deterioration that can be seen. In many cases there are check lists or systems that can be followed to determine and scale the severity of the deterioration. A good practice is taking photographs of spalled and sound concrete areas in order to perform further analysis instead of non-directly taking core samples from the structure. The survey process requires knowledge and experience to interpolate the results.

2.3.3 Delamination Survey

The purpose of this test is to measure the horizontal cracks between the reinforcing steel (cracks starts between the reinforcing steel at the reinforcing steel depth) before it becomes apparent at the concrete surface. Horizontal cracks can be noticed by a hollow sound when hit by a hammer or by chain dragging. Delaminations are marked and plotted on a deck plan view to present the extent of the delamination. Spalls and patches are also noted and plotted. The procedure is considered a quick and low cost method which does not require sophisticated equipment, and it gives reasonably accurate data for the repair/rehabilitation decisions. Other techniques and special equipment, such as ground penetration radar, can be used if more data is required or in some cases where the reinforcing steel is deeply imbedded.

2.3.4 Cover Depth Measurements

As previously mentioned, the cover depth is the first line of defense against corrosive agents attacking the reinforcing steel, such as chloride and carbonation. Sufficient cover depth delays the attack of corrosion agents. Reinforcing steel is detected by sending low-frequency electromagnetic field through the concrete. Steel interacts strongly with electromagnetic field which makes the cover depth meter detect the reinforcing steel

location (Mehta and Monteiro 2006). By performing a cover depth survey, it will be clear which areas have higher potential for corrosion based on the cover depth. If there is a congestion of bars and iron bearing aggregates, it becomes more challenging in taking cover depth surveys since they will interfere with the readings. However, it is still considered a good practice to determine the root causes of the deterioration, of which cover depth is one input parameter for corrosion.

2.3.5 Concrete Resistivity

A non-destructive technique is useful to monitor and inspect structures using the electrical resistivity of concrete (Polder, Andrade et al. 2000). The concrete resistivity is strongly influenced by the concrete quality (permeability) and the moisture content. Higher resistivity means the concrete is more resistive to aggressive materials which initiate corrosion in the reinforcing steel, while lower resistivity reflects that the reinforcing steel has a higher potential of corrosion since it will be easier for the aggressive materials to reach the reinforcing steel (Mehta and Monteiro 2006).

Measuring the concrete resistivity depends on the ions dissolved in the pore liquid which carry the electrical current. This application can be used in different techniques such as a single point probe, two points probe and a four points probe system. The most commonly used is the Werner Probe (four probe resistivity) which was developed for measuring soil resistivity. The probes have been modified with springs so they can be placed on the concrete surface without drilling holes. Current is passed by the outer probes, while the inner probes detect the potential difference (Broomfield 2007). The readings do not indicate if the reinforcing steel is in active corrosion or not, but they give additional information of where is the highest potential for corrosion taking place in the structure and the how resistive the concrete is to supporting corrosion (Polder, Andrade et al. 2000). The data interpretation for four probe resistivity is presented in Table 2.1.

In this research single point resistivity is used and it is represented by Equation 2.1 (Polder, Andrade et al. 2000).

$$\rho = \frac{R\pi D^2}{4L} \qquad \textbf{(Equation 2.1)}$$

Where,

ρ = resistivity of concrete (ohms-cm)

R = resistance of concrete (ohms)

D = diameter of the probe in contact with the concrete surface measuring resistance (cm)

L = clear cover depth + half the diameter of the reinforcing steel (cm)

Table 2.1 **Concrete Resistivity Interpretation Guidelines for Four Probe (Mehta and Monteiro 2006) [Used under fair use guidelines, 2011]**

Concrete resistivity (Ω-m)	Likely corrosion rate
>200	Negligible
100-200	Low
50-100	High
<50	Very high

Feliu conducted some tests using a disc method (single probe) using Newman's formula for onsite concrete resistivity measurements, the results are presented in Table 2.2.

Table 2.2 **Single Probe Concrete Resistivity Interpretation (Feliu, Andrade et al. 1996) [Used under fair use guidelines, 2011]**

Concrete resistivity (kΩ-cm)	Risk Levels
>100-200	Very low corrosion rates
10-100	Corrosion rate low to high
<10	Corrosion rate not controlled by resistivity

2.3.6 Half-Cell Potential

The Half-cell method is used to determine the corrosion activity of the reinforcing steel. The main requirement for this test to be successful is that the structure being tested is to have electrical continuity. The concrete being tested should be moist so it can maintain an electrical circuitry (ASTM C 876-91). The half-cell potential test is considered a simple device (Broomfield 2007). Also, it is considered a quick and inexpensive method to determine areas which require further investigation (Mehta and Monteiro 2006). The test setup consists of a copper rod submerged in a saturated copper-copper sulfate solution and confined in a rigid tube with a porous plug at its bottom, which is now a copper/copper sulfate electrode (CSE) half-cell. An electrical junction device is mounted at the bottom of the CSE half-cell to provide continuity between the concrete surface and the porous plug. A sponge pre-wetted with an electrolyte is used to provide a low electrical resistance. The potential difference between the half-cell and the reinforcing steel is measured using a high impedance voltmeter. Detailed test setup is presented in Figure 2.1 (ASTM C 876-91). Table 2.3 presents the data interpretation for the CSE half-cell potential.

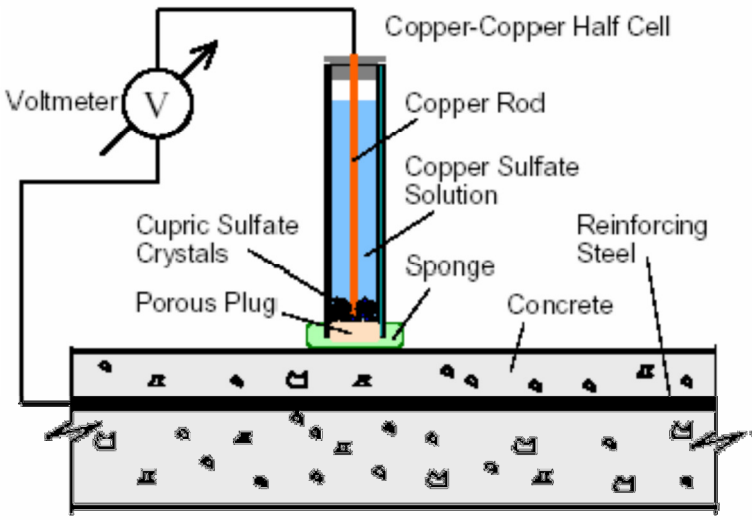

Figure 2.1 Half-Cell Potential Apparatus

Table 2.3 Corrosion Interpretation Using CSE Half-Cell (ASTM C 876-91)

Measured Potentials (mV)	Corrosion Condition
> -200	Low (10% risk of corrosion)
-200 to -350	Intermediate corrosion risk
< -350	High (>90% risk of corrosion)

2.3.7 Linear Polarization

This method gives real time readings of corrosion rate and metal lost, but it cannot accurately calculate and predict total section loss or concrete spalling rate (Broomfield 2007). It gives a snapshot of corrosion rate based on concrete temperature and moisture condition (Liu and Weyers 2003). With current technology, corrosion rate is the closest we can get to measure the rate of deterioration (Grantham, Herts et al. 1997; Broomfield 2007). Gowers and Millard described corrosion by, "Corrosion is a dynamic process subject to fluctuations and the interpretation of corrosion rate measurements should focus on the order of magnitude rather than the precise value obtained (Gowers and Millard 1999)".

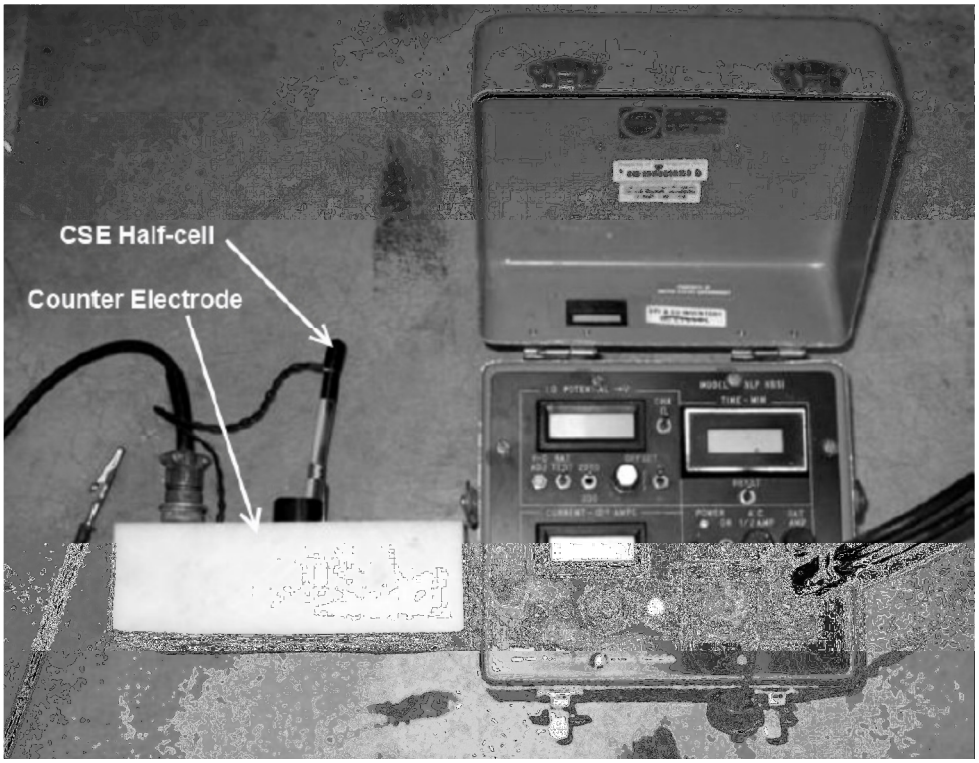

Figure 2.2 3LP Device Setup (Photograph Taken By Soundar S. G. Balakumaran 2010) [Used under fair use guidelines, 2011]

The three-electrode polarization method (3LP method), shown in Figure 2.2, is one of the common methods used to measure corrosion rate. Three electrodes are required for the 3LP method: "working electrode" is the reinforcing steel embedded in the concrete, "counter electrode" is a metallic object used to apply the polarizing current, and "standard half-cell" is used to measure the response of the reinforcing steel to the current applied via the counter electrode (Clear 1990). The test uses the Stern-Geary characterization of a polarization curve for corrosion. Corrosion current, $I_{corr,}$ is calculated using the Stern-Geary equation (Clear 1989; Liu and Weyers 2003), and is connected to corrosion current density (I_{corr}) by dividing by an estimated reinforcing bar surface polarized area (see Equation 2.2).

$$I_{corr} = \frac{\Delta I_{appl}(\beta_a \beta_c)}{1.2\Delta\emptyset(\beta_a + \beta_c)} = \frac{B}{R_p} \qquad \textbf{(Equation 2.2)}$$

Where,

I_{corr} = corrosion current (mA)

I_{appl} = current required to polarize the rebar by different potential values from static potential

$\Delta\Phi$ = absolute value of cathodic polarization potential minus the natural electrical half-cell potential

β_a = anodic tafel slope (mV/decade) = 150 mV/decade

β_c = cathodic tafel slope (mV/decade) = 250 mV/decade

R_p = Polarization resistance (ohms)

B = constant value between 26 and 52 mV, a values of 40 mV is used for the 3LP device.

Interpretations of corrosion current density readings are provided by the 3LP developer, but are generally considered in need of further evaluation (see Table 2.4).

Table 2.4 Interpretations for Corrosion Current Density for the 3LP Device (Clear 1989)

Corrosion Current Density, I_{corr} (mA/ft^2)	**Corrosion Damage State**
<0.2	No corrosion damage expected
0.2 – 1.0	Corrosion damage is possible in between 10 to 15 years
1.0 – 10	Corrosion damage expected between 2 to 10 years
>10	Corrosion damage expected in 2 years or less

2.3.8 Chloride Content

Two methods to measure chloride content in concrete are "acid soluble" (ASTM C 1152/C 1152M) and "water soluble" (ASTM C 1218/C 1218 M). Both may be performed by collecting core samples from the structure and cutting them at different depths, after that they are crushed smaller than the #30 sieve. Each sample should be tested separately to prevent any contamination between samples. A chloride profile should be plotted based on the chloride content measured at each depth. For decent plots it is recommend to take at least four readings at different depths (Broomfield 2007). For more details about how each test is conducted refer to ASTM C 1152/C 1152M for acid soluble test, and ASTM C 1218/C 1218 M for water soluble test. Table 2.5 presents one means of interpretation of acid soluble chloride values.

Table 2.5 Chloride Contents Corrosion Risk (Broomfield 2007) [Used under fair use guidelines, 2011]

% Chloride by mass of cement	% Chloride by mass of sample (concrete)	Risk
<0.2	<0.03	Negligible
0.2 – 0.4	0.03 – 0.06	Low
0.4 – 1.0	0.06 – 0.14	Moderate
>1.0	>0.14	High

The following equation maybe used to assess the penetration rate of chlorides. This model is based on Fick's second law of diffusion, although the influence of cracking is not included, still it gives good correlation. Also, the diffusion constant is highly variable and background chloride must be deducted from diffusion coefficient.

$$C_{(x,t)} = C_o\left(1 - erf\frac{x}{2\sqrt{D_c t}}\right) \qquad \textbf{(Equation 2.3)}$$

Where,

$C_{(x,t)}$ = chloride concentration (kg/m^3)

C_o = surface chloride concentration (kg/m^3)

D_c = diffusion coefficient (mm^2/year)

x = concrete cover depth (mm)

erf = statistical error function

2.4 Concrete Shrinkage

2.4.1 Introduction

Concrete changes in volume throughout its service life in a three-dimensional manner, it is dimensionally unstable (Mehta and Monteiro 2006). This change is mainly caused by shrinkage and creep. Shrinkage is defined as a volumetric change without applying any sustained loads. There are mainly four types of concrete shrinkage: plastic, drying, autogenous, and carbonation shrinkage (Aitcin, Neville et al. 1997; Holt and Leivo 2004). Based on Holt and Leivo, shrinkage can be divided into two categories, early age and long term. Early shrinkage occurs in the first 24 hours and it consists of drying, thermal and autogenous shrinkage, and is sensitive to internal stresses while concrete has a low strain capacity. While long term shrinkage occurs after 24 hours and it consists of drying, thermal, carbonation and further autogenous shrinkage (Holt and Leivo 2004). Also, excess of shrinkage can lead to cracks which may aid in premature deterioration of the structure (Holt and Leivo 2004).

When concrete is under sustained loading, inelastic deformations take place, this is also known as creep (Lamond 2006). There are two main types of creep, basic and drying creep. In this part of the literature review there is more focus on concrete shrinkage, deck cracking and shrinkage prediction models

2.4.2 Plastic Shrinkage

Plastic shrinkage takes place at the surface of fresh mixed concrete during its plastic state before gaining any significant strength (Soroushian and Ravanbakhsh 1998; Kwak and Ha 2006). When the surface water on the fresh placed concrete evaporates at a faster rate than the bleeding water from the concrete it causes plastic shrinkage. Plastic shrinkage cracking, however, usually occurs in thin structures (Senthilkumar and Natesan 2005). Although the cracks are mainly on the surface, they can extend to the reinforcing steel and cause premature deterioration (Kwak and Ha 2006). If bleeding, which can be noticed by a shiny concrete surface, is not occurring, the possibility of plastic shrinkage occurring is high. The factors influencing rapid water loss are concrete and air temperature, relative humidity, and wind velocity. Decreasing the water loss on a freshly placed concrete surface by fogging is one of the first precautions which needs to be considered to control plastic shrinkage.

2.4.3 Drying Shrinkage

Drying shrinkage is the volumetric change due to the removal of water from the hydrating cement paste to the surrounding environment. The volume of water lost in this reaction does not equal the volume change of drying concrete. Water movement occurs by diffusion within the concrete. The largest percentage of water loss is from the large capillary pores, however, the smaller portion of water loss from the small capillary voids results in the greatest portion of the drying shrinkage since they have greater tension in the pore water (Lamond 2006). Drying shrinkage consists of reversible and irreversible shrinkage from the loss of water to the environment. When the calcium silicate hydrate (CSH) bonding forces increase due to water lost, this water is considered irreplaceable due to the difficulty of water to separate the CSH sheets.

The factors that influence drying shrinkage are cement paste content, water/cement ratio, degree of hydration, characteristic and amounts of admixtures used, elastic modulus of

aggregates, relative humidity, and the surface area of concrete exposed to the environment.

Higher water/cement ratio results in a greater drying shrinkage occurrence. A study was conducted by Kim and Lee to measure drying shrinkage at different depths within the concrete. It showed that the exposed concrete surface resulted in the highest drying shrinkage as predicted by analytical results (Kim and Lee 1998). The impact of aggregates causing shrinkage was discussed by Kwan. It focused on how pretreating aggregates can have a positive impact in decreasing the shrinkage rates (Kwan, Fung et al. 2010). Another study on aggregate affects, showed that an increase in aggregates in concrete decreased the drying shrinkage (Fattuhi and Al-Khaiat 1999).

2.4.4 Autogenous and Chemical Shrinkage

Autogenous and chemical shrinkage, are described as the change in volume without exchanging moisture with the surrounding environment, they are related to the hydration of cement only (Holt and Leivo 2004; Barcelo, Moranville et al. 2005; Lamond 2006). As described by Holt, the difference between chemical and autogenous shrinkage, "The chemical shrinkage is an internal volume reduction while the autogenous shrinkage is an external volume change (Holt and Leivo 2004)".

Chemical and autogenous shrinkage are equal when concrete is in its plastic form. When the cement starts setting, chemical shrinkage has less influence on autogenous shrinkage (Holt 2001). Higher temperatures, low water/cement ratio, and fine grained materials such as micro-silica (silica fume) increase the amount of autogenous shrinkage. In the first 24 hours, autogenous shrinkage may be as much as 50% of the total shrinkage.

2.4.5 Carbonation Shrinkage

Carbonation shrinkage has a direct relation between different cement hydration products and the carbon dioxide present in the air. The hydration products that aids this reaction to

takes place are calcium hydroxide ($Ca(OH)_2$), calcium silicate hydrate (CSH), tricalcium silicate (C_3S), and dicalcium silicate (C_2S) and not only CH (Claisse, El-Sayad et al. 1999; Lamond 2006). It takes place simultaneously with drying shrinkage and in some cases this can be misleading (Lamond 2006). When carbon dioxide dissolved in water, it forms carbonic acid and then it reacts with cement hydration products, which stay in an alkali media. In low relative humidity, the possibility for carbonation to be present is low. This is due to insufficient water present to react with the carbon dioxide. The factors that depend on the carbonation rate are the presence of carbon dioxide and its concentration, relative humidity, permeability of concrete, time of exposure, and method of curing.

2.4.6 Cause of Deck Cracking

One visual indication of concrete deterioration is surface cracking. It can be noticed throughout the life of the concrete structure and can occur within the first 24 hours of placing the concrete. The reasons behind that can be due to many factors. Some of them are due to constituent materials such as the water used in mixing, chemicals added or types of aggregates used, the construction process starting with mixing until curing the concrete, physical properties such as the modules of elasticity of the concrete, the nature of the environmental exposure, and the types of loading being applied at the structure and their magnitude and frequency.

From the mode and characteristic of the crack and some history of the structure, the root cause of the crack can be determined. Knowing the mode of the crack (linear, pattern or random) is one of the important factors that is considered. The characteristics which are considered in a crack are surface width, depth, and the orientation, and cracking through or around coarse aggregates.

There are physical and chemical factors that influence concrete durability. Each of them has internal and external processes for physical and chemical factors. Freezing, thawing, and alkali-silica reactions are considered internal process for both factors. Abrasion and

corrosion of reinforcing steel are considered as external process for both factors. However, the environmental exposure conditions, time, and the voids in the concrete are dependent on chemical external process only of the structure (Weyers, Pyc et al. 2003). All of the physical and chemical factors have strong influence on bridge deck cracking.

Cracking due to drying shrinkage can occur due to two reasons, either excessive early age water loss or long term water loss. The mode of the crack for an early age water loss is a mud flat crack, and a long term water loss is linear mode crack. Plastic shrinkage cracking occurs because of excessive early age water loss also, but it has a random cracking mode with a wide surface and a shallow depth. While subsidence crackling occurs over reinforcing steel and follows the reinforcing steel in a linear mode, it occurs usually in flat slabs such as bridge decks.

2.5 Shrinkage Models

There are many methods and models to calculate shrinkage and creep. Five shrinkage models will be discussed and will be compared with the shrinkage readings on the lab cast slabs. The five models are American Concrete Institute (ACI 209R-92 model), Comite Euro-International Du Beton (CEB MC90 model), Gardner and Lockman (GL2000 model), Bazant – Baweja (B3 model), and AASHTO-LRFD. Mathematical models were developed to match large databases of measured results.

Those models are valid for moist-cured hardened concrete for at least one day, and loaded after one day or more after curing. The mean compressive strengths that the models are adequate for vary from 20 to 70 MPa (3,000 to 10,000 psi). Modifications of those models are for normal composite concrete, and they were not modified for concrete which contains high concentrations of silica fume, fly ash, or natural pozzolans.

Each shrinkage prediction model requires a different range of parameters. The ACI 209R-92 model requires ten parameters, the CEB MC90 model requires six, the GL2000 model requires eight parameters, the B3 model requires 12 parameters, and the AASHTO-LRFD requires four parameters. Details of these models are present in Guide

for Modeling and Calculating Shrinkage and Creep in Hardened Concrete, and in AASHTO-LRFD.

CHAPTER 3: METHODS AND MATERIALS

3.1 Introduction

The study was conducted on a total of nine specimens, six from the actual I81 failed bridge and three new specimens fabricated and cast in the lab. Three of the actual bridge deck specimens were strength tested and three were fatigue tested. A total of three specimens were fabricated and cast in the lab identical to the actual specimens from the bridge deck to establish a baseline for strength and fatigue performance. Measurements were taken prior to strength and fatigue testing, and also after fatigue testing.

3.2 I81 Deck Slabs

3.2.1 Introduction

After 17 years of service a section of a closure slab failed on I-81 near Marion, VA. Sections from the actual bridge deck were removed and delivered to the Civil Engineering Structures and Materials Laboratory at Virginia Tech. The section contains the entire closure pour section along with the adjacent deck slab, the end blocks (deck sections) on the slabs were field cut about 9 in. from the closure pour joint, see Figure 3.1. There is a slight difference in the dimensions of the other specimens due to construction and cutting precision, all slabs are shown in Appendix C.

Visual inspection was conducted on the field slabs in addition to corrosion readings, mechanical properties, permeability characteristics, and density and saturation characteristics. After examining the section they were sawed transversely into strips with a width of about 22 in. each.

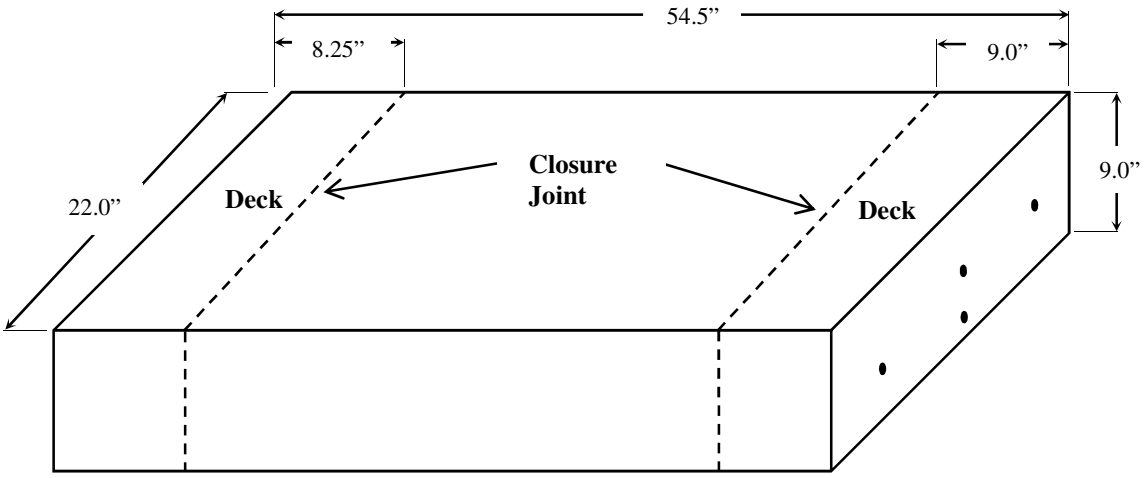

Figure 3.1 Specimen #6 Dimensions of Cut Section from the Bridge Deck

3.2.2 Visual Inspection

Visual inspection was conducted in two steps, using nondestructive and destructive methods. The nondestructive visual inspection measured dimensions of the slabs and specimens in addition to documentation of damage and a crack survey. Measurements were also made to determine the cold joints width using a feeler gauge. The destructive visual inspection required opening the specimens and checking the condition of the embedded ECR for corrosion and damage to the epoxy coating. Also for any deposits of calcium hydroxide, calcium carbonate and rust stains with the reinforcing bar trace.

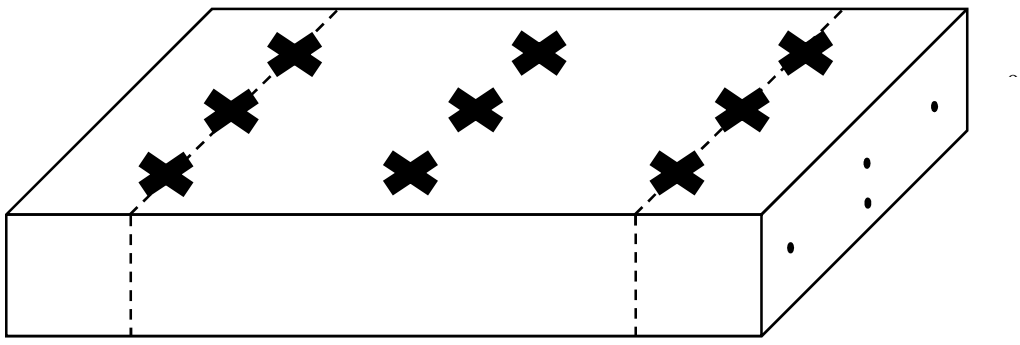

Figure 3.2 Cover Depths Measurement Locations

3.2.3 Cover Depth

Cover depths were measured in nine different locations in each specimen, three on each side of the closure pour joints and three in the center of the closure pour using a rebar locator Prometer 3,see Figure 3.2. In addition cover depths were taken at the exposed side bars on each side of the specimens on the deck slab using both a ruler and Prometer 3 to confirm the concrete cover depth measurements.

3.2.4 Half-cell Potentials

Half-cell potentials readings were collected at the same locations where the cover depth readings were taken, as shown in Figure 3.2. Measurements were conducted in accordance to the ASTM C 876-91 using a CSE electrode. ASTM C 876-91 states that the method is applicable for uncoated reinforcing steel, but it has been shown that it may be used on ECR (Brown, Weyers et al. 2006).

This test determines the corrosion activity of uncoated reinforcing steel, but it will be used for ECR.

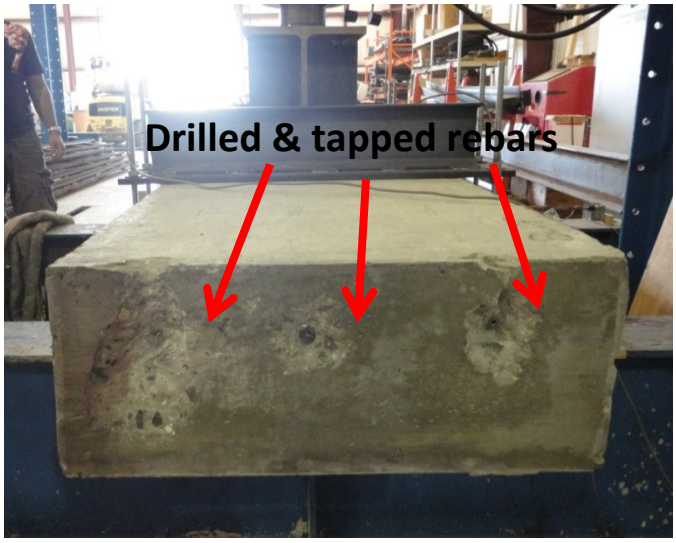

Figure 3.3 Drilled and Tapped Rebars to Measure Corrosion Readings

3.2.5 Linear Polarization

Three-electrode polarization method (3LP method) was used to measure the corrosion current density (I_{corr}) of the ECR. The test method and device were developed by Kenneth Clear (Clear 1990). It gives a snapshot of corrosion rate based on concrete temperature and moisture condition. The readings for the specimens were taken at the closure pour joint and at the middle of the closure pour for each bar from each side of each bar, see Figure 3.2.

3.2.6 Concrete Resistivity

Single point resistivity test was used for measuring the concrete resistivity of the specimens. Concrete resistivity is strongly influenced by the concrete quality (permeability) and the moisture content. The readings do not indicate if the reinforcing steel is in active corrosion or not, they give additional information of where the highest corrosion is taking place in the structure and how resistive the concrete is to supporting corrosion. Measurements were taken for each bar at the closure pour joint and at the center of the closure pour, see Figure 3.2.

3.2.7 Unit Weight, Percent Voids, and Percent Saturation Testing

Core samples were drilled from different locations from the bridge deck and closure pour concrete, as shown in Appendix B in Figures B.1 through B.4. Core tests included unit weight, percent voids, and percent saturation of the concrete. Concrete properties were measured at the top and bottom for the deck and closure pour, as shown in Appendix B in Figures B.1 through B.4. Testing was conducted in accordance with ASTM C 642 – 06, Standard Test Method for Density, Absorption, and Voids in Hardened Concrete.

3.2.8 Compressive Strength Testing

Seven core samples were drilled from the bridge deck and closure pour at locations shown in Appendix B in Figures B.1 through B.4, three from the deck and four from the closure pour. All coring was conducted using a water cooled diamond drill bit, with 4 in. inside diameter. Strength tests were conducted accordance with ASTM C39 / C39M – 10, Standard Test Method for Compressive Strength of Cylindrical Concrete Specimens.

3.2.9 Splitting Tensile Strength Testing

Core samples were drilled from the bridge deck and closure pour at locations shown in Appendix B in Figures B.1 through B.4, three from the deck, and four from the closure pour. They were conducted in accordance with ASTM C496 / C496M – 04, Standard Test Method for Splitting Tensile Strength of Cylindrical Concrete Specimens.

3.2.10 Modulus of Elasticity Testing

Core samples were drilled from the bridge deck and closure pour at locations shown in Appendix B in Figures B.1 through B.4, three from the deck, and four from the closure pour. Testing was conducted in accordance with ASTM C469 / C469M – 10, Standard Test Method for Static Modulus of Elasticity and Poisson's Ratio of Concrete in Compression.

3.3 Lab Cast Slabs

3.3.1 Introduction

Three slabs were fabricated and cast at the Civil Engineering Structures and Materials Laboratory in Blacksburg, VA. The concrete used in casting the slabs was A-4 ready mixed concrete which is standard for Virginia bridge decks (4000 psi at 28 days, VDOT

standard identification). Slabs closely match the geometry and materials of I81 deck slabs, see Figure 3.5. Reinforcing bar details for lab slabs are presented in Figure 3.4.

The actual bridge deck was constructed by closing one lane and shoulder of the bridge deck, and traffic was diverted to the other lane. After the construction work was completed the new deck lane and shoulder was opened to traffic and the other lane and shoulder were closed. Finally, when both lanes and shoulders were completed the two sections were connected using a closure pour. Whereas, the replicated laboratory slabs were cast by placing both bridge decks (exterior sides) at the same time then placing the closure pour after 30 days, as shown in Figure 3.5 and 3.6. The cast slabs had a width of 22 in., a thickness of 8.5 in., and a length of 8 ft-4 in. Slab cast sections were wet cured using wet burlap covered with a polyethylene sheet.

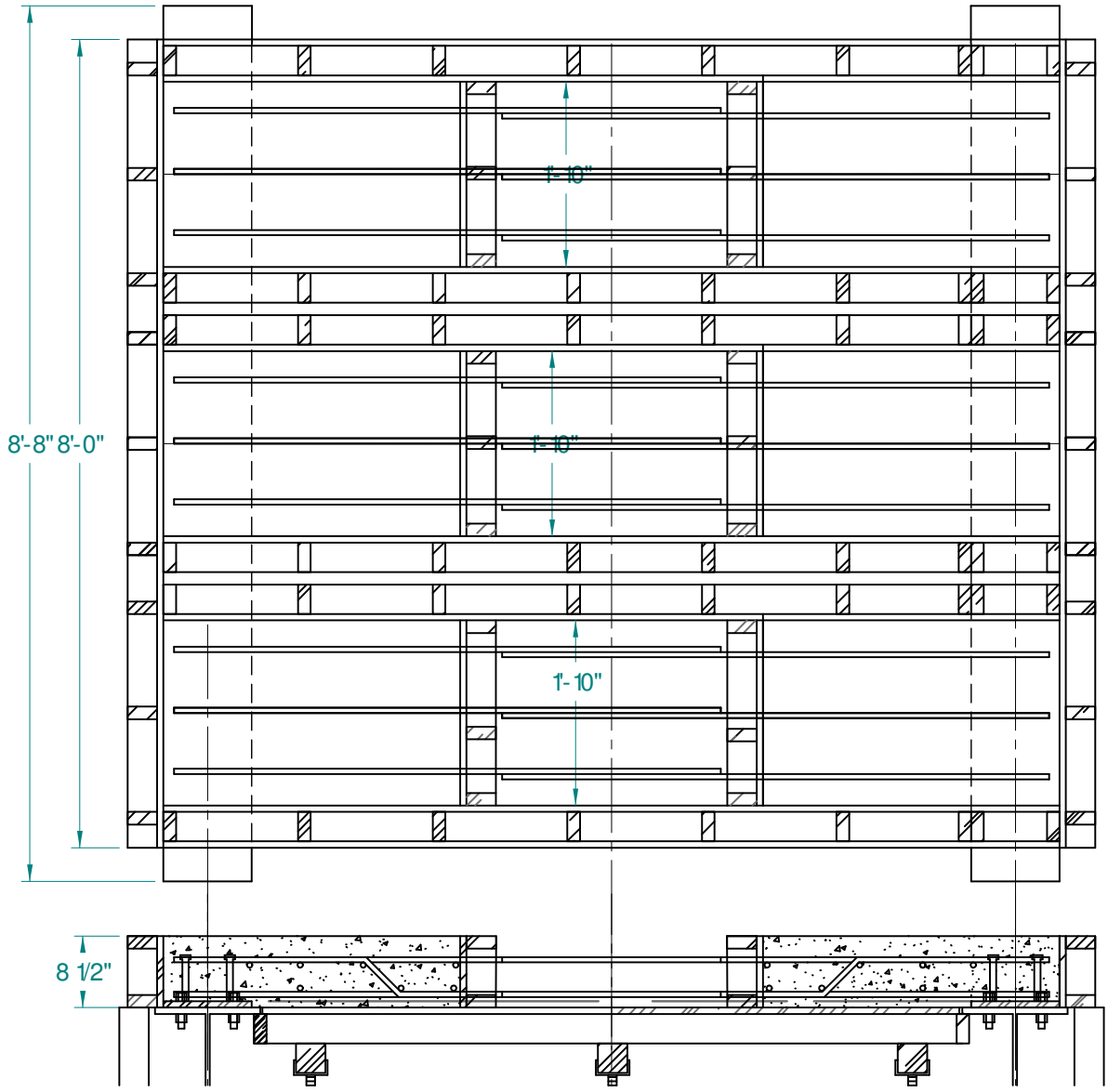

Figure 3.4 Lab Cast Slab Reinforcing Details

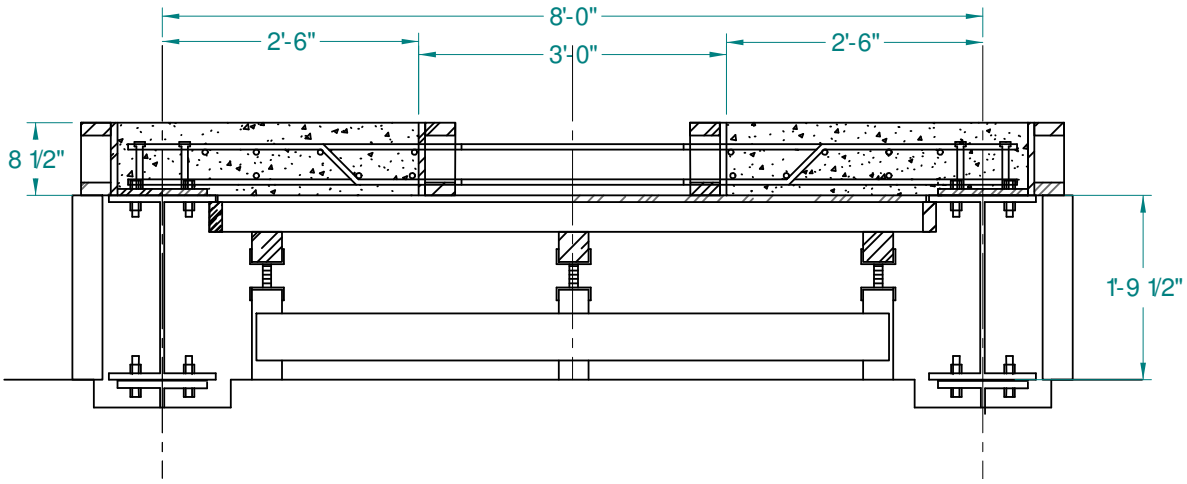

Figure 3.5 First Concrete Placement Setup

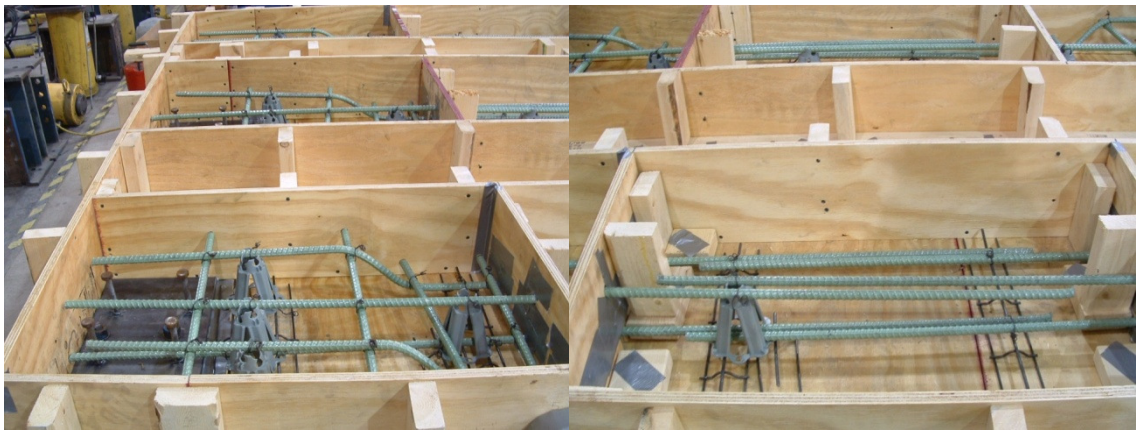

Figure 3.6 ECR and Form Work Setup before First Concrete Placement

Figure 3.7 and 3.8 show a cast slab after the first and second casting. Table 3.1 presents the mix designs for the two placements, total batched volume for the first and second placement were 4 cy each.

Figure 3.7 Closure after 30 days From First Concrete Placement

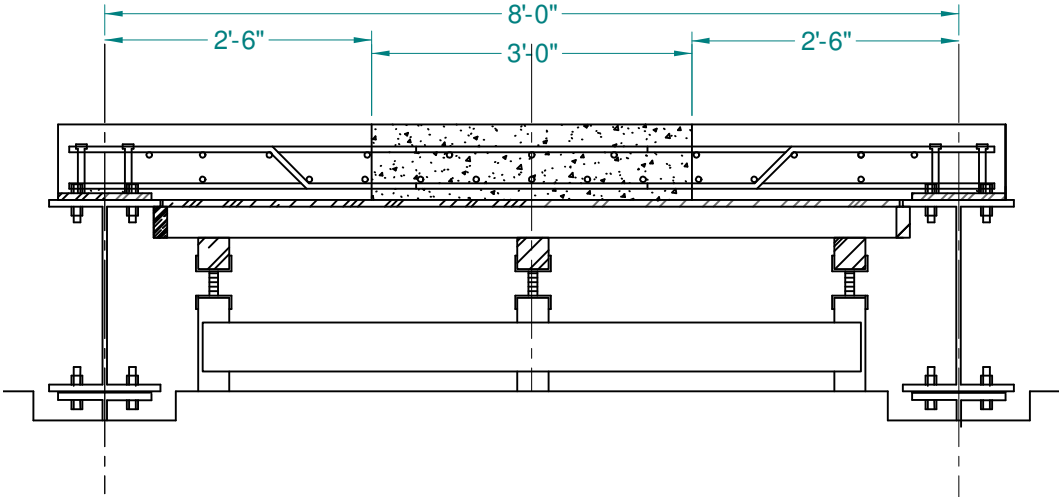

Figure 3.8 Second Concrete Placement Setup

Table 3.1 Cast Slab Mixture Proportions

Material	First Placement		Second Placement	
	Total Batched	Per cy	Total Batched	Per cy
Cement Type I, lbs.	2545	(636)	2535	(634)
Fly Ash, lbs.	635	(159)	665	(166)
Coarse Aggregate, lbs.	7060	(1765)	6980	(1745)
Fine Aggregate, lbs.	3840	(960)	3800	(950)
Water, lbs.	982	(246)	1130	(283)
Total, lbs.	15062	(3766)	15110	(3778)
AEA, fl. oz	6	(1.5)	5	(1.25)
MD W/R, fl. oz	76	(19)	76	(19)
Retarder, fl. oz	63	(16)	63	(16)

3.3.2 Compressive Strength Testing

Four inch by eight inch compressive strength test cylinders were cast for both the first and second concrete placement. The cylinders were cured in the same manner and adjacent to the casted bridge deck sections. Compressive test were conducted at seven, 28, 56, and 90 days in accordance with ASTM C39 / C39M – 10, Standard Test Method for Compressive Strength of Cylindrical Concrete Specimens. Two cylinders were tested at each age.

3.3.3 Splitting Tensile Strength Testing

Specimens were cast for the first and second placement using 4 in. by 8 in. plastic molds and were cured in the same manner and adjacent to the casted bridge deck sections. Tests were conducted at seven, 28, 56, and 90 days in accordance with ASTM C496 / C496M – 04, Standard Test Method for Splitting Tensile Strength of Cylindrical Concrete Specimens. Two cylinders were tested at each age.

3.3.4 Modulus of Elasticity Testing

Likewise, specimens were cast for the first and second placement and cured in the same conditions and adjacent to the casted bridge deck sections. Testing was conducted at seven, 28, 56, and 90 days, in accordance with ASTM C469 / C469M – 10, Standard Test Method for Static Modulus of Elasticity and Poisson's Ratio of Concrete in Compression. Two cylinders were tested at each age.

3.3.5 Water Ponding Testing

Ponding test was performed for each closure pour joint on each lab cast slab. Water was ponded for a period of 24 hours over each closure pour joints for each slab, see Figure 3.9. Water pond test was conducted to determine if the cast closure pour joints had opened wide enough to allow water leakage through the joint similar to the deck joints.

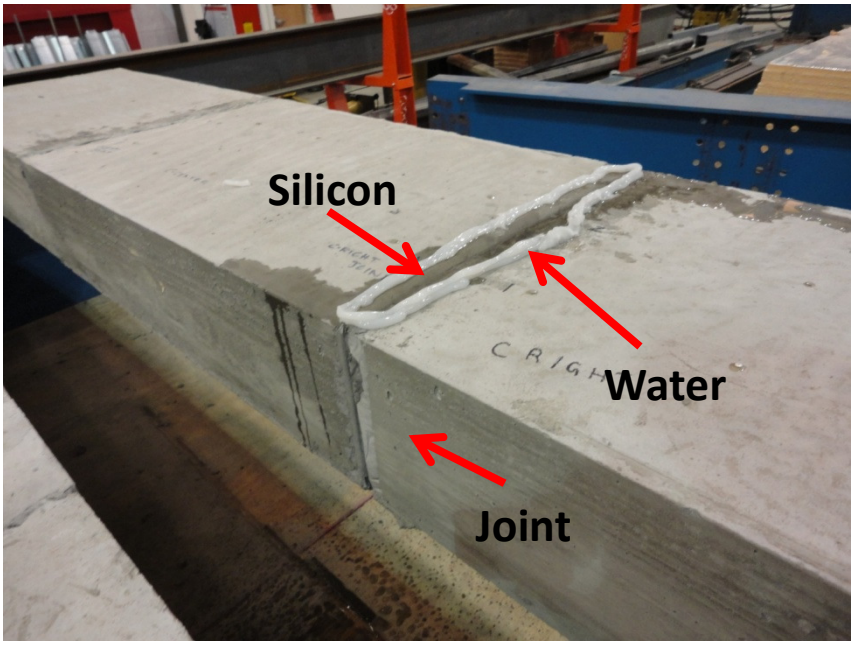

Figure 3.9 Water Ponding Test across the Joint

3.3.6 Shrinkage Testing

Concrete shrinkage measurements were performed during both the first and second placement and classified as restrained shrinkage testing by taking shrinkage measurements on demec points on slab surface. The restrained shrinkage testing data collection was conducted for a period of 180 days.

Shrinkage Measurements

Shrinkage measurements were taken on the actual slabs by placing Demec points on each slab. Demec points were placed using epoxy on the slab surface. A Demec gage was used to measure the length change between the points as shrinkage occurred, see Figure 3.10. Measurements were conducted for a period of 180 days for the deck on each side (first placement), closure pour which connects each side of the deck (second placement), and across the closure pour joint (between the first and second placement). The time interval between the first and second placement was 30 days. Figure 3.11 illustrates the location of the demec points.

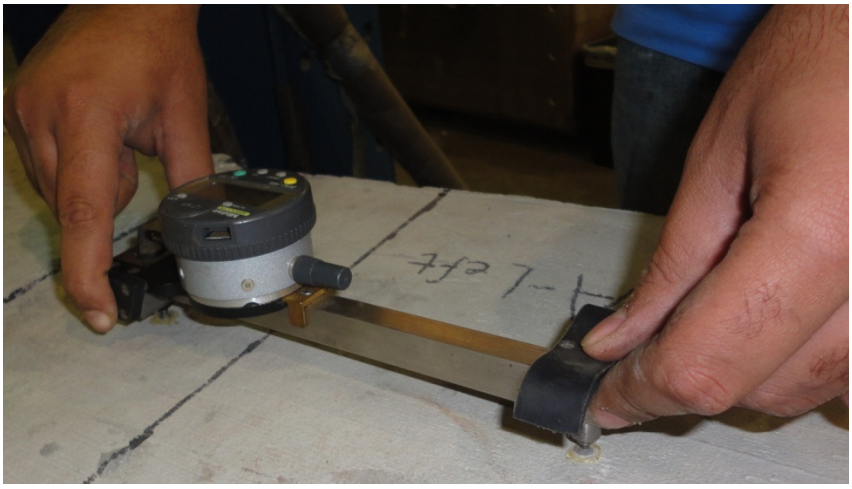

Figure 3.10 A Demec Gage Measuring Demec Points

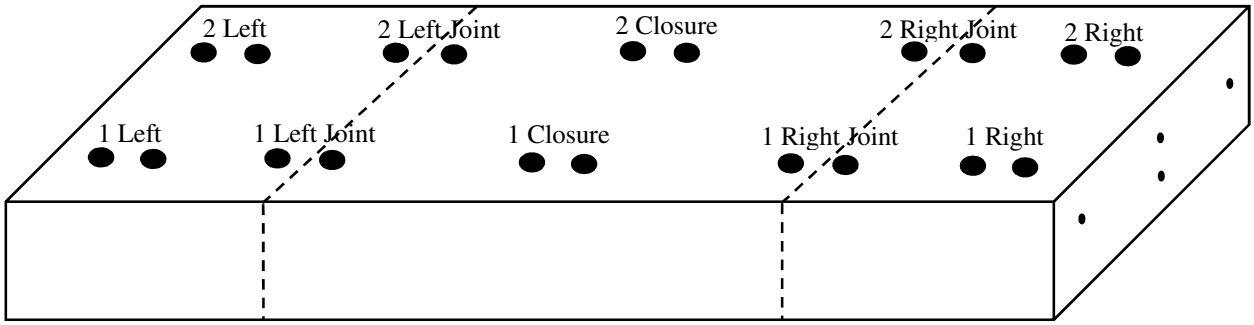

Figure 3.11 Location of The Demec Points on Lab Cast Slab

Unrestrained Shrinkage Measurements

Unrestrained shrinkage measurements were conducted on concrete prisms with a dimension of 3in. x 3in. x 11in.. Measurements were conducted in accordance with ASTM C 157/C 157M – 08, Standard Test Method for Length Change of Hardened Hydraulic-Cement Mortar and Concrete and performed for both the first and second placements. Three different curing conditions were evaluated as presented below:

1. Placed one day in mold, and then they were placed half an hour in lime bath before initial measurements were taken. After that they were placed again six days in lime bath before placing them in the shrinkage room with a temperature of 73 ºF ± 3 ºF and 50% ± 4% relative humidity.
2. Placed one day in mold, and then they were placed half an hour in lime bath before initial measurements were taken. After that they were placed again six days in lime bath before placing next to the laboratory slabs with varying in temperature and humidity.
3. Placed six days in mold, after that initial measurements were taken before placing specimens next to the laboratory slabs with varying temperature and humidity.

Length change measurements were conducted for a period of 180 days. For the first placement eight prisms were tested, three for the first curing condition, two for the second curing condition, and three for the third curing condition. For the second

placement ten prisms were tested, three each for the first and second curing conditions, and four for the third curing condition.

3.3.7 Shrinkage Prediction Models

The first curing condition unrestrained shrinkage data were compared with different shrinkage prediction models to identify the best prediction model, since the prisms were placed in a controlled environment. The comparison shrinkage models used were ACI 209R-92 model, Bazant-Baweja B3 model, CEB MC90 model, GL2000 model, and AASHTO-LRFD model (AASHTO 2007; ACI Committee 209 2008).

CHAPTER 4: RESULTS & DISCUSSIONS

4.1 Concrete Properties

4.1.1 Concrete Properties of I81 Deck Slabs

Samples were cored from different locations from the slabs, eight from the closure and six from the deck. Compressive strength, modulus of elasticity, unit weight, percent voids, and percent saturation were measured for those core samples. The results are presented in Table 4.1 and 4.3 for the core samples from Virginia Interstate 81 at Mile Marker 43 South Bound travel lane (I-81MM43SB) closure pour concrete. Table 4.2 and 4.4 presents the results for the core samples for the deck concrete from I-81MM43SB.

Table 4.1 Closure Pour Compressive Strength, Modulus, and Unit Weight

Concrete Type	Core Number	Compressive Strength (psi)	Modulus of Elasticity (10^6 psi)	Unit Weight (lb/ft^3)
Closure	S1C1	6760	4.26	147.5
Closure	S1C2	8510	4.50	147.0
Closure	S2C1	7590	4.49	146.4
Closure	S2C4	7730	-	146.5
Average		**7650**	**4.42**	**146.8**

Table 4.2 Deck Compressive Strength, Modulus, and Unit Weight

Concrete Type	Core Number	Compressive Strength (psi)	Modulus of Elasticity (10^6 psi)	Unit Weight (lb/ft^3)
Deck	S2C2	4620	3.19	142.9
Deck	S2C3	6760	4.50	142.9
Deck	S2C5	5600	3.58	143.1
Average		**5660**	**3.76**	**143.0**

From the results presented in Tables 4.1 and 4.2 it was noticed that the closure concrete had a higher compressive strength, modulus of elasticity, and unit weight. Compressive strength is higher at lower w/c ratio and lower air content. Higher compressive strength results in an increased modulus of elasticity. The increase in unit weight indicates denser concrete which indicates a lower air content.

Table 4.3 Closure Pour Unit Weight, Percent Voids, and Percent Saturation

Concrete Type	Core Section	Unit Weight (lbs./ft^3)	% Voids	% Saturation
Closure	S1C1 Top	146.6	12.7	85.5
	S1C1 Bottom	148.8	11.6	88.6
Closure	S1C2 Top	147.7	12.7	85.1
	S1C2 Bottom	148.6	11.5	84.5
Closure	S2C1 Top	147.9	12.4	85.4
	S2C1 Bottom	147.6	10.3	82.2
Closure	S2C4 Top	146.3	13.1	84.1
	S2C4 Bottom	147.4	11.7	84.1
Average Top		**147.1**	**12.7**	**85.1**
Average Bottom		**148.1**	**11.3**	**84.8**
Average Top and Bottom		**147.6**	**12.0**	**85.0**

From Table 4.3 it can be observed that there is different concrete at the top and bottom of the closure. The top section has a lower unit weight, compared to the bottom section, and a higher percentage of voids. This may be due to lower air contents. The average saturation percentage values are about equal for the top and bottom of the closure concrete. The percentage of saturation are influenced by the size and structure of the pores, thus the top may have larger pores.

Table 4.4 Deck Unit Weight, Percent Voids, and Percent Saturation

Concrete Type	Core Section	Unit Weight (lbs./ft^3)	% Voids	% Saturation
Deck	S2C2 Top	146.4	12.6	82.5
	S2C2 Bottom	142.4	11.8	77.4
Deck	S2C3 Top	136.8	15.1	73.8
	S2C3 Bottom	146.4	10.5	77.2
Deck	S2C5 Top	140.1	12.7	71.6
	S2C5 Bottom	145.8	10.2	83.7
Average Top		**141.1**	**13.5**	**76.0**
Average Bottom		**144.9**	**10.8**	**79.4**
Average Top and Bottom		**143.0**	**12.1**	**77.7**

From Table 4.4 it can also be observed that there is different concrete at the top and bottom of the deck. The top section has a lower unit weight, compared to the bottom section, and a higher percentage of voids which indicates differences in air content. This can be due to differences pour volume and size distribution. The average saturation percentage values are lower for the top closure concrete than the bottom closure concrete. This can be related to the unit weight and percentage of voids, which indicates a difference air content and pore size, compared to the bottom deck concrete, results in a lower percentage of saturation.

The differences between the closure and deck concrete is mainly due to the air content, moisture content, and pore size distribution. The closure concrete had a denser concrete compared to the deck concrete which is shown in Tables 4.1 and 4.2. As presented in Tables 4.3 and 4.4, the closure and deck concrete results have the same pattern for the top and bottom sections. This indicates that they are both affected by the same conditions. Mainly, the reason that the closure concrete is denser, which may be due to low w/c ratio and lower air content, which resulted in a higher unit weight and saturation percentage versus a higher voids percentage.

4.1.2 Concrete Properties of Lab Cast Slabs

Fresh concrete properties of the first and second placement are shown in Table 4.5. The time between the first and second placement was 30 days. Tables 4.6 and 4.7 present the average of two specimens for the compressive strength, splitting tensile strength, and modulus of elasticity for the lab cast slabs.

Table 4.5 Fresh Concrete Properties of First and Second Placement

Properties	First Placement	Second Placement
Unit Weight (lbs./ft^3)	139.5	139.9
Slump (in.)	4.75	5.5
Air Entrainment (%)	4	5.5
Temperature (^{o}F)	70	60

Table 4.6 First Placement Compressive Strength, Splitting Tensile, and Modulus of Elasticity

Age (Days)	Average Compressive Strength (psi)	Average Splitting Tensile Strength (psi)	Average Modulus of Elasticity (x 10^6 psi)
7	5930	610	4.05
14	5920	685	4.46
29	6510	720	4.53
56	6630	740	4.60
90	6650	760	4.58

Table 4.7 Second Placement Compressive Strength, Splitting Tensile, and Modulus of Elasticity

Age (Days)	Average Compressive Strength (psi)	Average Splitting Tensile Strength (psi)	Average Modulus of Elasticity (x 10^6 psi)
7	4930	585	4.90
28	6140	605	5.46
56	6280	645	5.80
90	6400	650	6.11

For the closure concrete the compressive strengths for the lab cast slabs at the age of 90 days were 15% greater than the I81 deck slabs at the age of 17 years. For the deck concrete the compressive strength for the I81 slabs at the age of 17 years was 15 % greater than the lab cast slabs at the age of 90 days. Modulus of elasticity was higher for the lab cast slabs, both for the deck and closure at 90 days, in comparison to the I81 slabs at the age of 17 years, a difference was 22% for the deck and 45% for the closure. Comparing the modulus of elasticity for the first and second placement, from Tables 4.6 and 4.7, it can be noticed that the modulus of elasticity are higher for the second placement than the first placement which is opposite from what is expected. Since the compressive strengths for the first placement are higher than the second placement, it is expected that the modulus of elasticity of the first placement to be higher than the second placement.

4.2 Corrosion Measurements

4.2.1 Introduction to Corrosion Measurements

Corrosion measurements are discussed individually for I81 deck slabs and lab cast slabs in sections 4.2.2 and 4.2.4. This discussion will consist of corrosion potential, resistivity, and corrosion current density measurements. All corrosion measurements will be plotted as a scatter diagram, separately for the I81 deck and lab cast slabs, in order to illustrate

general observations between values. Finally the measurements difference between the joint and closure pour will be discussed.

Chloride measurements of the I81 deck slabs are presented and discussed in section 4.2.4. Samples were taken from 12 locations from the four deck slabs. The samples locations were adjacent to the cut slabs at the closure pour joints of sides 1 and 2 as shown in Appendix B. Chloride content sample depth ranges were 2-3 and 3-4 inches.

4.2.2 Corrosion Measurements of I81 Deck Slabs

The results for the corrosion related measurements for the I81 deck slabs are presented in Tables 4.8 and 4.9. Tables 4.8 and 4.9 presents the corrosion potentials, resistivity, and corrosion current density at the closure pour joint and within the closure pour respectively. Top bar cover depths ranged from 2.64 to 5.0 in. for all of the slabs. VDOT specifies a cover depth of 2.5 in. for cast in place deck slabs, and not less than 0.5in.. Also, electrical continuity checks were performed between each ECR and it showed that all of the ECR was continuous between each bar combination.

As shown in Table 4.8, the potential measurements, Slab 1 has a relatively high standard deviation, especially for Side 1. Slab 2, Slab 4, and Slab 7 are more uniform with a lower standard deviation value than Slab 1. For the resistivity measurements, Slab 4 has a higher standard deviation value at Side 1 and 2 compared to the other slabs. The corrosion current density measurements for all the slabs are highly variable at Side 1 and 2 with standard deviation equal to or exceeding the average in some cases. Analyses of the results are presented later.

Table 4.8 Corrosion Measurements for I81 Deck Slabs at the Closure Pour Joints

Slab #	Bar #	E_{corr} (mV)		R (kΩ-cm)		i_{corr} (mA/ft^2)	
		Side 1	Side 2	Side 1	Side 2	Side 1	Side 2
Slab 1	TB	-413	-231	211	96	0.80	0.48
	BB 1	-261	-115	163	71	0.45	0.19
	BB 2	-199	-119	99	42	0.44	0.19
	BB 3	-277	-90	163	190	0.26	0.03
	Average	-288	-139	159	100	0.49	0.22
	STDV	90	63	46	64	0.23	0.19
Slab 2	TB	-148	-139	76	193	0.21	0.12
	BB 1	-119	-119	88	140	0.33	0.06
	BB 2	-166	-173	27	42	0.19	0.16
	BB 3	-147	-83	152	42	0.21	0.10
	Average	-145	-129	86	104	0.23	0.11
	STDV	19	38	51	75	0.06	0.04
Slab 4	TB	-58	-207	296	216	0.22	1.12
	BB 1	-71	-146	149	226	0.01	0.06
	BB 2	-66	-170	119	30	0.75	0.20
	BB3	-75	-129	126	259	0.03	0.08
	Average	-68	-163	172	183	0.25	0.36
	STDV	7	34	83	104	0.34	0.51
Slab 7	TB	-189	-135	72	55	0.03	1.36
	BB 1	-142	-180	62	66	0.07	0.03
	BB 2	-200	-164	139	83	0.84	0.68
	BB 3	-186	-172	153	168	0.41	0.33
	Average	-179	-163	106	93	0.34	0.60
	STDV	26	20	46	51	0.37	0.57

As shown in Table 4.9, the potential measurements, Slab 7 followed by Slab 1 both have a relatively high standard deviation, especially for Side 1. Slab 2 and Slab 4 are more uniform with a lower standard deviation value than Slab 7 and Slab 1. For the resistivity measurements, Slab 7 followed by Slab 4 both have a higher standard deviation value at Side 1 and 2 compared to Slab 1 and Slab 2. The corrosion current density measurements for all the slabs are highly variable at Side 1 and 2 with standard deviation equal to or exceeding the average in some cases. Analyses of the results are presented later.

Table 4.9 Corrosion Measurements for I81 Deck Slabs within the Closure Pour

Slab #	Bar #	E_{corr} (mV)		R (kΩ-cm)		i_{corr} (mA/ft^2)	
		Side 1	Side 2	Side 1	Side 2	Side 1	Side 2
Slab 1	TB	-422	-287	233	350	0.45	0.15
	BB 1	-296	-188	233	396	0.18	0.06
	BB 2	-207	-190	233	233	0.21	0.06
	BB 3	-323	-226	233	233	0.10	0.01
	Average	-312	-223	233	303	0.24	0.07
	STDV	89	46	0	83	0.15	0.06
Slab 2	TB	-136	-135	96	194	0.05	0.02
	BB 1	-130	-128	161	82	0.20	0.02
	BB 2	-149	-175	91	194	0.05	0.04
	BB 3	-167	-135	180	198	0.07	0.03
	Average	-146	-143	132	167	0.09	0.03
	STDV	16	21	45	57	0.07	0.01
Slab 4	TB	-171	-210	256	119	0.07	0.44
	BB 1	-127	-173	145	131	0.01	0.02
	BB 2	-201	-174	217	19	0.22	0.08
	BB 3	-199	-151	107	443	0.01	0.02
	Average	-175	-177	181	178	0.08	0.14
	STDV	35	24	68	184	0.10	0.20
Slab 7	TB	-5.8	-151	93	226	0.01	0.39
	BB 1	-202	-213	177	56	0.03	0.03
	BB 2	-221	-224	723	326	0.38	0.57
	BB 3	-12.3	-171	98	110	0.16	0.13
	Average	-110	-190	273	180	0.15	0.28
	STDV	117	34	302	121	0.17	0.24

For Slab 1, the corrosion density measurements shown in Tables 4.8 and 4.9, indicate higher active corrosion than Slabs 2, 4, and 7. Resistivity readings in the closure concrete indicate that either the concrete is dry or the epoxy coating is increasing the resistivity values.

4.2.3 Corrosion Measurements of I81 Deck Slabs – Closure Pour vs. Closure Joints

Corrosion measurements for the I81 deck slabs are plotted as a scatter diagram comparing the closure pour corrosion measurements versus the closure joints measurements, as shown in Figures 4.1 through 4.3.

Figure 4.1 shows a scatter diagram for corrosion potentials versus resistivity for I81 deck slabs. It can be noticed that the corrosion potentials for the closure pour and the closure joints measurements are less than -200 mv which indicates low corrosion activity, although some values are showing higher corrosion activity. The resistivity measurements for the closure pour indicate higher resistivity compared to the closure joints measurements. Higher resistivity indicates better concrete quality or an interference from the epoxy coating since it is generally considered a nonconductive material if not saturated.

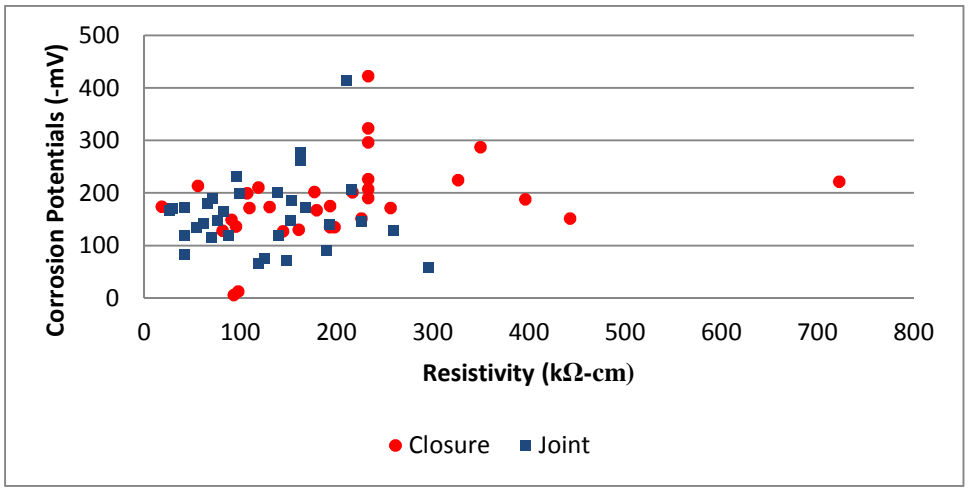

Figure 4.1 Corrosion Potentials vs. Resistivity for I81 Slabs

Figure 4.2 shows a scatter diagram for corrosion potentials versus corrosion current density for I81 deck slabs. It can be noticed that the corrosion potentials for the closure pour and the closure joints measurements are less than -200 mv which indicates low corrosion activity, although some values are showing higher corrosion activity. Corrosion current density measurements for the closure joints indicate higher corrosion activity compared to the closure pour measurements. Most of the measurements of the

closure pour are less than 0.2mA/ft^2, which indicates very low corrosion activity. While the closure joints measurements are highly variable showing low to high corrosion rates.

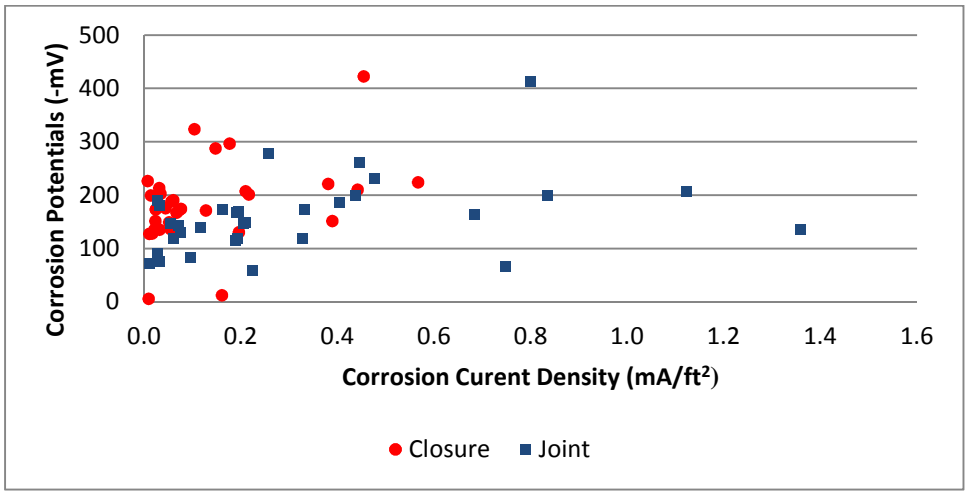

Figure 4.2 Corrosion Potentials vs. Corrosion Current Density for I81 Slabs

Figure 4.3 shows a scatter diagram for resistivity versus corrosion current density for I81 deck slabs. It can be noticed that the resistivity measurements for the closure pour indicate higher resistivity compared to the closure joints measurements. Higher resistivity indicates better concrete quality or an interference from the epoxy coating since it maybe more of a nonconductive material. Corrosion current density measurements for the closure joints indicate higher corrosion activity compared to the closure pour measurements. Most of the measurements of the closure pour are less than 0.2mA/ft2, which indicates very low corrosion activity. While the closure joints measurements are highly variable showing low to high corrosion activity.

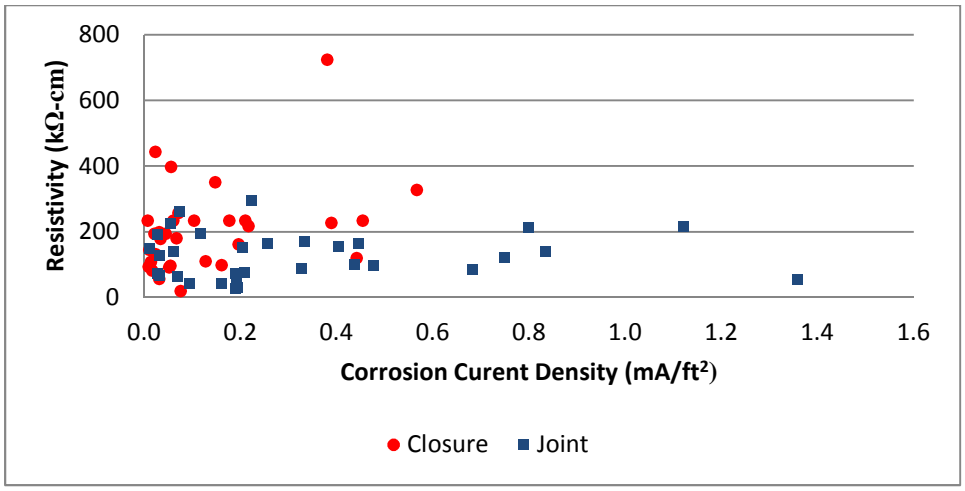

Figure 4.3 Resistivity vs. Corrosion Current Density for I81 Slabs

It can be noticed from the scatter diagrams that there is higher corrosion activity across the closure joints based on the corrosion current density measurements. Corrosion potentials and resistivity measurements indicated uncertain signs of corrosion activity compared to the corrosion current density.

4.2.4 Corrosion Measurements of Lab Cast Slabs

Tables 4.10 and 4.11 represent the results of the corrosion related measurements for the lab cast decks. Cover depths were measured with a range from 2.64 to 4.2 in. for the three slabs. Those results are similar to the deck slabs cover depths range. The tests were conducted on three bars (TB, BB 1, and BB 3) out of four bars on each side of the slabs. Since the top bar is located directly over the bottom middle rebar, this made the cover meter ineffective in locating the bottom bar. Electrical continuity checks were performed for each single bar between Side 1 and 2, and it showed that each spliced ECR bar is continuous between both sides, as shown in Figure 4.4.

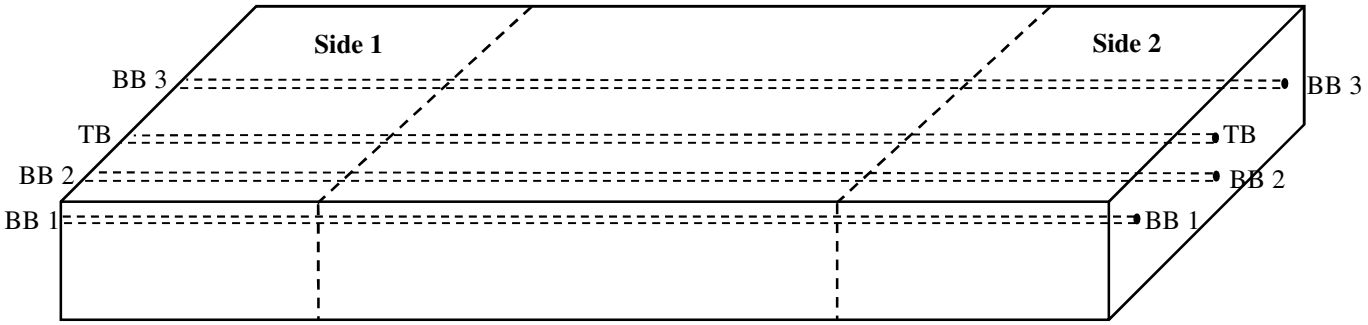

Figure 4.4 Continuity Readings Locations for Lab Cast Slab

Table 4.10 Corrosion Measurements for Lab Cast Slabs at the Closure Pour Joints

Slab #	Bar #	E_{corr} (mV)		R (kΩ-cm)		i_{corr} (mA/ft^2)	
		Side 1	Side 2	Side 1	Side 2	Side 1	Side 2
Slab A	TB	-25	-123	169	138	0.010	0.023
	BB 1	-65	-150	67	140	0.011	0.007
	BB3	-40	-190	113	164	0.004	0.004
	Average	-43	-154	116	147	0.01	0.01
	STDV	20	34	51	15	0.00	0.01
Slab B	TB	-70	-124	22	125	0.015	0.009
	BB 1	-103	-157	61	134	0.011	0.105
	BB 3	-91	*	239	*	0.136	*
	Average	-88	-141	107	129	0.05	0.06
	STDV	17	23	116	7	0.07	0.07
Slab C	TB	-139	-142	108	47	0.015	0.005
	BB 1	-188	-104	72	72	0.005	0.007
	BB 3	-144	-149	157	132	0.127	0.007
	Average	-157	-132	112	83	0.05	0.01
	STDV	27	24	43	44	0.07	0.00

Note: * Data unavailable, ECR could not be located

As shown in Table 4.10, the potential, resistivity, and corrosion current density measurements at the closure pour joints indicated a relatively uniform condition with a low standard deviation for all three lab cast slabs. Analyses of the results are presented later. Some results for Slab B bottom bar (BB 3) are not presented since the ECR could not be located as stated previously.

Table 4.11 Corrosion Measurements for Lab Cast Slabs within the Closure Pour Concrete

Slab #	Bar #	E_{corr} (mV)		R (kΩ-cm)		i_{corr} (mA/ft^2)	
		Side 1	Side 2	Side 1	Side 2	Side 1	Side 2
Slab A	TB	-40	-129	233	161	0.003	0.017
	BB 1	-76	-155	217	110	0.006	0.003
	BB 3	-42	-190	205	256	0.003	0.003
	Average	-53	-158	218	176	0.00	0.01
	STDV	20	31	14	75	0.00	0.01
Slab B	TB	-65	-133	126	89	0.022	0.012
	BB 1	-107	-210	135	62	0.007	0.005
	BB 3	-47	*	166	*	0.006	*
	Average	-73	-172	142	75	0.01	0.01
	STDV	31	54	21	19	0.01	0.01
Slab C	TB	-150	-138	326	215	0.010	0.009
	BB 1	-206	-106	443	133	0.004	0.005
	BB 3	-145	-143	256	280	0.019	0.004
	Average	-167	-129	342	209	0.01	0.01
	STDV	34	20	94	74	0.01	0.00

Note: * Data unavailable

As shown in Table 4.11, the potential, resistivity, and corrosion current density measurements within the closure pour concrete indicate relatively uniform conditions with a low standard deviation for all three lab cast slabs. Analyses of the results are presented later. Some results for Slab B bottom bar (BB 3) are not presented since the ECR could not be located as previously stated.

4.2.5 Corrosion Measurements of Closure Pour – I81 Slabs vs. Lab Cast Slabs

Corrosion measurements for the closure pour are plotted as a scatter diagram comparing the I81 slabs measurements versus the lab cast slabs measurements, as shown in Figures 4.5 through 4.7.

Figure 4.5 shows a scatter diagram for corrosion potentials versus resistivity for the closure pour of the I81 slabs versus the lab cast slabs measurements. It can be noticed that the corrosion potentials for the I81 deck slabs indicating higher corrosion activity compared to the lab cast slabs measurements. The lab cast slabs corrosion potentials are

less than -200 mv which indicates low corrosion activity, while the I81 deck slabs measurements are indicating higher corrosion activity with corrosion potentials greater than -200 mv. The resistivity measurements for the I81 deck and lab cast slabs indicate high resistivity with a similar range of measurements.

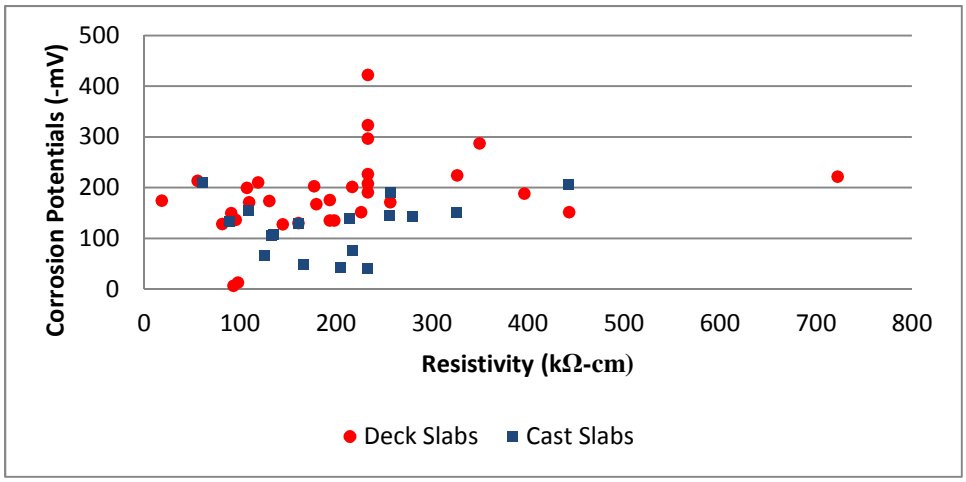

Figure 4.5 Closure Pour Corrosion Potentials vs. Resistivity for Deck vs. Cast Slabs

Figure 4.6 shows a scatter diagram for corrosion potentials versus corrosion current density for the closure pour of the I81 slabs versus the lab cast slabs measurements. It can be noticed that the corrosion potentials for the I81 deck slabs indicating higher corrosion activity compared to the lab cast slabs measurements. The lab cast slabs corrosion potentials are less than -200 mv which indicates low corrosion activity, while the I81 deck slabs measurements are indicating higher corrosion activity with corrosion potentials greater than -200 mv. Corrosion current density measurements for the I81 deck slabs indicate higher corrosion activity compared to the lab cast slabs measurements. All of the measurements of the lab cast slabs are less than 0.2mA/ft^2, which indicates no corrosion activity.

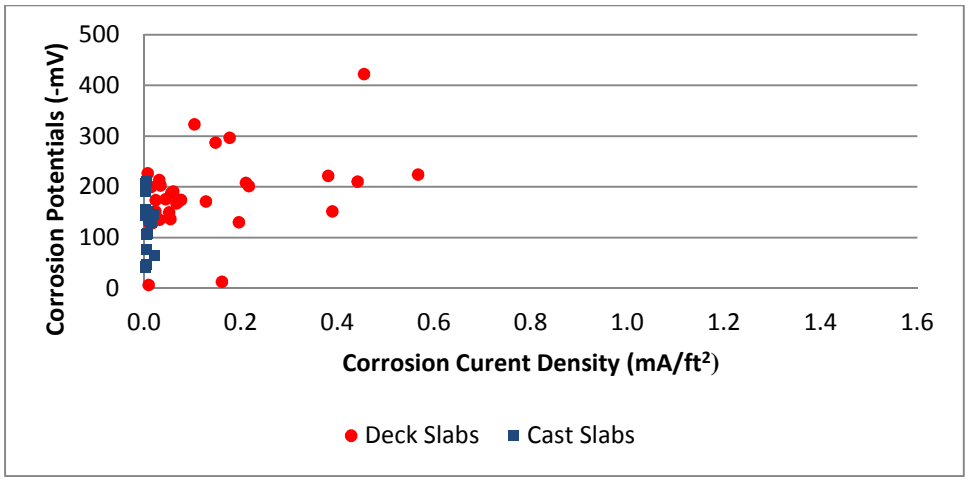

Figure 4.6 Closure Pour Corrosion Potentials vs. Corrosion Current Density for Deck vs. Cast Slabs

Figure 4.7 shows a scatter diagram for resistivity versus corrosion current density for the closure pour of the I81 slabs versus the lab cast slabs measurements. The resistivity measurements for the I81 deck and lab cast slabs indicate high resistivity with a similar range of measurements. Corrosion current density measurements for the I81 deck slabs indicate higher corrosion activity compared to the lab cast slabs measurements. All of the measurements of the lab cast slabs are less than 0.2mA/ft^2, which indicates no corrosion activity.

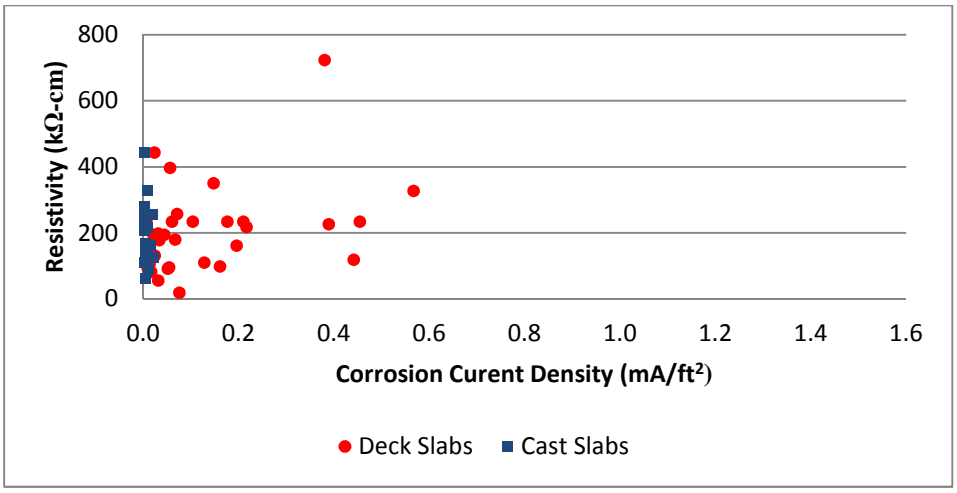

Figure 4.7 Closure Pour Resistivity vs. Corrosion Current Density for Deck vs. Cast Slabs

It can be noticed from the scatter diagrams of the closure pour that there is higher corrosion activity at the I81 deck slabs compared to the lab cast slabs based on the corrosion current density measurements. The lab cast slabs indicated no corrosion

activity based on the corrosion current density measurements which were less than 0.2mA/ft^2. Corrosion potentials and resistivity measurements indicated uncertain signs of corrosion activity compared to the corrosion current density.

4.2.6 Corrosion Measurements of Closure Pour Joints – I81 Slabs vs. Lab Cast Slabs

Corrosion measurements for the closure pour joints are plotted as a scatter diagram comparing the I81 slabs measurements versus the lab cast slabs measurements, as shown in Figures 4.8 through 4.10.

Figure 4.8 shows a scatter diagram for corrosion potentials versus resistivity for the closure pour joints of the I81 slabs versus the lab cast slabs measurements. It can be noticed that the corrosion potentials for the I81 deck slabs indicating higher corrosion activity compared to the lab cast slabs measurements. The lab cast slabs corrosion potentials are less than -200 mv which indicates low corrosion activity, while the I81 deck slabs measurements are indicating higher corrosion activity with corrosion potentials greater than -200 mv. The resistivity measurements for the I81 deck and lab cast slabs indicate high resistivity with a similar range of measurements.

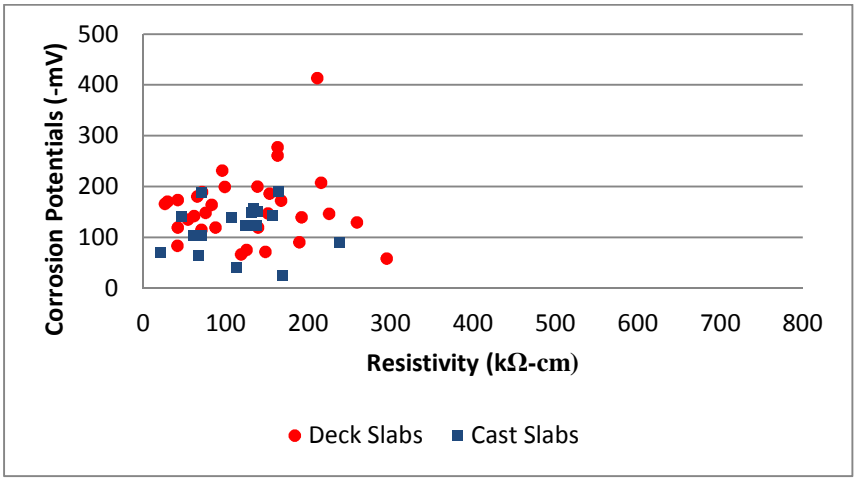

Figure 4.8 Closure Joints Corrosion Potentials vs. Resistivity for Deck vs. Cast Slabs

Figure 4.9 shows a scatter diagram for resistivity versus corrosion current density for the closure pour joints of the I81 slabs versus the lab cast slabs measurements. The resistivity measurements for the I81 deck and lab cast slabs indicate high resistivity with a similar range of measurements. Corrosion current density measurements for the I81 deck slabs indicate higher corrosion activity compared to the lab cast slabs measurements. All of the measurements of the lab cast slabs are less than 0.2mA/ft^2, which indicates no corrosion activity.

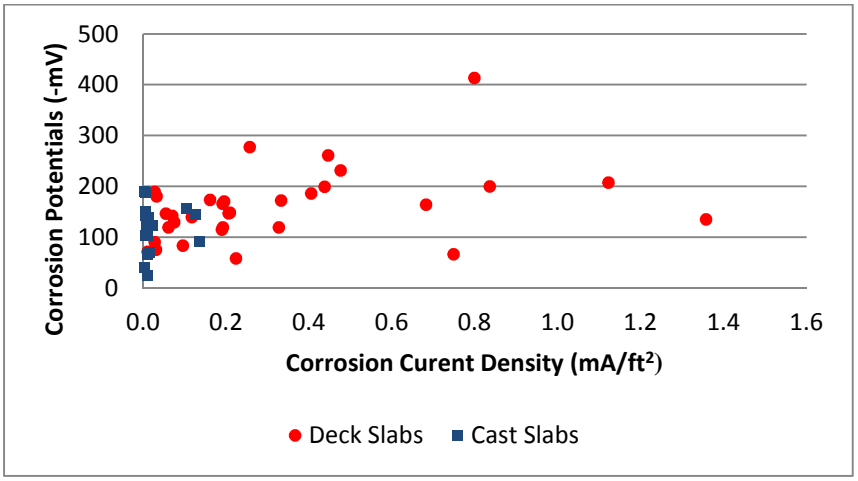

Figure 4.9 Closure Joints Corrosion Potentials vs. Corrosion Current Density for Deck vs. Cast Slabs

Figure 4.10 shows a scatter diagram for resistivity versus corrosion current density for the closure pour joints of the I81 slabs versus the lab cast slabs measurements. The resistivity measurements for the I81 deck and lab cast slabs indicate high resistivity with a similar range of measurements. Corrosion current density measurements for the I81 deck slabs indicate higher corrosion activity compared to the lab cast slabs measurements. All of the measurements of the lab cast slabs are less than 0.2mA/ft2, which indicates no corrosion activity.

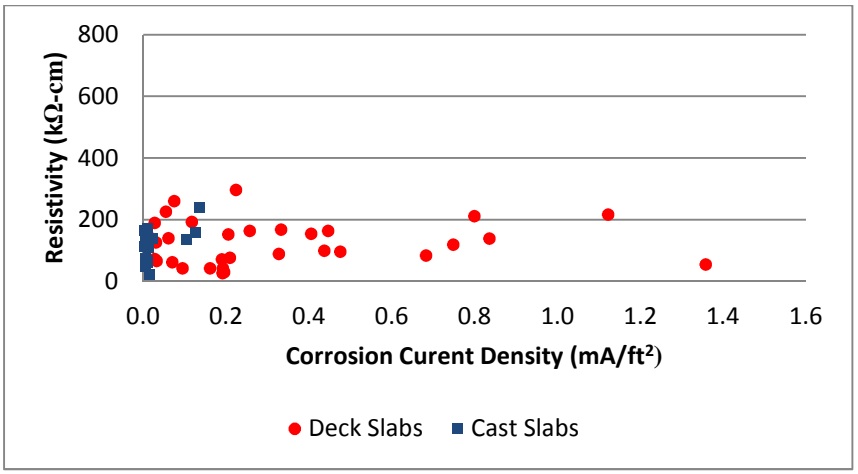

Figure 4.10 Closure Joints Resistivity vs. Corrosion Current Density for Deck vs. Cast Slabs

It can be noticed from the scatter diagrams of the closure pour joints that there is higher corrosion activity at the I81 deck slabs compared to the lab cast slabs based on the corrosion current density measurements. The lab cast slabs indicated no corrosion activity based on the corrosion current density measurements which were less than 0.2mA/ft^2. Corrosion potentials and resistivity measurements indicated uncertain signs of corrosion activity compared to the corrosion current density.

4.2.7 Chloride Measurements in I81 Deck Slabs

The results for the chloride content in I81 closure pour joints are presented in Table 4.12. Powdered samples were taken from 12 locations from the four deck slabs. The samples locations were adjacent to the cut slabs at the closure pour joints of sides 1 and 2 as shown in Appendix B. Chloride content depth ranges were at 2-3 and 3-4 inches. Acid soluble chloride contents were determined in accordance with ASTM C1152.

The results indicate that chlorides are present at general bars depths (3-4 in.) in the closure pour joints varying from 1.64 to 4.69 lbs/yd^3. Also, the chloride contents at average depths of 2.5 and 3.5 in. are similar rather than decreasing with depth. This indicates that the leaking closure pour joints facilitated the chloride movement to the bar

depth. According the chloride values are sufficient to initiate corrosion of the ECR as determined by Brown with a range of 0.13 to 3.00 lbs/yd^3 for ECR (Brown 2002).

Table 4.12 Chloride Content in Closure Pour Joints of I81 Deck Slabs

Sample Location	Joint	Sample Range (in.)	Chloride Content (lbs/yd^3)
Adjacent to Test Section One	Side 1	2-3	4.21
		3-4	4.40
	Side 2	2-3	4.11
		3-4	3.83
Adjacent to Test Section Two	Side 1	2-3	3.26
		3-4	3.50
	Side 2	2-3	3.20
		3-4	4.69
Adjacent to Test Section Three	Side 1	2-3	0.08
		3-4	2.47
	Side 2	2-3	1.80
		3-4	2.30
Adjacent to Test Section Four	Side 1	2-3	2.84
		3-4	2.72
	Side 2	2-3	2.62
		3-4	2.65
Adjacent to Test Section Seven	Side 1	2-3	4.65
		3-4	3.44
	Side 2	2-3	1.35
		3-4	1.64
Adjacent to Test Section Eight	Side 1	2-3	3.68
		3-4	3.55
	Side 2	2-3	2.19
		3-4	1.99
Average	Side 1	2-3	3.12
		3-4	3.35
	Side 2	2-3	2.55
		3-4	2.85
STDV	Side 1	2-3	1.48
		3-4	0.63
	Side 2	2-3	0.91
		3-4	1.07

The results for the chloride content in I81 closure pour are presented in Table 4.13. Powdered samples were taken from six locations from the two deck slabs. The samples locations were at the center of the closure pour as shown in Appendix B. Chloride

content sample ranges were at 0-1, 1-2, 2-3 and 3-3.5 in.. Acid soluble chloride contents were determined in accordance with ASTM C1152.

Table 4.13 Chloride Content in Closure Pour of I81 Deck Slabs

Sample Location	Sample Range (in.)	Chloride Content (lbs/yd^3)
Slab One (1-2)	0-1	15.3
	1-2	3.0
	2-3	0.3
	3-3.5	-
Slab One (1-4)	2-3	12.2
	3-4	-
	2-3	0.2
	3-3.5	0.3
Slab One (1-6)	2-3	14.1
	3-4	2.7
	2-3	0.3
	3-3.5	-
Slab Two (2-2)	0-1	16.0
	1-2	7.9
	2-3	1.0
	3-3.5	-
Slab Two (2-4)	0-1	11.4
	1-2	2.4
	2-3	0.6
	3-3.5	-
Slab Two (2-6)	0-1	14.3
	1-2	3.0
	2-3	-
	3-3.5	0.7
Average	0-1	13.88
	1-2	3.80
	2-3	0.48
	3-3.5	0.50
STDV	0-1	1.77
	1-2	2.31
	2-3	0.33
	3-3.5	0.28

The results indicate that chlorides are present in low concentrations, which are considered as background readings, at general bars depths (2-3.5 in.) in the closure pour varying from 0.2 to 1.0 lbs/yd^3. This indicates that the concrete cover depths are adequate and are acting as a barrier against chlorides.

It can be noticed that the closure pour joints chloride content are higher varying from 1.64 to 4.69 lbs/yd^3 from the closure pour chloride content which vary from 0.2 to 1.0 lbs/yd^3. Also, the chloride contents for the closure pour joints are similar at average depths of 2.5 and 3.5 in., while the closure pour chloride contents decrease with depth. Thus confirming that leaking closure pour joints facilitated the chloride movement to the bar depth, while for the closure pour the concrete cover depth was acting as a barrier against chlorides.

4.2.8 Chloride Permeability in I81 Deck Slabs

The results for the chloride permeability in I81 closure pour joints are presented in Table 4.14. One 4 in. diameter core was taken from each of slabs 1 and 2. To maintain the moisture content, the core samples were sealed with shrink wrap, aluminum foil and duct tape. Then the cores were sliced 2 in. from the top (top sample) and another 2 in. (bottom sample). Chloride permeability sample ranges were at 0-2 in. (top sample) and 2-4 in. (bottom sample) for each of the two cores. Testing was first conducting for the slices, top and bottom, as received moisture content. The top and bottom slices were tested again, in accordance to AASHTO T277, by vacuum saturating the slices. This test measures the concrete resistivity and the unit it is measured in is coulombs.

Table 4.14 Chloride Permeability in Closure Pour of I81 Deck Slabs, Coulombs

Core	As Received Moisture		Saturated	
	Top (0-2 in.)	Bottom (2-4 in.)	Top (0-2 in.)	Bottom (2-4 in.)
1-1	880	826	2371	1722
1-2	446	969	1362	1882
2-1	547	784	1639	1919
2-2	543	700	1375	1610
Average	604	820	1687	1783

The results indicate that chloride permeability is very low for the as received moisture condition specimens since all of the measurements were below 1000 coulombs. For the saturated specimens the values ranged between 1000 and 2000 coulombs which is indicates low chloride permeability. Core 1-1 was the only value which was over 2000 coulombs this indicates that the chloride permeability is moderate.

4.3 Visual Observation of Extracted Bars

4.3.1 Photographs of Visual Inspection

Samples were cut from different places from the bridge deck across the joints as shown in Appendix B. The samples were stored without damaging and exposing the ECR embedded into the concrete by keeping the concrete around the ECR in its place.

Figures 4.11 and 4.12 presents the visual inspection of samples C2-S1 Bottom Bar 1 and C2-S1 Top Bar 2, as shown in Appendix B. As shown in Figure 4.11 arrow 1, the bar is corroded across the joint and as shown by the change of epoxy color. Figure 4.12 shows signs of spotted deposits, arrow 2, on the bar surface, with less signs of corrosion, arrow 3, as compared to the top bar show in Figure 4.11. Figure 4.13 shows white and yellow deposits in the concrete along the bar trace underneath the bar, as shown by arrow 2 in Figure 4.12.

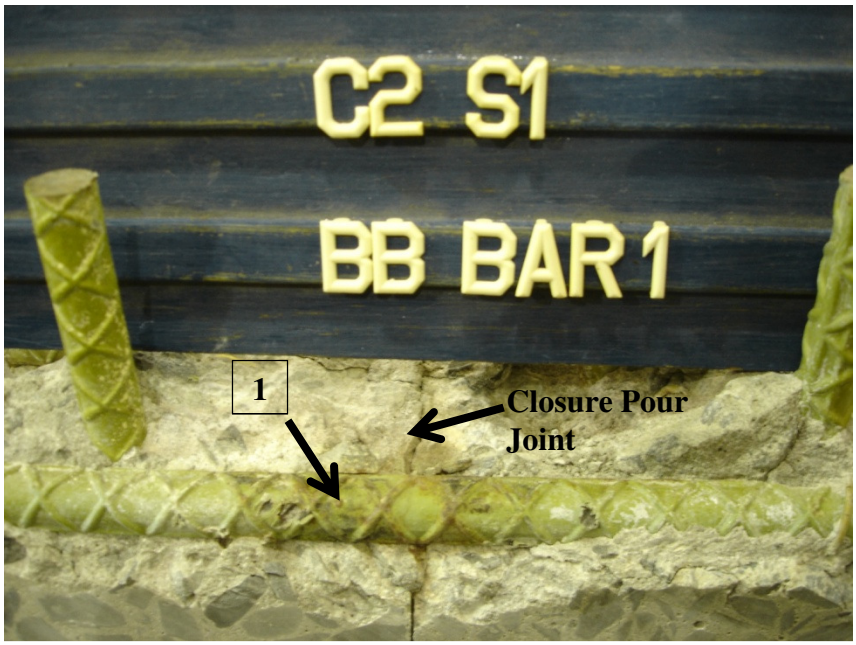

Figure 4.11 C2-S1 Bottom Bar from Side On

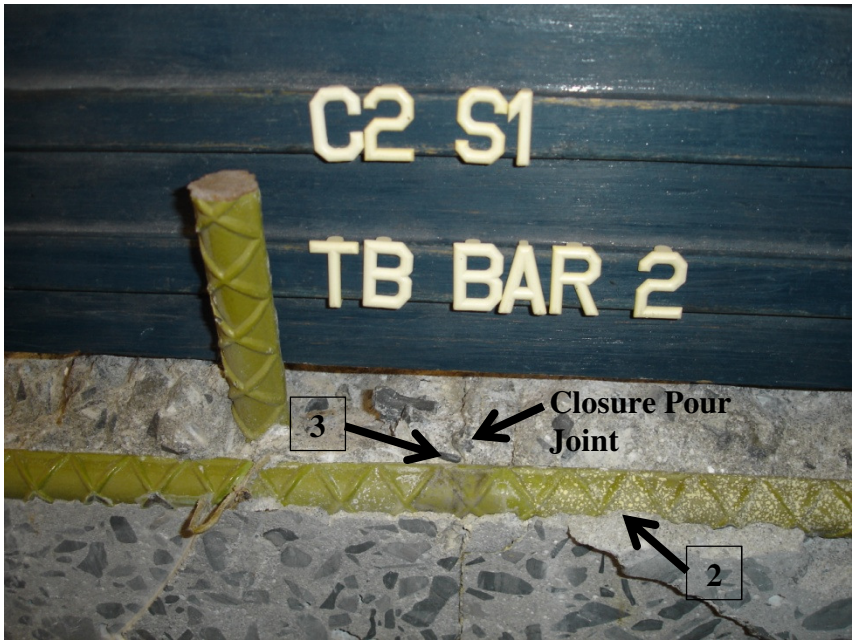

Figure 4.12 C2-S1 Top Bar 2

Figure 4.13 C2-S1 Top Bar 2 after Removing Bar

The sample shown in Figure 4.14 was taken from the bottom of slab three across joint one, as shown in Appendix B. Samples shown in Figures 4.15 and 4.16 were taken from the top of the same slab. Figure 4.14 shows some precipitation, arrow 4, at the top of the bar and corrosion, arrow 5, at the bottom of the bar. Figure 4.15 and 4.16 shows the bar corroded across the joint, arrow 6. Also, white and yellow deposits, arrow 7, can be seen on the concrete and bar on one side of the bar.

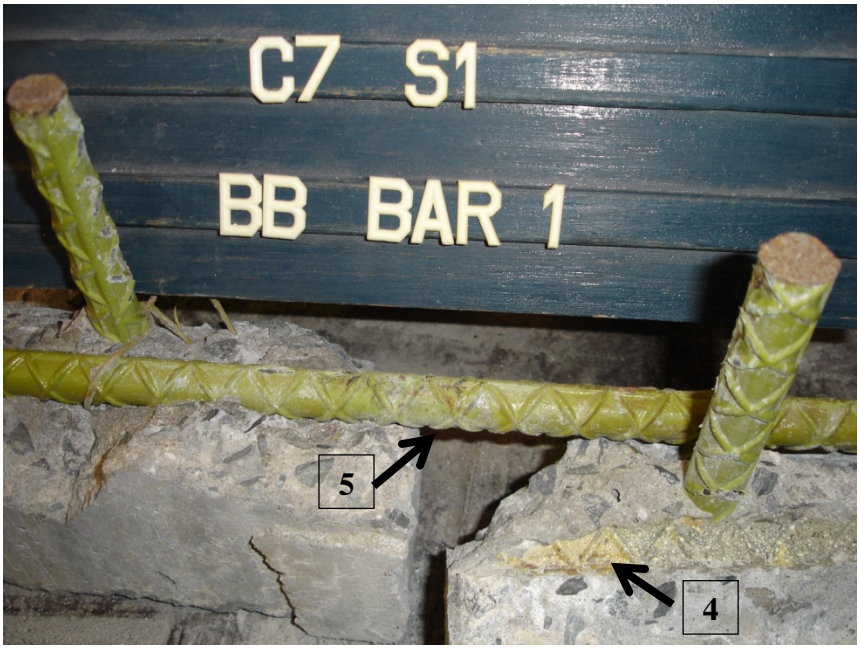

Figure 4.14 C7-S1 Bottom Bar 1

Figure 4.15 C7-S1 Top Bar 2 without Concrete

Figure 4.16 C7-S1 Top Bar 2 after removing Bar

The samples shown in Figure 4.17 and 4.18 were taken from the top of slab four across joint two, as shown in Appendix B. Samples shown in Figures 4.19 and 4.20 were taken from the bottom of the same slab. Figure 4.17 and 4.18 shows some deposits, arrow 9, at the top of the bar and corrosion, arrow 8, at the bottom of the bar. Figure 4.19 and 4.20 shows the bar at the top of the bottom bar with some precipitation, arrow 11, and corrosion, arrow 10, at the joint.

Figure 4.17 C8-S2 Top Bar 2 without Concrete

Figure 4.18 C8-S2 Top Bar 2 after Removing Bar

Figure 4.19 C8-S2 Bottom Bar 1 without Concrete

Figure 4.20 C8-S2 Bottom Bar 1 after Removing Bar

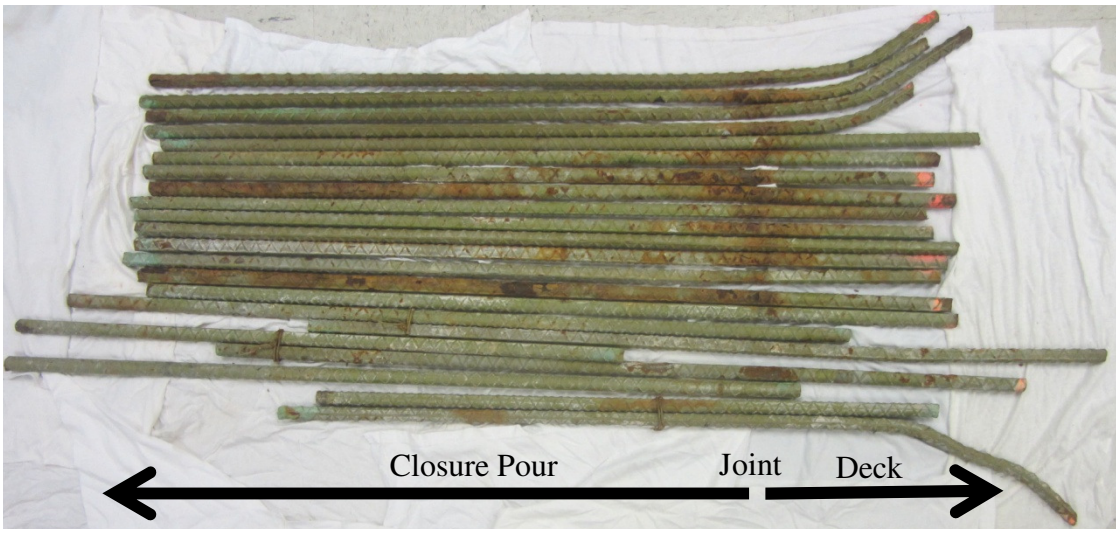

Figure 4.21 Corrosion Extent of Extracted ECR Bars

All of the samples taken from different locations from the slabs, deposits and corrosion were observed at the joint and moving along the bar and bar trace in both the closure and the deck concrete. Although corrosion was noticed in some bars, the epoxy coating was difficult to peel off the reinforcing bar. The bars were soaked for two weeks in water to aid the epoxy debondment from the bars to have a closer look at the corrosion under the coating, and to measure the integrity of the epoxy coating. This had no effect on debonding the epoxy from the bars, although there were some places were the coating was peeled off due to the corrosion of the bar, as shown in Figure 4.19.

The extent of the corrosion of the ECR beyond the joint interface is illustrated in Figure 4.21 of ECR bars recovered at the job site. As shown, corrosion of the ECR varied from 4 to 31 inches.

4.3.2 Scanning Electron Microscope (SEM) of Concrete Sample at Joint

After opening the samples across the joints and observing yellow and white precipitation in the ECR trace, further analysis was required to identify the chemistry of the precipitations. Six concrete images and corresponding chemical compositions were taken

using a Scanning Electron Microscope (SEM). Table 4.15 presents the unaided eye visual description for each of the SEM sample areas.

Table 4.15 Samples at Joints Image Areas Description

Sample Number	Image Areas	Description
One	I81MM43SB-1 I81MM43SB-2	Area 1 contains yellow deposit. Area 2 is outside yellow area, just outside of yellow deposit.
Two	I81MM43SB-3 I81MM43SB-5	Area 5 is far outside of yellow area and it is located at edge with small yellow coating in a square. Area 3 is concrete.
Three	I81MM43SB-6 I81MM43SB-7	Areas 6 and 7 are adjacent to ridge impression made by reinforcing lug.
Four	I81MM43SB-8 I81MM43SB-9	Areas 8 and 9 are adjacent to ridge impression made by reinforcing lug.
Five	I81MM43SB-10 I81MM43SB-11	These two are at the edge of the coating with the coating thickness. Area 10 is the fracture edge of the concrete. Area 11 is the coating.
Six	I81MM43SB-12 I81MM43SB-13	Area 12 and 13 are at the fractured edge of the concrete, areas are similar.

Figure 4.22 presents a SEM micrograph of sample area one, it shows two image areas. I81MM43SB-1 is on the yellow deposit, while I81MM43SB-2 is just outside the yellow deposit and coating. Table 4.16 presents the chemical composition of the two locations on sample one. Location 1 shows high carbon content compared to location 2, which indicates that the yellow precipitation is calcium carbonate where water penetrates the closure pour, dissolves the $Ca(OH)_2$ in the hydrated cement then reacts with carbon dioxide in the air to form calcium carbonate. The present of calcium carbonate within the ECR trace away from the joint indicates a higher level of water content within the interface between the ECR and concrete. Water movement within the ECR trace would have been from the joint line inward, indicating a higher void volume at ECR- Concrete interface. While location 2 shows high silicon content compared to location 1, which

indicates that it is hydrated cement since silicates are commonly present in hydrated cement as tricalcium silicate (C_3S) and dicalcium silicate (C_2S).

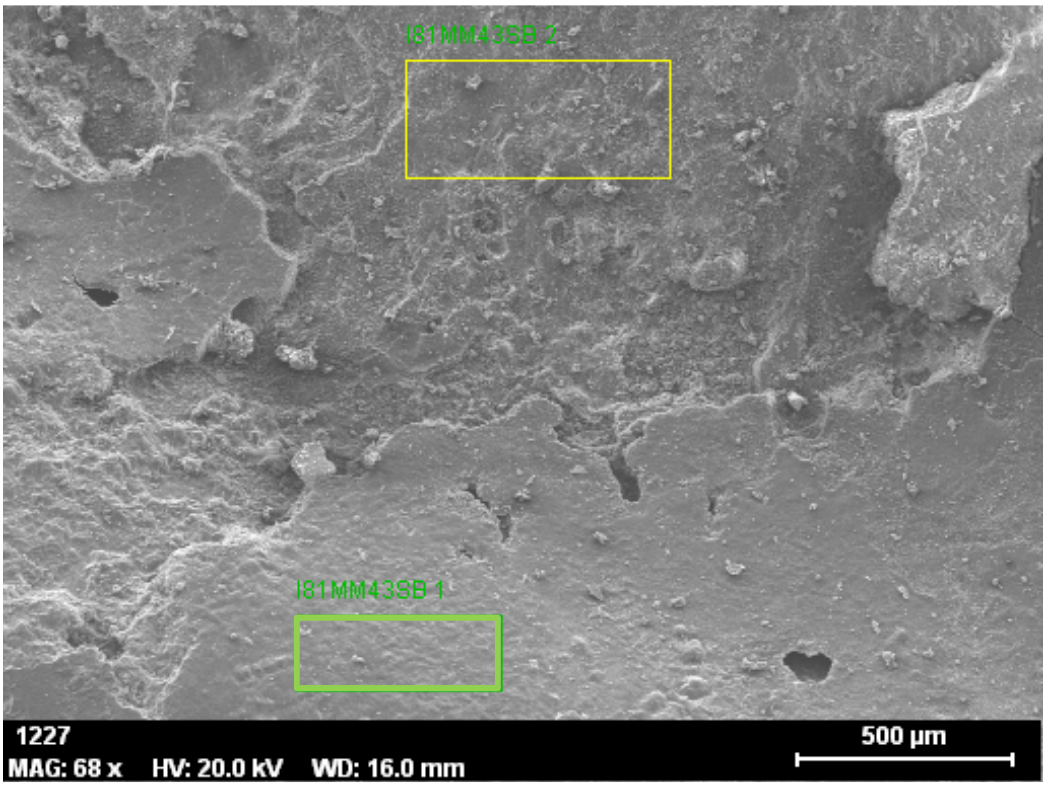

Figure 4.22 Sample One SEM Micrograph I81MM43SB-1 and I81MM43SB-2

Table 4.16 Sample One EDS Chemical Composition I81MM43SB-1 and I81MM43SB-2

	Mass Percent (%)									
Spectrum	**C**	**O**	**Na**	**Mg**	**Al**	**Si**	**K**	**Ca**	**Ti**	**Fe**
I81MM43SB-1	16.57	58.19	1.76	0.92	1.18	2.71	0.49	17.21	0.43	0.55
I81MM43SB-2	5.21	57.32	0.81	1.04	2.22	10.30	1.22	19.55	0.14	2.19
Difference Between 1 and 2	11.36	0.87	0.95	-0.12	-1.04	-7.59	-0.73	-2.34	0.29	-1.64

Figure 4.23 presents a SEM micrograph of sample two, it shows two image areas. I81MM43SB-3 is on the concrete, while I81MM43SB-5 is on a small yellow deposit at the edge of the sample. Table 4.17 presents the chemical composition of the two locations on sample two. Locations 3 and 5 show relatively low carbon content and

higher silicon content. This indicates that the hydrated cement carbonated when the sample was exposed to air.

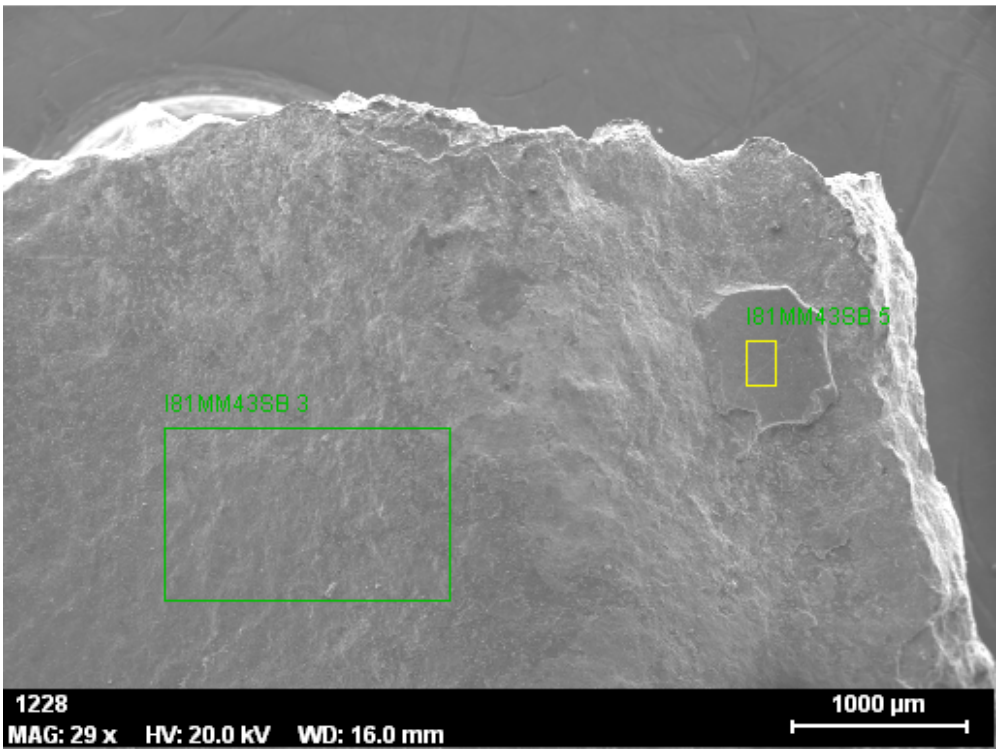

Figure 4.23 Sample Two SEM Micrograph I81MM43SB-3 and I81MM43SB-5

Table 4.17 Sample Two EDS Chemical Composition I81MM43SB-3 and I81MM43SB-5

	Mass Percent (%)									
Spectrum	**C**	**O**	**Na**	**Mg**	**Al**	**Si**	**K**	**Ca**	**Ti**	**Fe**
I81MM43SB-3	7.16	56.56	0.07	0.16	0.52	5.66	0.68	28.04	0.07	1.07
I81MM43SB-5	5.94	56.51	0.95	1.00	2.81	9.83	1.09	19.93	0.00	1.95
Mean value	6.55	56.54	0.51	0.58	1.67	7.75	0.88	23.99	0.03	1.51
Sigma	0.86	0.03	0.62	0.59	1.62	2.94	0.29	5.74	0.05	0.62
Sigma mean	0.61	0.02	0.44	0.42	1.15	2.08	0.21	4.06	0.03	0.44

Figure 4.24 presents a SEM micrograph of sample three, it shows two image areas. I81MM43SB-6 and I81MM43SB-7 which are both adjacent to ridge impression made by reinforcing lug. Table 4.18 presents the chemical composition of two locations on sample three. Locations 6 and 7 show higher carbon and relatively higher silicate

content, and lower calcium content. This may indicate that the hydrated cement carbonated over a longer period, as air and moisture moved along the ECR-concrete interface.

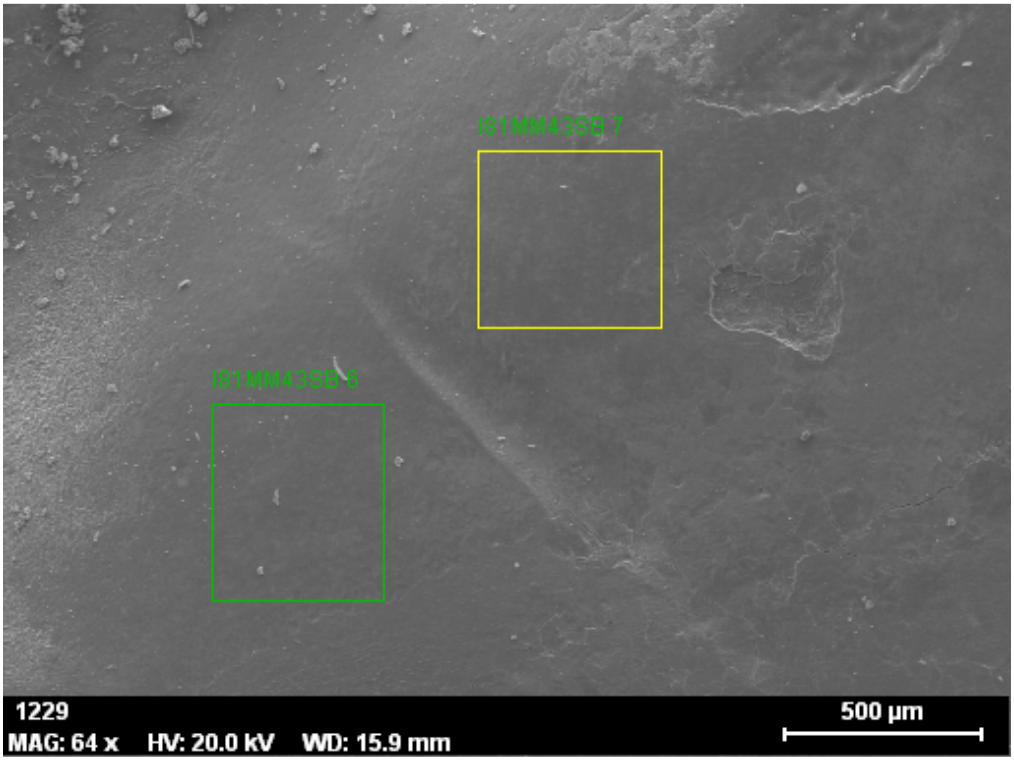

Figure 4.24 Sample Three SEM Micrograph I81MM43SB-6 and I81MM43SB-7

Table 4.18 Sample Three EDS Chemical Composition I81MM43SB-6 and I81MM43SB-7

	Mass Percent (%)									
Spectrum	**C**	**O**	**Na**	**Mg**	**Al**	**Si**	**K**	**Ca**	**Ti**	**Fe**
I81MM43SB-6	11.73	59.08	1.75	0.43	1.75	8.55	3.18	12.02	0.42	1.09
I81MM43SB-7	20.06	62.24	1.07	0.34	1.37	4.53	1.71	6.99	0.53	1.16
Difference Between 6 and 7	-8.33	-3.16	0.68	0.09	0.38	4.02	1.47	5.03	-0.11	-0.07

Figure 4.25 presents a SEM micrograph of sample four, it shows two image areas. I81MM43SB-8 and I81MM43SB-9 which are both adjacent to ridge impression made by reinforcing lug. Table 4.19 presents the chemical composition of two locations on

sample four. Locations 8 and 9 show high carbon and silicon content, and low calcium content, they have similar results to locations 6 and 7 discussed previously. This indicates that it is carbonated section of hydrated cement.

Figure 4.25 Sample Four SEM Micrograph I81MM43SB-8 and I81MM43SB-9

Table 4.19 Sample Four EDS Chemical Composition I81MM43SB-8 and I81MM43SB-9

	Mass Percent (%)									
Spectrum	**C**	**O**	**Na**	**Mg**	**Al**	**Si**	**K**	**Ca**	**Ti**	**Fe**
I81MM43SB-8	22.28	63.45	0.60	0.11	0.62	3.78	1.00	6.88	0.34	0.94
I81MM43SB-9	19.69	59.66	1.15	0.37	1.27	4.02	1.29	10.99	0.37	1.19
Mean value	20.99	61.55	0.88	0.24	0.95	3.90	1.14	8.94	0.35	1.06
Sigma	1.83	2.68	0.39	0.18	0.46	0.17	0.20	2.91	0.02	0.18
Sigma mean	1.29	1.89	0.27	0.13	0.32	0.12	0.14	2.05	0.02	0.12

Figure 4.26 presents a SEM micrograph of sample five, it shows two image areas. I81MM43SB-10 is on the fracture edge of the concrete, while I81MM43SB-11 is on the precipitated products. Table 4.20 presents the chemical composition of two locations on

sample five. Location 11 shows higher carbon content, and lower calcium and silicon content from location 10. This can be concluded to be calcium carbonate in location 11, while location 10 is hydrated cement with some traces of carbon.

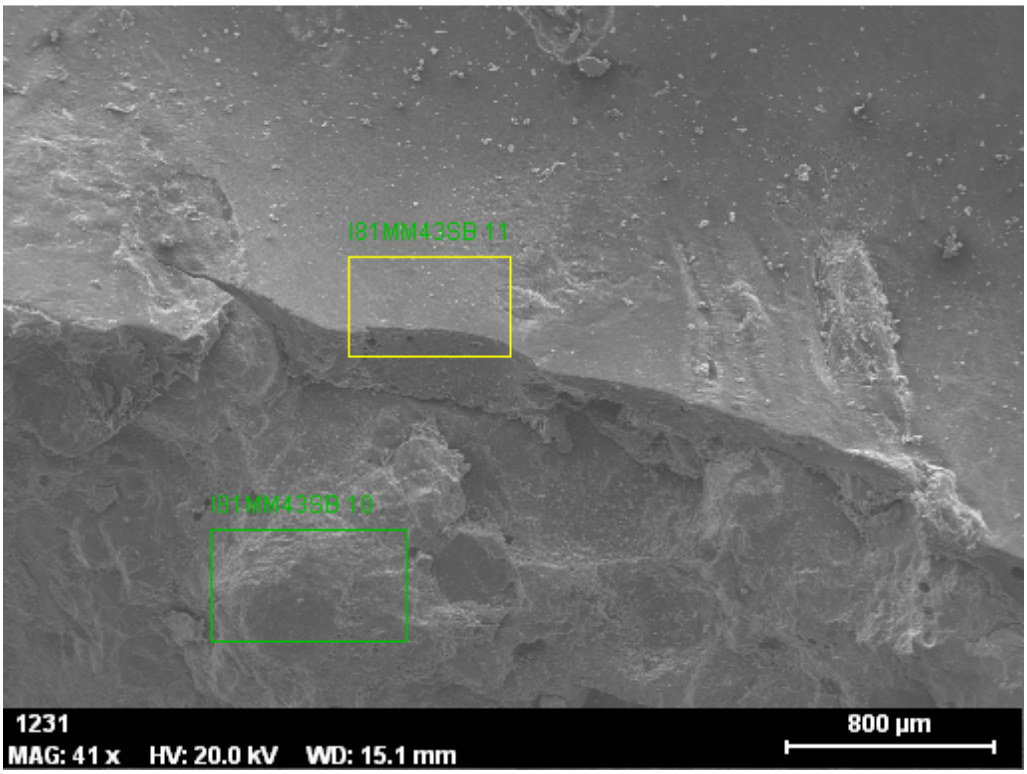

Figure 4.26 Sample Five SEM Micrograph I81MM43SB-10 and I81MM43SB-11

Table 4.20 Sample Five EDS Chemical Composition I81MM43SB-10 and I81MM43SB-11

	Mass Percent (%)									
Spectrum	**C**	**O**	**Na**	**Mg**	**Al**	**Si**	**K**	**Ca**	**Ti**	**Fe**
I81MM43SB-10	3.95	55.12	0.61	0.44	2.14	18.22	0.70	17.41	0.00	1.40
I81MM43SB-11	10.48	61.06	2.07	0.59	1.42	9.09	1.36	13.26	0.27	0.40
Difference Between 10 and 11	-6.53	-5.94	-1.46	-0.15	0.72	9.13	-0.66	4.15	-0.27	1.00

Figure 4.27 presents a SEM micrograph of sample six, it shows two image areas. I81MM43SB-12 and I81MM43SB-13 are both at fractured edge of the concrete. Table 4.21 presents the chemical composition of two locations on sample six. Locations 12 and

13 show low carbon content, and high calcium and silicon content. This can be concluded to be hydrated cement with traces of little carbonation. Silicates are commonly present in hydrated cement as tricalcium silicate (C_3S) and dicalcium silicate (C_2S).

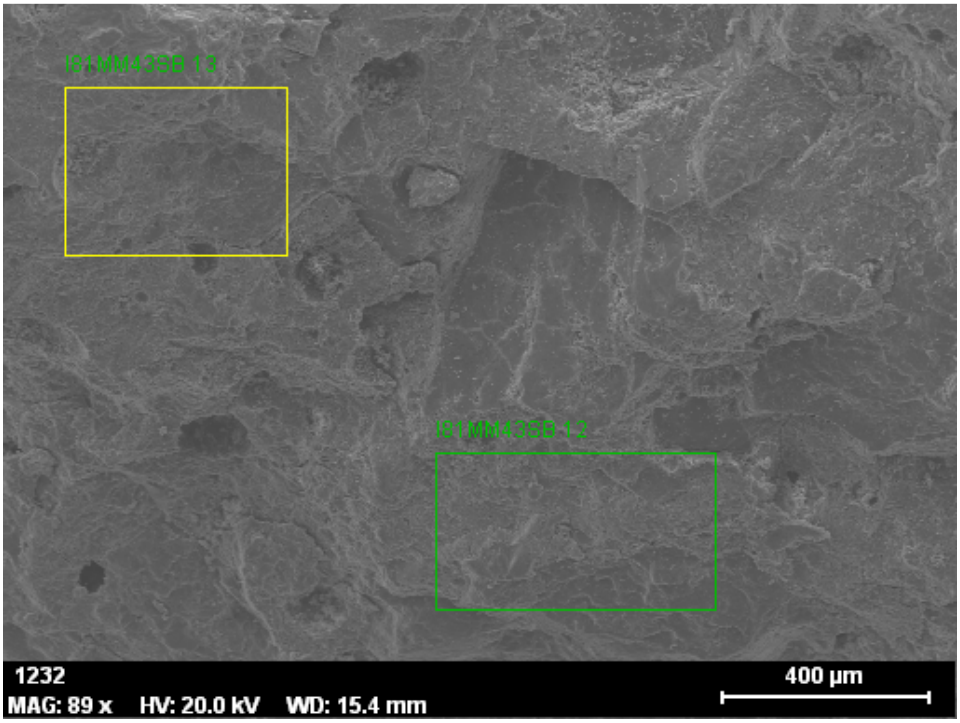

Figure 4.27 Sample Six SEM Micrograph I81MM43SB-12 and I81MM43SB-13

Table 4.21 Sample Six EDS Chemical Composition I81MM43SB-12 and I81MM43SB-13

	Mass Percent (%)									
Spectrum	**C**	**O**	**Na**	**Mg**	**Al**	**Si**	**K**	**Ca**	**Ti**	**Fe**
I81MM43SB-12	1.91	57.08	0.00	0.00	1.94	17.66	0.61	19.39	0.00	1.42
I81MM43SB-13	2.05	57.60	0.00	0.12	2.49	12.11	0.59	23.34	0.00	1.70
Mean value	1.98	57.34	0.00	0.06	2.22	14.88	0.60	21.37	0.00	1.56
Sigma	0.10	0.37	0.00	0.09	0.39	3.93	0.02	2.80	0.00	0.20
Sigma mean	0.07	0.26	0.00	0.06	0.28	2.78	0.01	1.98	0.00	0.14

4.3.3 Joint Opening Measurements

Closure joint openings from the I81 bridge deck were measured using a feeler gauge to determine the approximate construction joint width. Some parts of the closure joints, at side 1 and 2, were filled with debris on the four I81 bridge deck slabs which made it difficult to measure the true joint width in certain locations. The measurements were measured on the side of the slabs from top to bottom, since the top surface of the slabs were rough and there was more filling of the joints which made it difficult to measure the true joint width. The feeler gauge, a thinner steel piece used to measure small gaps. Thus, there is a possibility for denting or damaging the tip of the gauge which affects its precision.

For slab one the construction joint width for side 1 and 2 ranged from 0.009 to 0.016 in.. Slab two joint measurements ranged from 0.010 to 0.016 in.. Slab three joint measurements ranged from 0.009 to 0.020 in.. Slab four joint measurements ranged from 0.010 to 0.025 in.. This indicates that the closure joints are not fully sealed and are strongly influenced by the shrinkage of the concrete which causes those joints to open. For reinforced concrete under service load ACI 224R recommends that the crack width is kept below 0.007 in. for deicing chemicals (chlorides) (Abou-Zeid, Fowler et al. 2001). This threshold value has been exceeded in the I81 bridge deck closure joints which increases the risk of chloride attack.

4.4 Shrinkage Bars and Deck Shrinkage

4.4.1 Unrestrained Shrinkage

Figures 4.28 through 4.35 present unrestrained drying shrinkage for the first and second concrete placement for the lab cast slabs. A total of eight prism specimens were tested for the first placement, and a total of ten prism specimens were tested for the second placement. Each set of prism specimens, for the first and second placement, were separated into three different curing conditions, presented in Table 4.22. For the first placement eight prisms were tested, three for the first curing condition, two for the

second curing condition, and three for the third curing condition. For the second placement ten prisms were tested, three each for the first and second curing conditions, and four for the third curing condition.

Table 4.22 Prism Specimens Curing Conditions

Series	Curing Conditions Description
One	Place one day in mold, and then place half an hour in lime bath before taking initial measurements. After that place specimens again six days in lime bath before placing them in shrinkage room.
Two	Place one day in mold, and then place half an hour in lime bath before initial measurements were taken. After that place specimens again six days in lime bath before placing next to the slabs in normal conditions.
Three	Place six days in mold, after the initial measurements before placing specimens next to the slabs in normal conditions.

The shrinkage behavior of the first placement was similar for series one, two, and three, as shown in Figures 4.28 through 4.30. They exhibited a similar trend throughout the 180 days of testing duration, and the final readings at 180 days were 700 microstrain. Each series was averaged and compared with other series, as shown in Figure 4.31. Series one exhibited a slower shrinkage rate since it was placed in the shrinkage room, while series one and two were placed in ambient conditions next to the lab cast slabs.

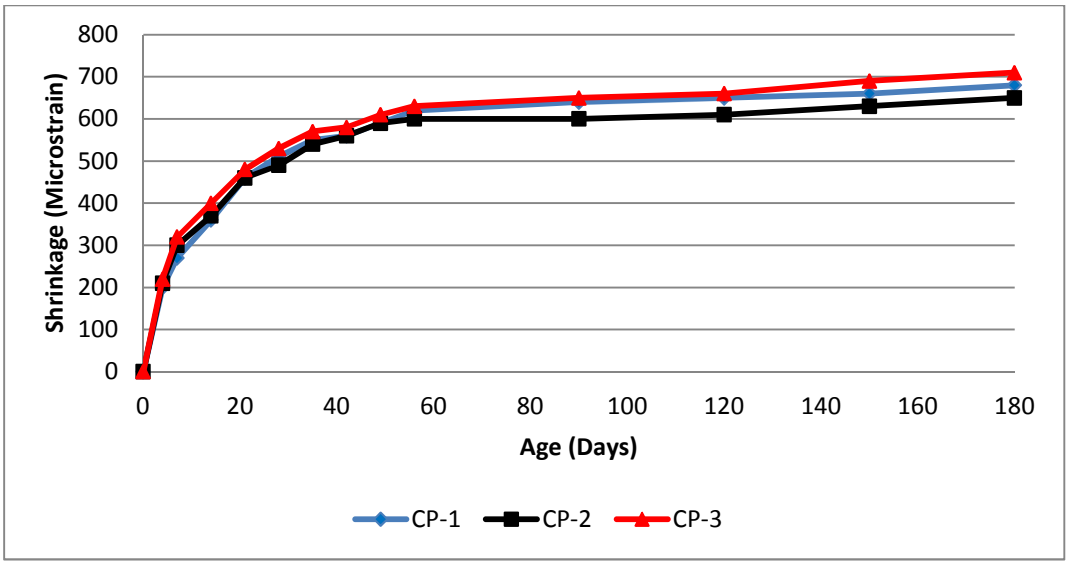

Figure 4.28 Drying Shrinkage of First Placement (Series 1)

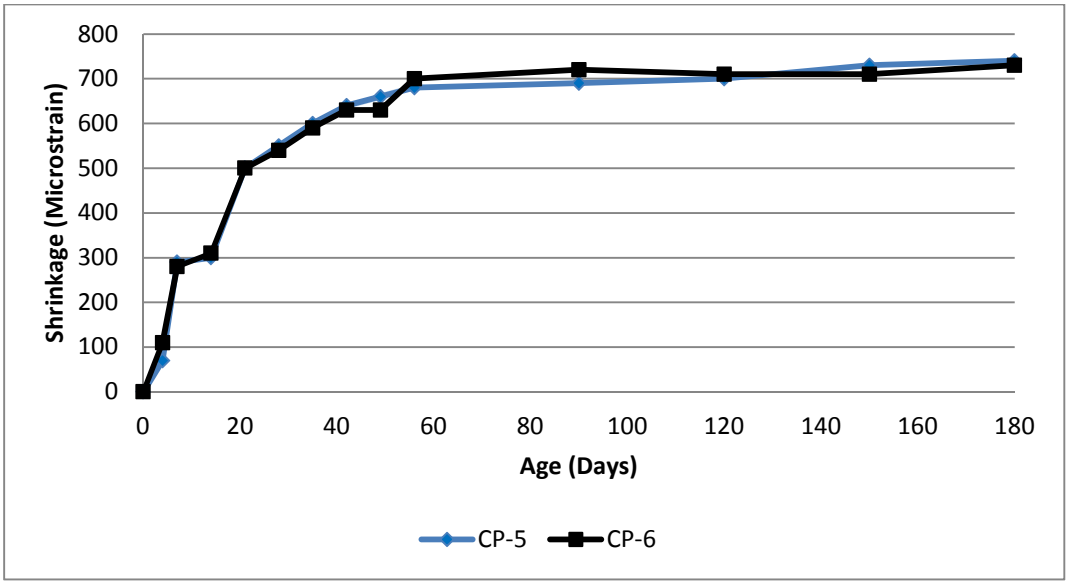

Figure 4.29 Drying Shrinkage of First Placement (Series 2)

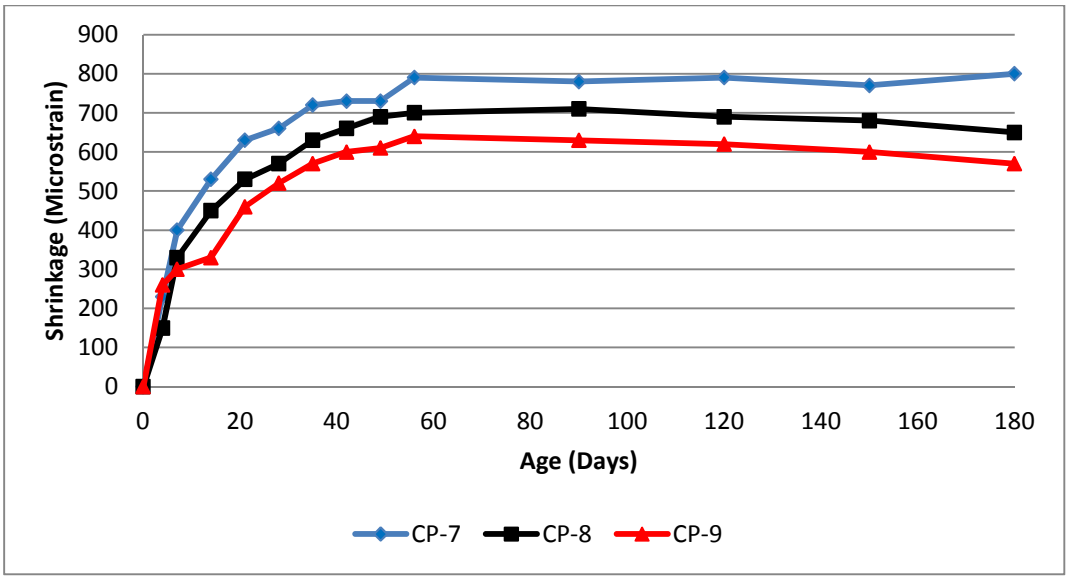

Figure 4.30 Drying Shrinkage of First Placement (Series 3)

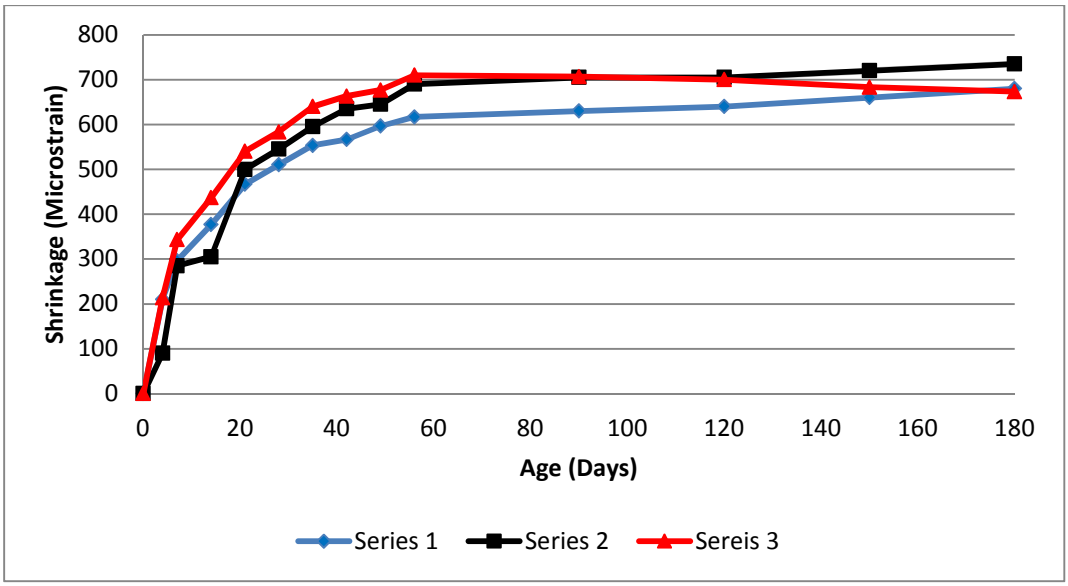

Figure 4.31 Average Drying Shrinkage for All Series of First Placement

The shrinkage behavior of the second placement was similar for series one, two, and three, as shown in Figures 4.32 through 4.34. They exhibited a similar trend throughout the 180 days of testing duration. The final readings at 180 days were 740 microstrain, 5% more than the first placement. Each series was averaged and compared with other series, as shown in Figure 4.35. Series one which was placed in the shrinkage room

exhibited a slower shrinkage rate, while series two and three were placed in ambient conditions next to the lab cast slabs and they had a similar shrinkage rate.

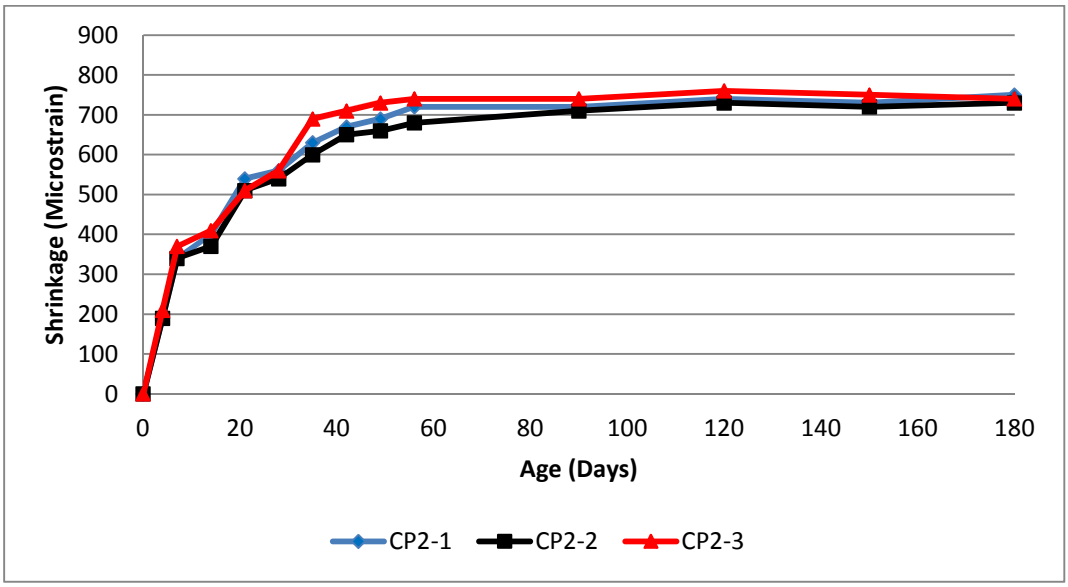

Figure 4.32 Drying Shrinkage of Second Placement (Series 1)

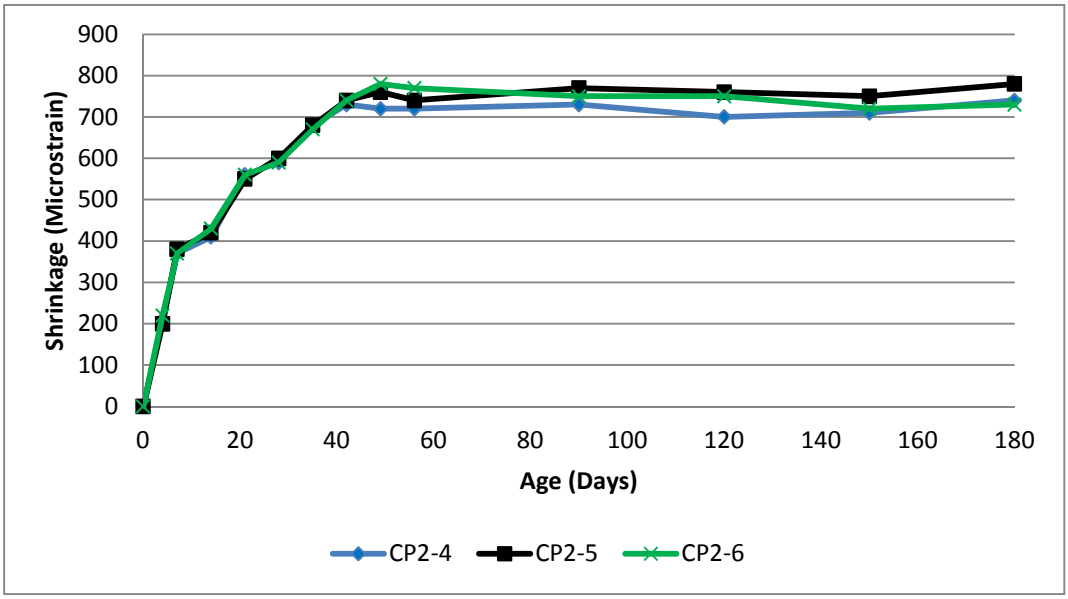

Figure 4.33 Drying Shrinkage of Second Placement (Series 2)

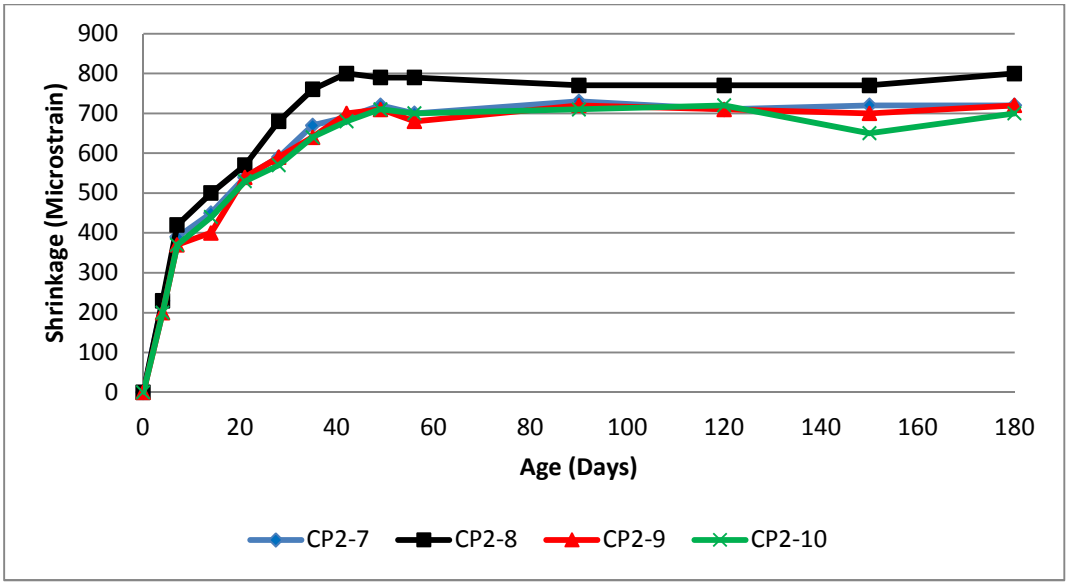

Figure 4.34 Drying Shrinkage of Second Placement (Series 3)

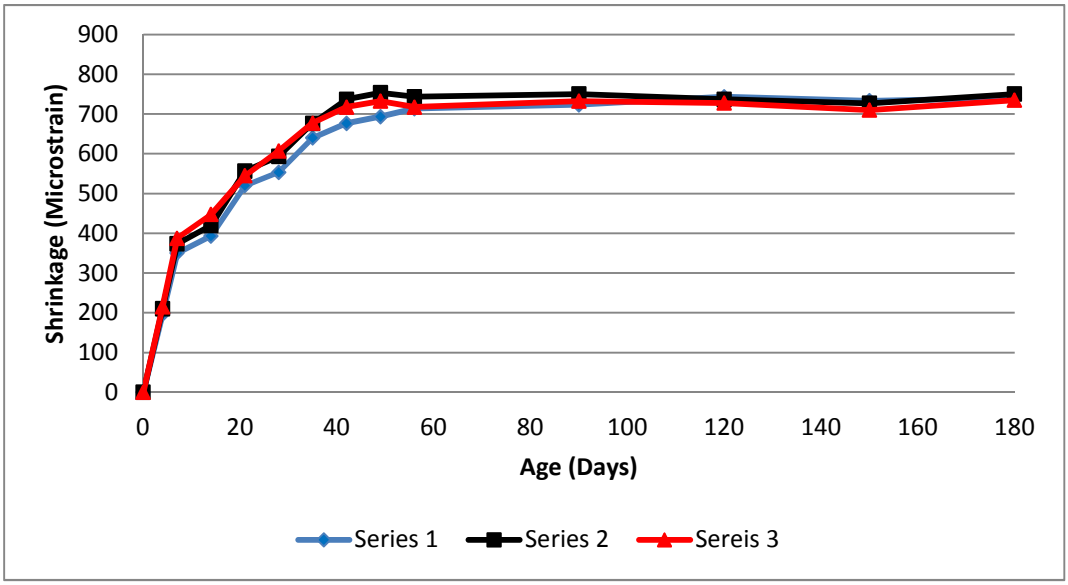

Figure 4.35 Average Drying Shrinkage for All Series of Second Placement

4.4.2 Restrained Shrinkage

Figures 4.36 through 4.40 present restrained drying shrinkage for the first and second concrete placement for three lab cast slabs. A Demec gage was used to measure the length change between the points as shrinkage occurred on the top surface of the slabs.

Four shrinkage readings were measured after seven days from placing the first placement (deck) from each slab, two readings from the right deck and two from the left deck. After 30 days the second placement was poured for the closure. Two shrinkage readings were measured from the closure, and additional four measurements were measured across the joint, between the deck and closure, after seven days from placing the first placement. Shrinkage readings were measured for 180 days. The three slabs were labeled as Slab A, Slab B, and Slab C.

Figure 4.36 presents the shrinkage of the left side of the three slabs for the first placement of concrete. All of the shrinkage readings are following the same trend and a final reading of 285 microstrains at 180 days. Slab C Left-2 exhibited a higher shrinkage rate of 340 mirostrains at 180 days among the other five readings. The second placement (closure pour) was placed after 30 days of the first placement, and it is represented with a dashed line in Figure 4.36. It can be noticed that by the time the closure pour was placed 50% of the shrinkage occurred. Before placing the closure pour the bottom part of the formwork was assembled, at that time it can be noticed that the shrinkage rate flattens while placing the closure pour and then shrinkage continues at a slower rate after the casting the closure pour.

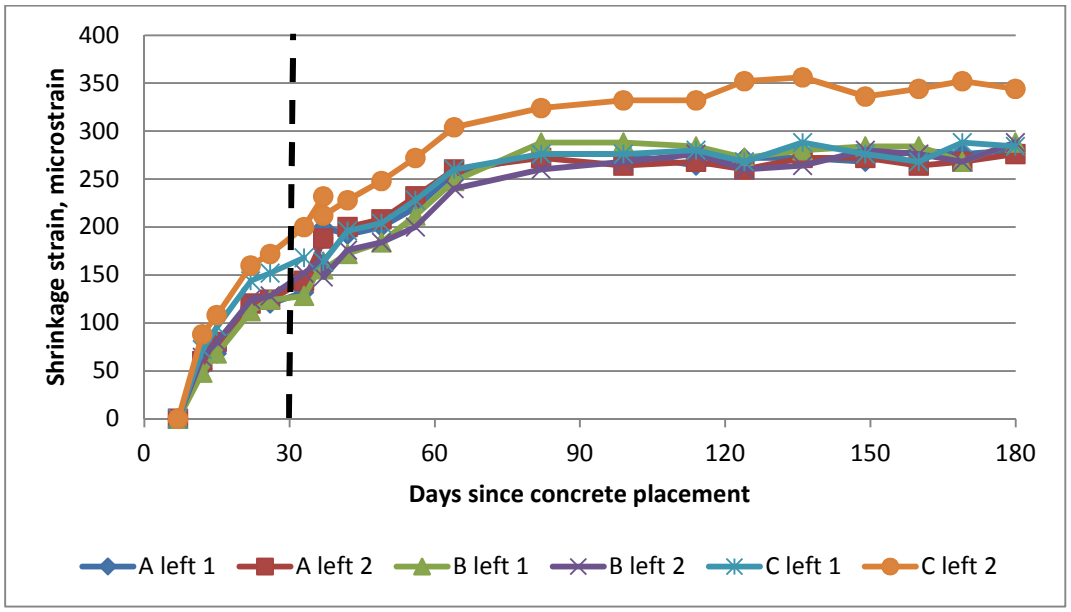

Figure 4.36 Slab Shrinkage Readings for Left Side of First Placement

Figure 4.37 presents the shrinkage of the right side of the three slabs for the first placement of concrete. All of the shrinkage readings are following the same trend, and the final readings varied from 300 to 350 microstrains at 180 days. The second placement (closure pour) was placed after 30 days of the first placement, and it is represented with a dashed line in Figure 4.37. It can be noticed that by the time the closure pour was placed 50% of the shrinkage occurred. Before placing the closure pour the bottom part of the formwork was assembled, at that time it can be noticed that the shrinkage rate flattens while placing the closure pour and then shrinkage continues at a slower rate after the casting the closure pour.

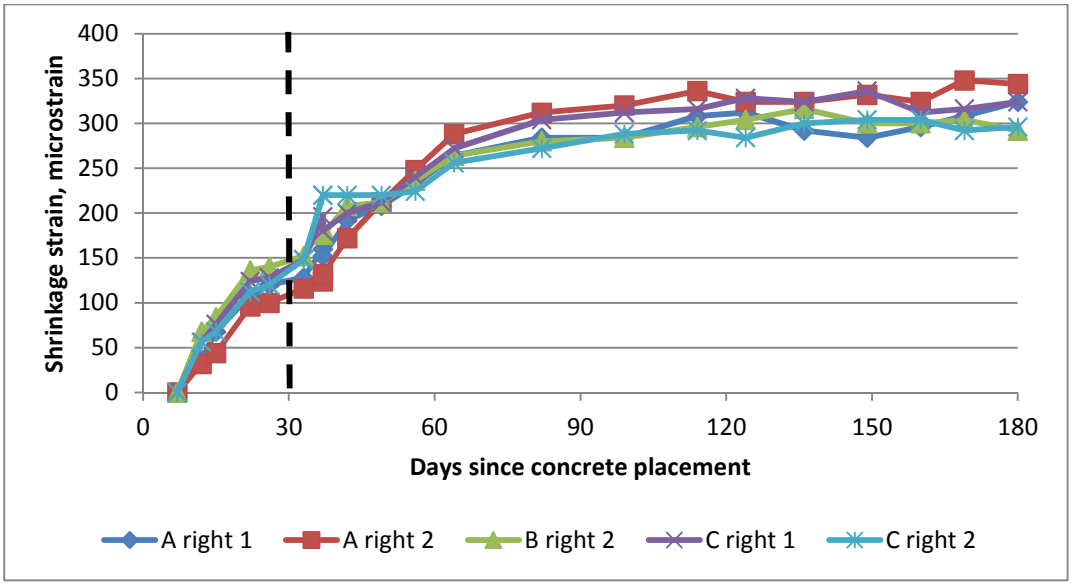

Figure 4.37 Slab Shrinkage Readings for Right Side of First Placement (Deck)

Figure 4.38 presents the shrinkage of the left joint of the three slabs. Slab A shrinkage readings are following the same trend averaging 235 microstrains at 180 days. Slab B shrinkage behavior represents an unusual behavior with fluctuation in data averaging 75 microstrains at 180 days. Demec points have been detached few times during the testing period due to surrounding working environment. This had a significant impact on the data for Slab B. Slab C shrinkage was less than Slab A with a similar overall trend of the results with 195 microstrains at 180 days.

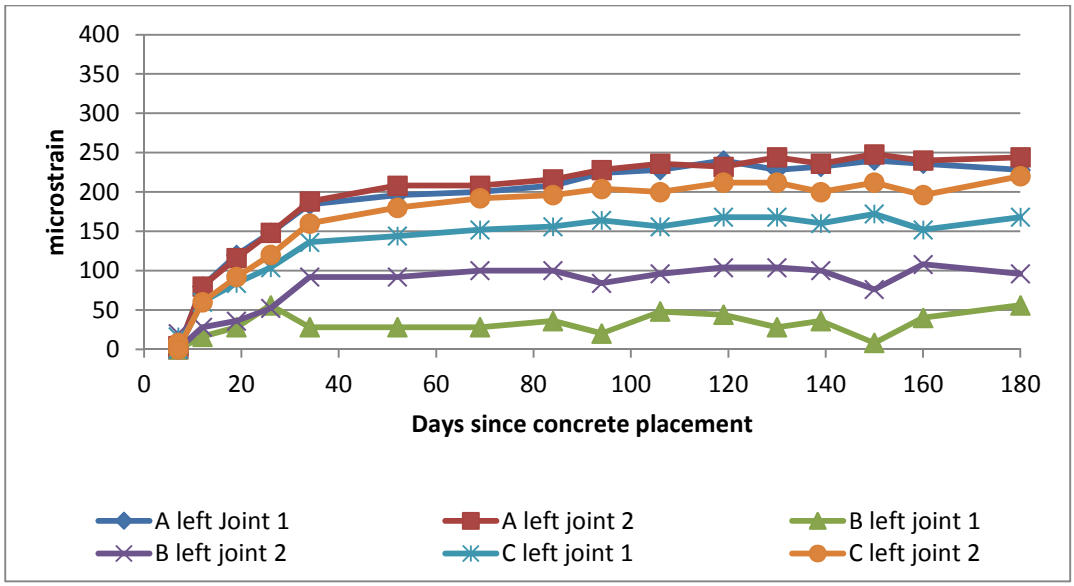

Figure 4.38 Slab Shrinkage Readings for Left Joint between Deck and Closure

Figure 4.39 presents the shrinkage of the right joint of the three slabs. There is a high variability in readings for the three slabs ranging from 125 to 370 microstrains. Slab A shrinkage readings were 310 microstrains at 180 days. For Slab B one of the demec points on B right 1 was detached chipping the concrete under it. This occurred after 52 days of casting the slabs. Slab B shrinkage based on right joint 2 only was 135 microstrains at 180 days. Slab C shrinkage is less than Slab A with 160 microstrains at 180 days.

Shrinkage for the closure pour and the deck are at different rates. The time the closure pour is placed, 30 days, 50% of the shrinkage occurred already in the deck. Also, the shrinkage is measured across the joint which strongly influence the shrinkage readings, as noticed in Figure 4.38 and 4.39.

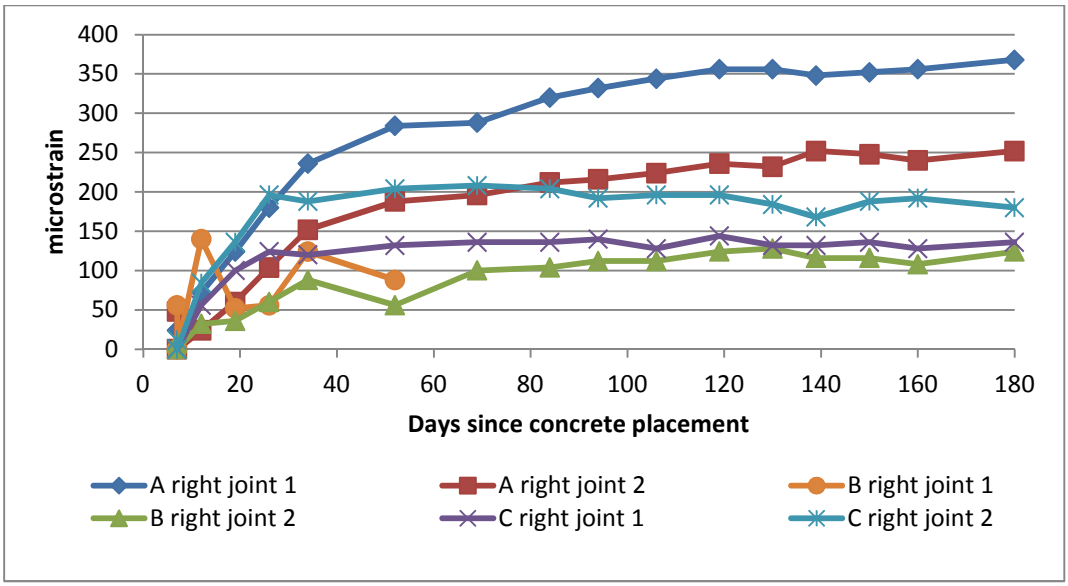

Figure 4.39 Slab Shrinkage Readings for Right Joint between Deck and Closure

Figure 4.40 presents the shrinkage of the closure for the three slabs for the second placement of concrete. All of the shrinkage readings are following the same trend, and there final readings varied from 390 to 450 microstrains at 180 days.

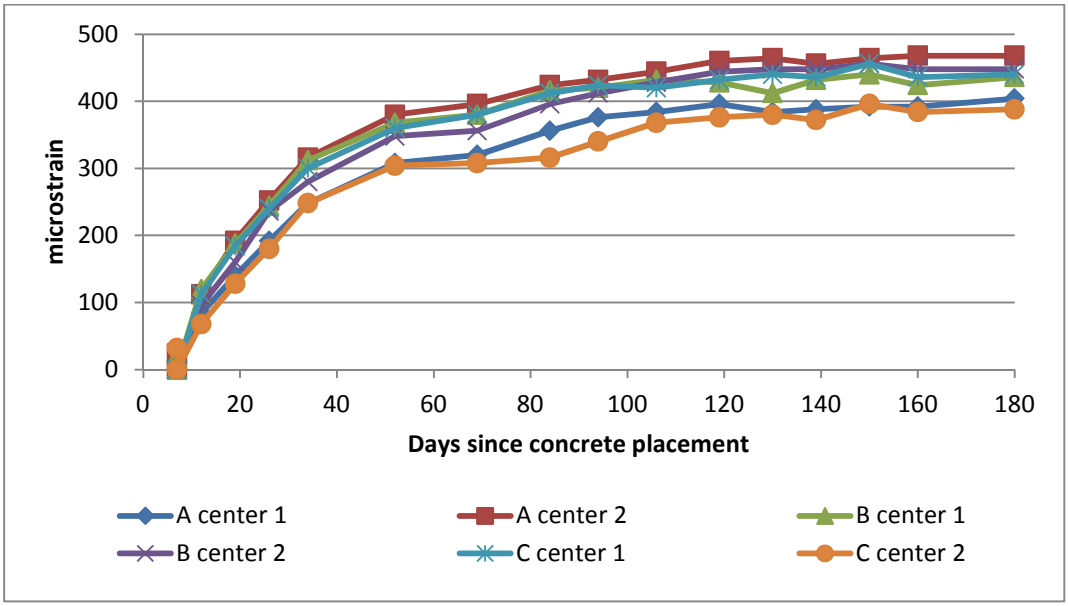

Figure 4.40 Slab Shrinkage Readings for Second Placement (Closure)

There were some variations in the shrinkage readings of the lab cast slabs. Some of those fluctuations were due to temperature and relative humidity variability. Another factor

which had a strong impact on Slab B was the detachment of the demec points during testing. This was clearly reflected on the demec readings across the slab joints. The total shrinkage average displacement of each slab was 0.033 in., and all of the three slabs a negligible difference from the average displacement with a difference less than 3%. This was determined by taking the average of the measured ultimate shrinkage at 180 days for the lab cast slabs, and multiplying it by the length that the measured ultimate shrinkage at 180 days exhibited. For the left and right deck, and the closure pour the length was taken as 28 in.. For the measurements across the joints the length was taken as 8 in., which is the length of the demec gage.

The unrestrained shrinkage had a higher rate of shrinkage compared to restrained shrinkage. All of the unrestrained shrinkage occurred after 50 days, for the first and second placement, for the three tested series. For the restrained shrinkage it took over 80 days for all of the shrinkage to occur. The relative humidity and temperature in the laboratory conditions varied during the testing period.

4.4.3 Demec Readings After Unbolting Lab Cast Slabs

Tables 4.23 through 4.25 present the change in length of the lab cast slabs due to the restraining effect to simulate the actual condition of the bridge deck. The demec points on the slabs were measured at two points for each location on the slabs before unbolting them and letting them relax. After unbolting the slabs the demec gauge was fluctuating, so the slabs were left for 24 hours to relax and then the measured readings were stable.

As presented in Table 4.23 the right joint of Slab A shows a higher difference than the left joint, although the readings are close at the points measured in those locations. This might be due to some imperfections in Slab A during the construction process. The total difference was -1.86×10^{-3} in..

Table 4.24 presents Slab B with a difference of 8.48×10^{-4} in.. Slab B exhibited an unexpected result from other slabs. This might be due to some debris inside the joint which is affecting the results.

Table 4.25 presents Slab C and it shows that the right and left joint are exhibiting a difference. The total difference was -7.65×10^{-3} in.. Slab A and C exhibited the expected behavior of a restrained end condition, although the displacements were very small.

Table 4.23 Slab A Demec Readings Before and After Unbolting

Location	Point	Before Unbolting (mm)	After Unbolting (mm)	Difference (mm)	Difference (με)
A-Left	1	-0.01	-0.016	0.006	24
	2	0.003	0.003	0	0
A-Left Joint	1	-0.05	-0.037	-0.013	-52
	2	0.007	0.02	-0.013	-52
A- Center	1	-0.055	-0.073	0.018	72
	2	-0.023	-0.019	-0.004	-16
A-Right Joint	1	-0.096	-0.051	-0.045	-180
	2	-0.127	-0.057	-0.07	-280
A-Right	1	0.011	0.011	0	0
	2	0.041	0.004	0.037	148

Table 4.24 Slab B Demec Readings Before and After Unbolting

Location	Point	Before Unbolting (mm)	After Unbolting (mm)	Difference (mm)	Difference (με)
B-Left	1	-0.007	-0.01	0.003	12
	2	X	X	X	X
B-Left Joint	1	0.043	0.023	0.02	80
	2	0.038	0.077	-0.039	-156
B- Center	1	-0.044	-0.027	-0.017	-68
	2	-0.058	-0.063	0.005	20
B-Right Joint	1	X	X	X	X
	2	0.036	0	0.036	144
B-Right	1	X	X	X	X
	2	0.014	-0.046	0.06	240

Table 4.25 Slab C Demec Readings Before and After Unbolting

Location	Point	Before Unbolting (mm)	After Unbolting (mm)	Difference (mm)	Difference (με)
C-Left	1	-0.005	-0.02	0.015	60
	2	0.009	0.015	-0.006	-24
C-Left Joint	1	0.05	0.175	-0.125	-500
	2	0.009	0.116	-0.107	-428
C- Center	1	-0.114	-0.129	0.015	60
	2	0.005	-0.015	0.02	80
C-Right Joint	1	0.024	0.13	-0.106	-424
	2	0.046	0.186	-0.14	-560
C-Right	1	0.037	0.043	-0.006	-24
	2	0.021	0.004	0.017	68

Changes in lengths were noticed at the joints after unrestraining the lab cast slabs. This indicates that restraining the lab cast slabs resulted in keeping the closure joints open. The lab cast slabs are restrained from both ends which causes the closure joints to open due to the shrinkage of the closure pour, and the right and left side of the deck. This causes tensile stress in the reinforcing steel across the closure joints, since the concrete stress at the joint is equal to zero. When the lab cast slabs are unbolted they become unrestrained which causes the reinforcing steel to relax and closes the closure joints. Slabs A and C exhibited those results, while Slab B had unexpected results which were discussed previously. This simulates the actual condition of the bridge deck were restraining was occurring which helped the closure joints to stay open for steel aggressors.

4.5 Comparison of Unrestrained Shrinkage Models

Five models were used to predict the unrestrained shrinkage and compare it with the actual measured results. They were calculated at seven, 14, 28, 56, 90, 150, and 180 days. A sensitivity analysis for different parameters in the shrinkage model equations was conducted for each of the five models to compare it with actual measured results, as presented in Figures 4.41 through 4.51. This was done by inputting a range of different

parameter values and comparing them with the actual measured results for the first and second placements. The average relative humidity in the laboratory were varying, from 40% to 92%, throughout the testing period, from December 2010 to June 2011, for series two and three. Series one specimens were placed in a controlled environment of 50% RH.

Figure 4.41 presents a sensitivity analysis for different relative humidity (40%, 50%, 60%, and 70% RH) performed for ACI 209R-92 for a range of relative humidity for cement type I. ACI 209 R-92 under predicted shrinkage for the first 90 days then it started to give closer results especially for 40% and 50% RH.

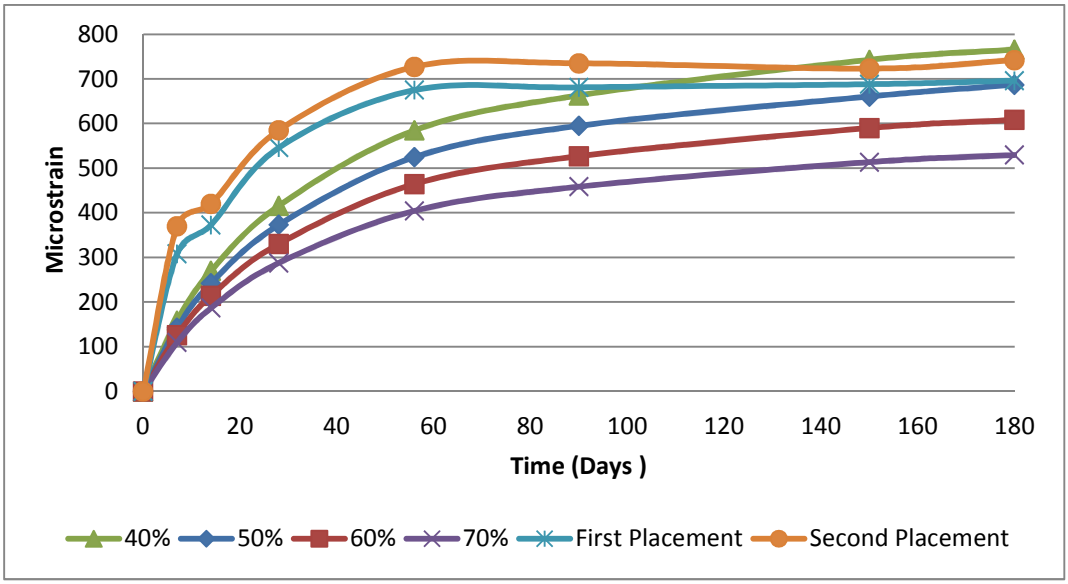

Figure 4.41 ACI 209R-92 Sensitivity Analysis for Relative Humidity

Figure 4.42 presents a sensitivity analysis for different relative humidity (40%, 50%, 60%, and 70% RH) performed for B3 for a range of relative humidity for cement type I. B3 under predicted more than 200 microstrain at 180 days.

Figure 4.43 presents a sensitivity analysis for different relative humidity (40%, 50%, 60%, and 70% RH) performed for B3 for a range of relative humidity for cement type II. B3 under predicted more than 300 microstrain at 180 days.

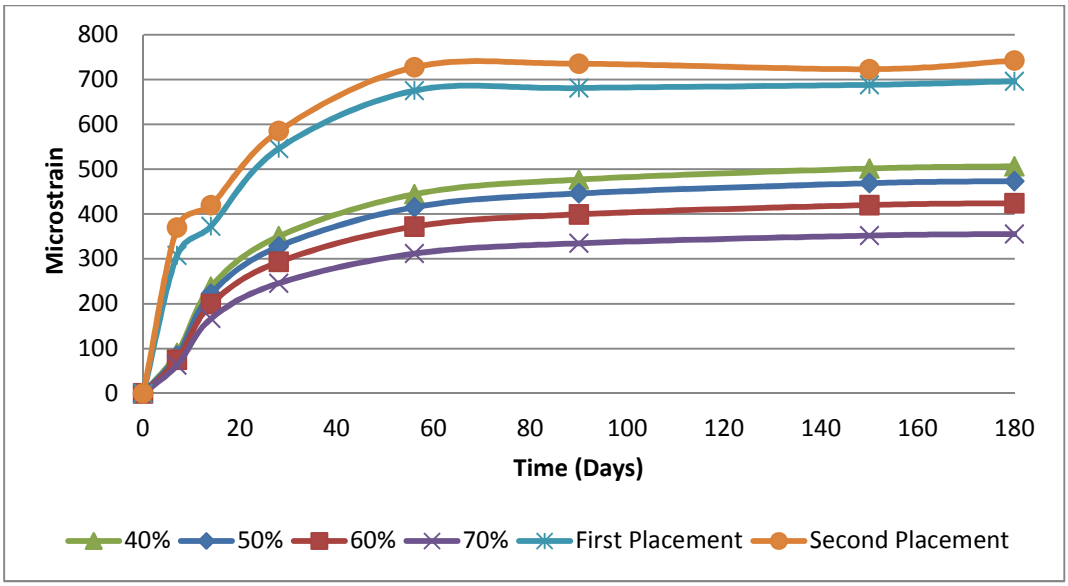

Figure 4.42 B3 Sensitivity Analysis for Relative Humidity (Cement Type I)

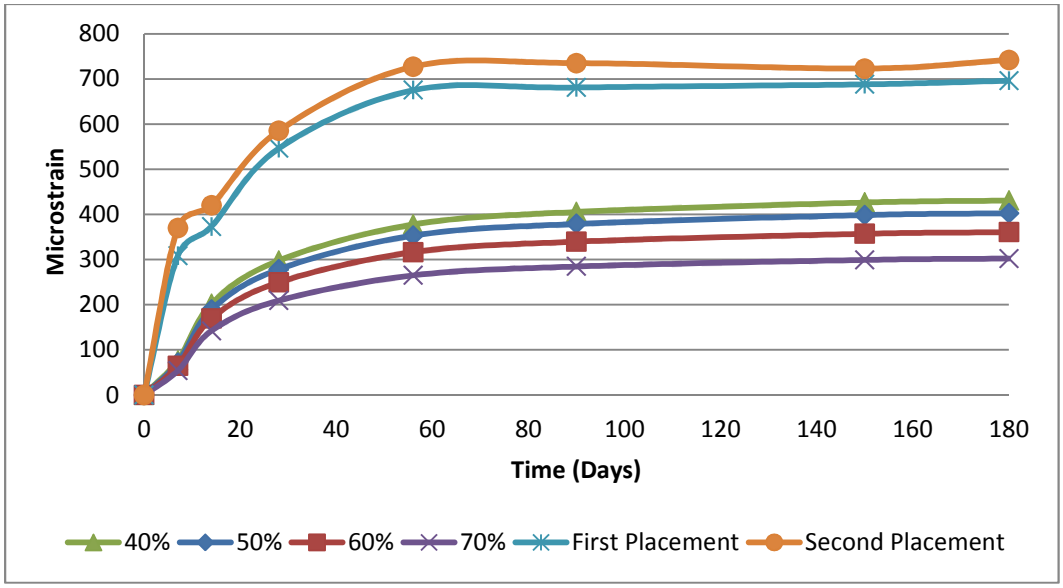

Figure 4.43 B3 Sensitivity Analysis for Relative Humidity (Cement Type II)

Figure 4.44 presents a sensitivity analysis for different cement type correction factors performed for B3 model. Cement type I correction factor is equal to 1.00, cement type II correction factor is equal to 0.85, and 1.5 correction factor was used to get a close fit to the actual measured values. Cement type II have a lower shrinkage rate compared to cement type I. When using 1.5 as a cement type correction factor it under predicts for the first 90 days and then fits the actual measurements between 90 and 180 days.

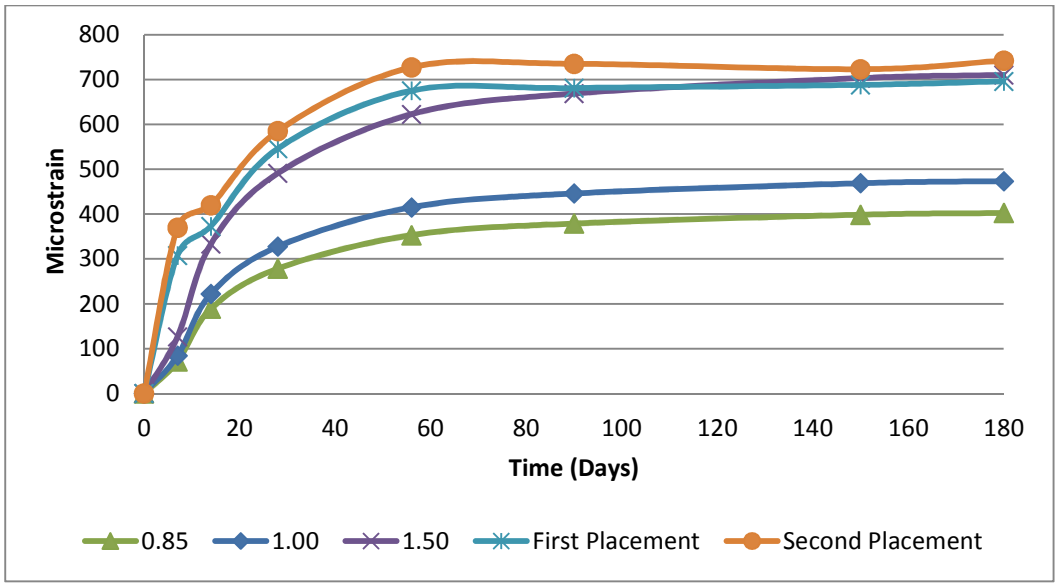

Figure 4.44 B3 Sensitivity Analysis for Cement Type

Figure 4.45 presents a sensitivity analysis performed for CEB 90 for a range of relative humidity (40%, 50%, 60%, and 70% RH) for cement type I. CEB 90 had a similar behavior as B3, presented in Figure 4.49, which under predicted more than 200 microstrain at 180 days.

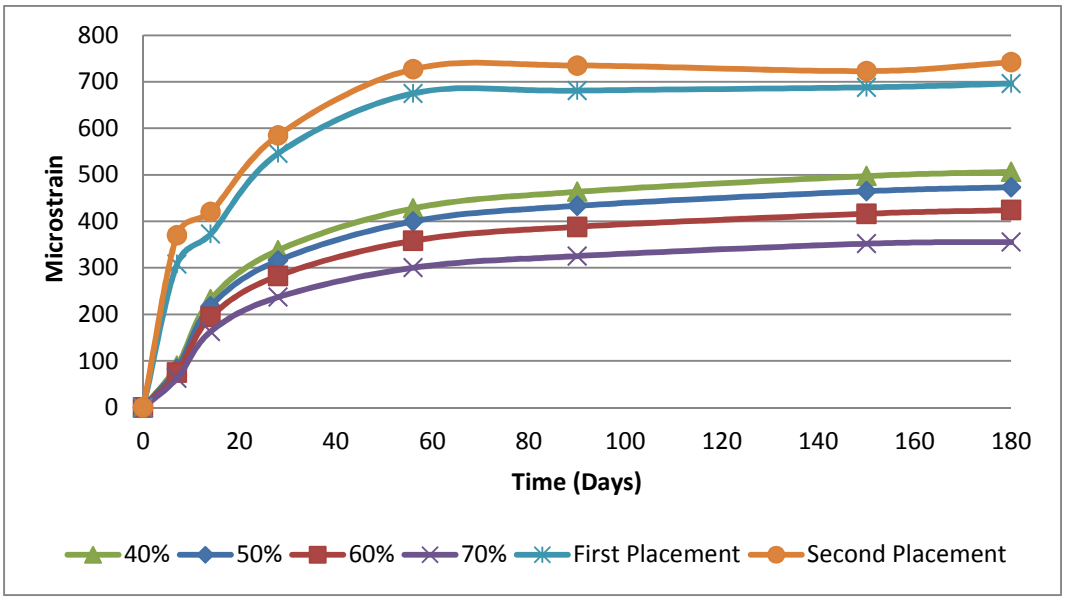

Figure 4.45 CEB 90 Sensitivity Analysis for Relative Humidity

Figure 4.46 presents a sensitivity analysis performed for GL2000 for a range of relative humidity (40%, 50%, 60%, and 70% RH) for cement type I. GL2000 had a similar behavior as ACI 209R-92, presented in Figure 4.41. It under predicted shrinkage for the first 90 days then it started to give closer results especially for lower RH as it got closer to 180 days.

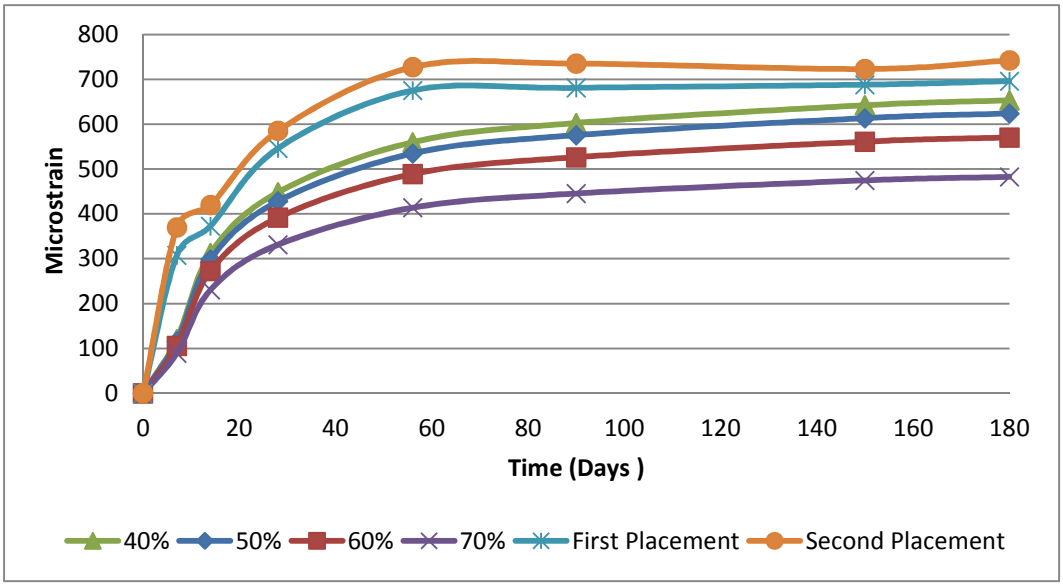

Figure 4.46 GL2000 Sensitivity Analysis for Relative Humidity (Cement Type I)

Figure 4.47 presents a sensitivity analysis performed for GL2000 for a range of relative humidity (40%, 50%, 60%, and 70% RH) for cement type II. GL2000 had a similar behavior as CEB 90 and B3 which under predicted more than 200 microstrain at 180 days.

Comparing cement type I and II, cement type I had a better fit for the actual measurements for the first and second placement. While cement type II under predicted the actual measurements.

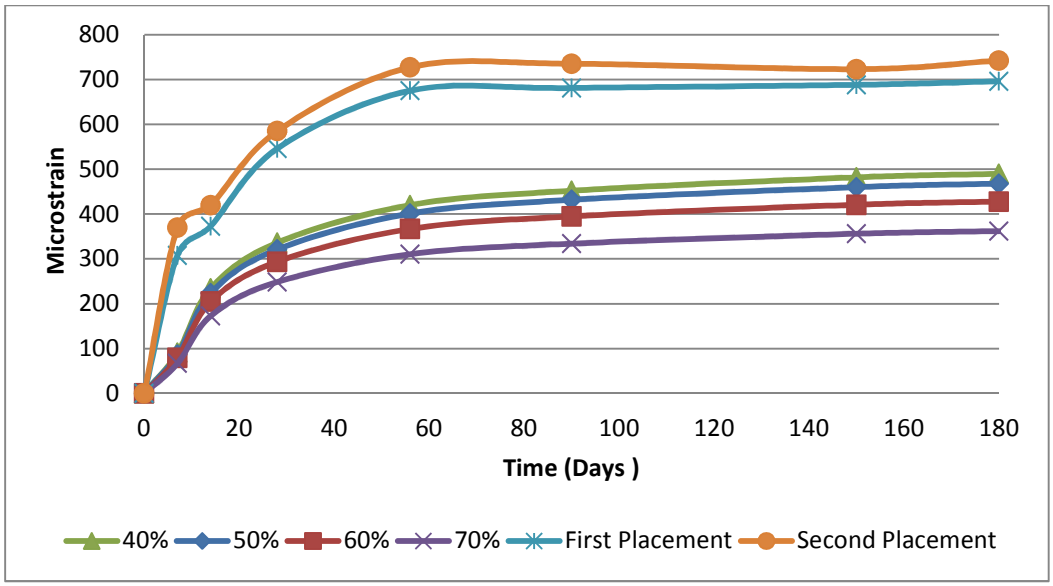

Figure 4.47 GL2000 Sensitivity Analysis for Relative Humidity (Cement Type II)

Figure 4.48 presents a sensitivity analysis performed for GL2000 for different cement types. Cement type I correction factor is equal to 1.00, cement type II correction factor is equal to 0.75, and 1.2 correction factor was used to get a close fit to the actual measured values. Cement type II have a lower shrinkage rate compared to cement type I. When using 1.2 as a cement type correction factor it under predicts for the first 90 days and then fits the actual measurements between 90 and 180 days.

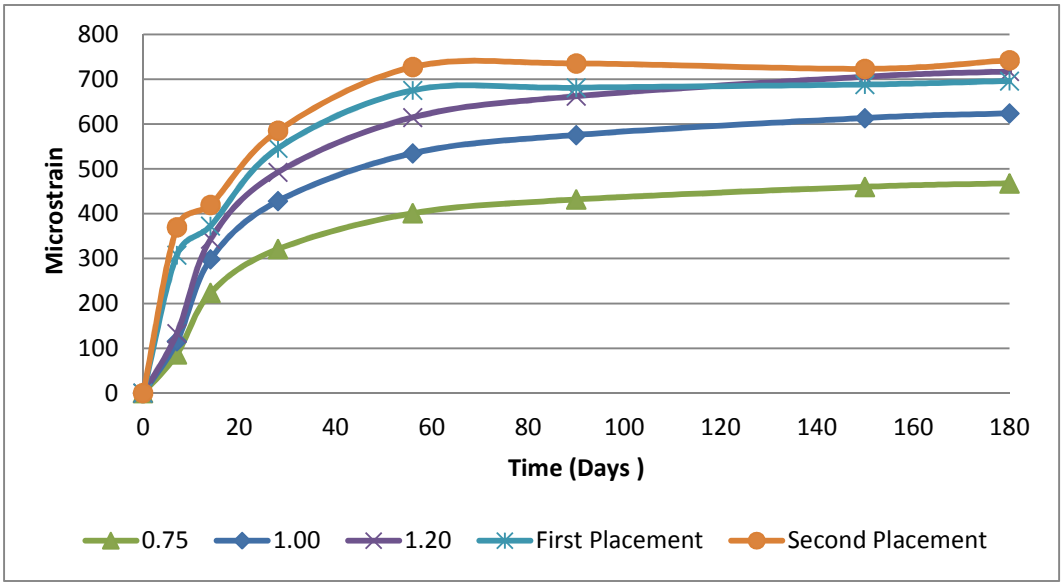

Figure 4.48 GL2000 Sensitivity Analysis for Cement Type

Figure 4.49 presents a sensitivity analysis performed for AASHTO-LRFD for a range of relative humidity (40%, 50%, 60%, and 70% RH). AASHTO-LRFD under predicted the shrinkage early stages until about 60 days then it start to decrease the difference. Still it under predicted shrinkage and it was off by more than 100 microstrain at 180 days.

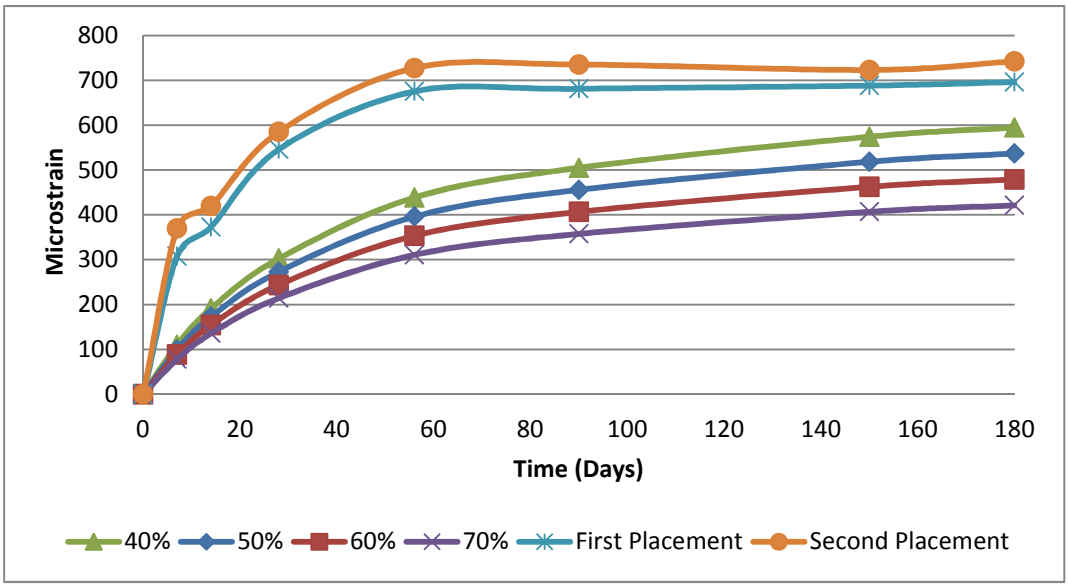

Figure 4.49 AASHTO-LRFD Sensitivity Analysis for Relative Humidity

Figure 4.50 presents a comparison for the previous five models for 50% RH. RH is the only varying factor in our testing for the prisms placed beside the casted slab, since they were exposed for 180 days for an uncontrolled RH. While the prisms placed in the humidity chamber had a controlled RH of 50%. The other parameters we have them specific and we are certain of them.

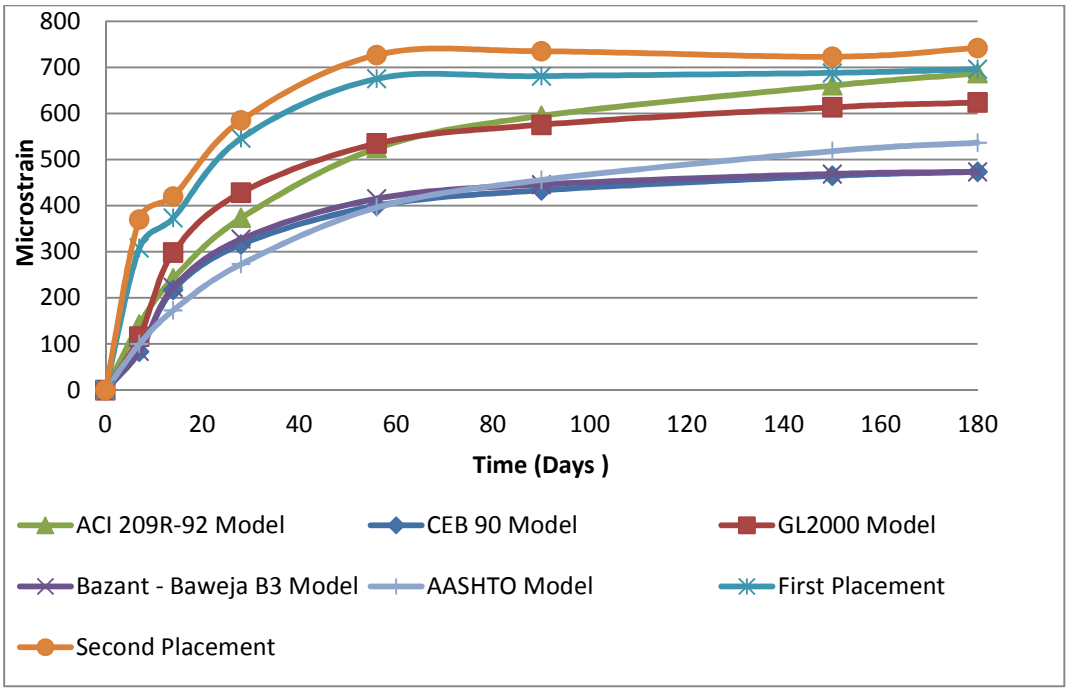

Figure 4.50 Shrinkage Models Comparison for 50% Relative Humidity

Figure 4.51 presents a sensitivity analysis performed for ACI 209R-92 for a range of α (flatter hyperbolic form) with 50% RH, α can be applied in Equation 4.1. ACI 209 R-92 under predicted shrinkage for α equal to one, but as the value of α increased the slope became steeper for the first 20 to 30 days, and then flattens. The best fit for both placements is when α is equal to 1.25.

$$\varepsilon_{sh}(t, t_c) = \frac{(t-t_c)^{\alpha}}{f+(t-t_c)^{\alpha}} \varepsilon_{shu} \qquad \textbf{(Equation 4.1)}$$

Figures 4.52 and 4.53 present the residual microstrain difference between α equal 1.25 and both the first and second placement. The residual microstrain were plotted using the predicted values minus the measured values, and the vertical error bars for each plot shows the standard deviation of the measured values and the predicted values. If the residual values are negative it means the model underestimated the shrinkage, and if the residual values are positive it means the model overestimated the shrinkage. The error was 10% for the first placement and 4% for the second placement at 180 days for α equal 1.25.

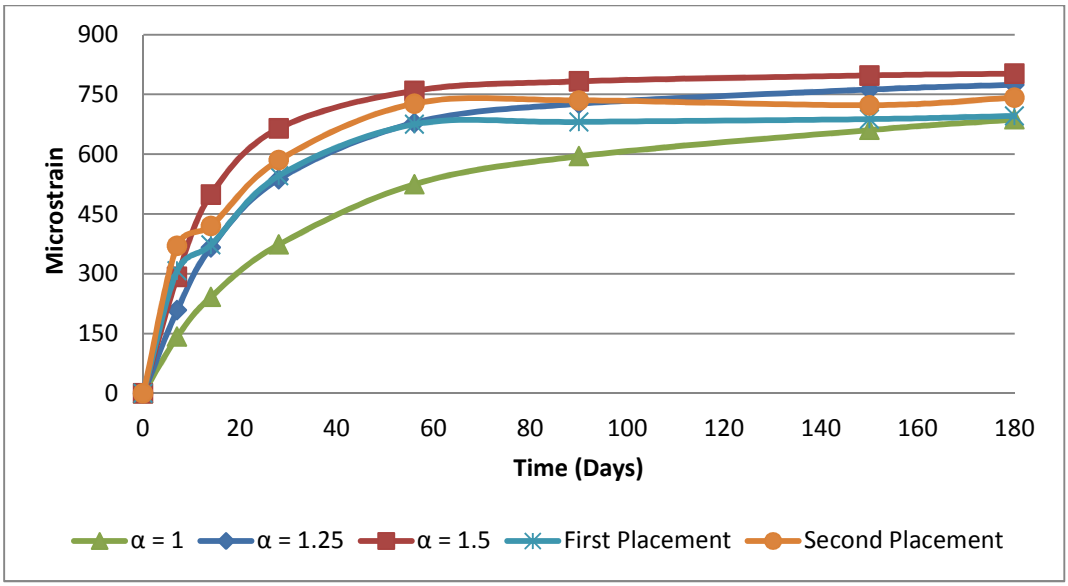

Figure 4.51 ACI 209R-92 Sensitivity Analysis for α with 50% RH

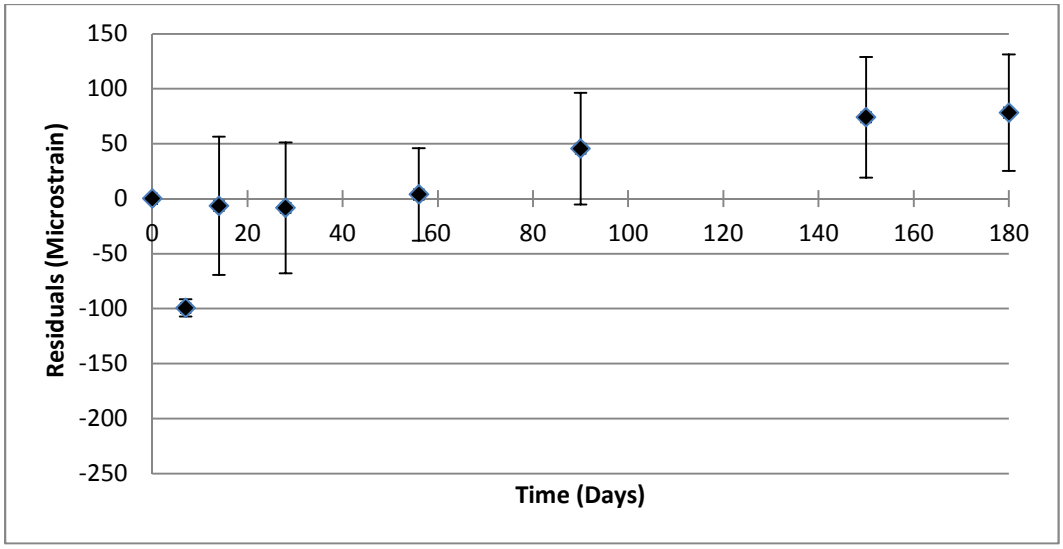

Figure 4.52 ACI 209R-92 Residuals for First Placement

The residuals for the first placement, shown in Figure 4.52, are close to zero residuals for the first 60 days which indicates precise model shrinkage. From 60 to 180 days, the values become more positive which indicates that the ACI 209R-92 model overestimated the shrinkage. The residuals for the second placement, shown in Figure 4.53, are under

estimating the shrinkage for the first 60 days, and then the values become more positive which indicates that the ACI 209R-92 model is overestimating the shrinkage.

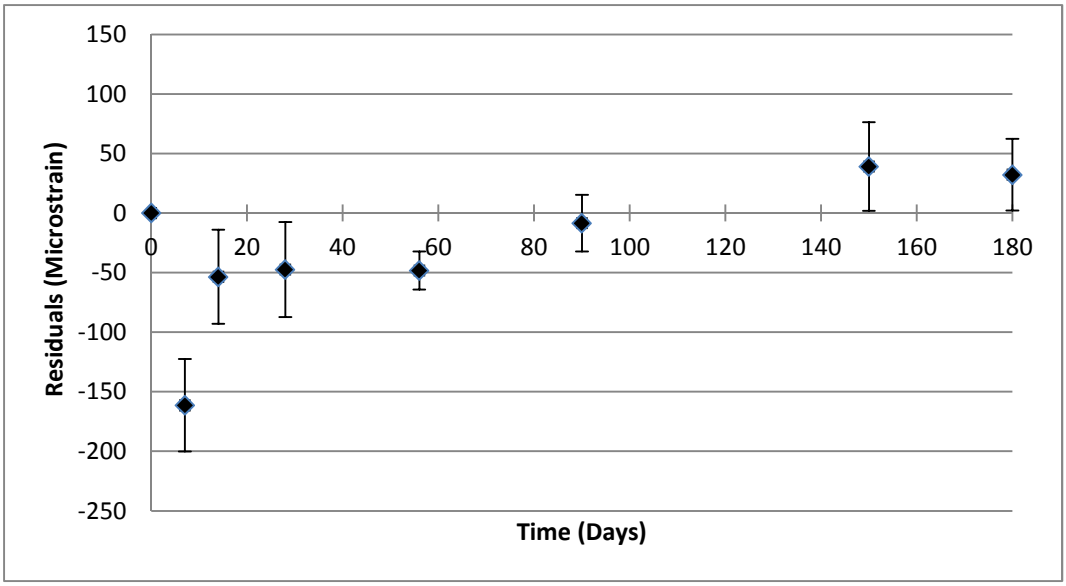

Figure 4.53 ACI 209R-92 Residuals for Second Placement

Using 1.2 for the cement correction factor for the GL 2000 predicted closer results than using the recommended values for cement type I and II. For the B3 model, a cement correction factor of 1.5 predicted closer results than the recommended values for cement type I and II. The GL 2000 and B3 models under predicts for the first 90 days and then fits the actual measurements between 90 and 180 days. From the five models used to predict the unrestrained shrinkage the ACI 209-92 was the best predictor followed by the GL 2000 and B3 models using the modified cement correction factors.

CHAPTER 5: CONCLUSIONS

The following conclusions can be made from this study:

1. Cover depths are adequate and they provide good protection against chloride attacks within the closure pour but not the cracked areas.
2. Concrete shrinkage is adequate to open the construction joint.
3. Corrosion activity is higher closer to the construction joint for I81 bridge deck slabs.
4. Corrosion potentials are higher for I81 bridge deck slabs than lab cast slabs.
5. Resistivity measurements showed good quality of concrete for I81 bridge deck and lab cast slabs.
6. Corrosion current densities for I81 bridge deck slabs are higher than lab cast slabs.
7. Corrosion current densities are higher across the joints from the closure pour for I81 bridge deck slabs.
8. Chloride content along the depth of the joint were relatively uniform for the depths of 2-4 inches from the top surface of the I81 bridge deck slabs (1.64 to 4.69 lbs/yd^3).
9. Chloride content within the closure pour were very low from 2-3.5 inches (0.2 to 1.0 lbs/yd3) from the top surface of the I81 bridge deck slabs.
10. Epoxy adhesion was in good condition on the ECR, since it could not be peeled even after soaking the ECR for two weeks in water. Although corrosion was occurring under the epoxy coating and it lost adhesion in some places.
11. The ACI 209R-92 was the best predictor model for drying shrinkage followed by the GL2000 and B3 models. While the other two models predicted significantly drying shrinkage.

CHAPTER 6: RECOMMENDATIONS

The following recommendations can be made from the following study:

1. Frequent inspection and closely monitoring bridges with similar conditions at least every two years. This includes visually checking leaking joints for deposits and rust stains. Also, measuring corrosion current densities for the reinforcing steel at different location on the bridge deck.
2. Use corrosion resistance reinforcement, such as stainless steel bars (ASTM A955 or A1035), to maintain a longer deck service life. This will decrease rehabilitation work for the bridge deck and will increase its service life.
3. Seal construction joints with flexible sealants to prevent chlorides from attacking the reinforcing steel.

REFERENCES

AASHTO (2007). "AASHTO LRFD Bridge Design Specifications, 4th Edition." American Association of State Highway and Transportation Officials.

Abou-Zeid, M., D. W. Fowler, et al. (2001). "Control of Cracking in Concrete Structures."

ACI Committee 209 (2008). "Guide for Modeling and Calculating Shrinkage and Creep in Hardened Concrete (ACI 209.2R-08)." American Concrete Institute: 45.

Aitcin, P.-C., A. M. Neville, et al. (1997). "Integrated view of shrinkage deformation." Concrete international **19**(Compendex): 35-41.

ASTM C 876-91 "C876-91, Standard test method for half cell potentials of uncoated reinforced steel in concrete." Annual Book of ASTM Standard **4**.

Balakumaran, S. S. G. (2010). Influence of Bridge Deck Concrete Parameters on the Reinforcing Steel Corrosion, Virginia Polytechnic Institute and State University.

Barcelo, L., M. Moranville, et al. (2005). "Autogenous shrinkage of concrete: a balance between autogenous swelling and self-desiccation." Cement and Concrete Research **35**(1): 177-183.

Bentur, A., S. Diamond, et al. (1997). Steel corrosion in concrete : fundamentals and civil engineering practice. London ; New York, E & FN Spon.

Böhni, H. (2005). Corrosion in reinforced concrete structures. Cambridge, England, Woodhead Publishing;.

Broomfield, J. P. (2007). Corrosion of steel in concrete : understanding, investigation and repair. London ; New York, Taylor & Francis.

Brown, M. C. (2002). Corrosion Protection Service Life of Epoxy Coated Reinforcing Steel in Virginia Bridge Decks. Doctor of Philosophy, Virginia Polytechnic Institute and State University.

Brown, M. C., R. E. Weyers, et al. (2006). "Service life extension of virginia bridge decks afforded by epoxy-coated reinforcement." Journal of ASTM International **3**(Compendex).

Claisse, P. A., H. El-Sayad, et al. (1999). "Permeability and pore volume of carbonated concrete." ACI Materials Journal **96**(Compendex): 378-381.

Clear, K. C. (1989). "Measuring rate of corrosion of steel in field concrete structures." Transportation Research Record(Compendex): 28-37.

Clear, K. C. (1990). Test procedures, data analysis, and general information. 3-LP Package. K.C.C. Inc. Sterling, VA.

Clear, K. C., W. H. Hartt, et al. (1995). Performance of Epoxy-Coated Reinforcing Steel in Highway Bridges. United States**:** 174p.

Dickie, R. A., J. S. Hammond, et al. (1981). "INTERFACIAL CHEMISTRY OF THE CORROSION OF POLYBUTADIENE-COATED STEEL." Industrial & Engineering Chemistry, Product Research and Development **20**(Compendex): 339-343.

Fattuhi, N. I. and H. Al-Khaiat (1999). "Shrinkage of Concrete Exposed to Hot and Arid Climate." Journal of Materials in Civil Engineering **11**(1): 66-75.

Feliu, S., C. Andrade, et al. (1996). "A new method forin-situ measurement of electrical resistivity of reinforced concrete." Materials and Structures **29**(6): 362-365.

FHWA. (2010). Retrieved 4th February, 2011, from http://www.fhwa.dot.gov/bridge/nbi/defbr10.cfm.

Gowers, K. R. and S. G. Millard (1999). "Electrochemical techniques for corrosion assessment of reinforced concrete structures." Proceedings of the Institution of Civil Engineers: Structures and Buildings **134**(Compendex): 129-137.

Grantham, M. G., B. Herts, et al. (1997). "The use of linear polarisation corrosion rate measurements in aiding rehabilitation options for the deck slabs of a reinforced concrete underground car park." Construction and Building Materials **11**(4): 215-224.

Holt, E. and M. Leivo (2004). "Cracking risks associated with early age shrinkage." Cement and Concrete Composites **26**(5): 521-530.

Holt, E. E. (2001). "Early age autogenous shrinkage of concrete." VTT Publications(Compendex).

Kim, J. K. and C. S. Lee (1998). "Prediction of differential drying shrinkage in concrete." Cement and Concrete Research **28**(7): 985-994.

Koch, G. H., M. P. H. Brongers, et al. (2002). Corrosion Cost and Preventive Strategies in the United States**:** 790p.

Kwak, H. G. and S. J. Ha (2006). "Plastic shrinkage cracking in concrete slabs Part I: a numerical model." Magazine of Concrete Research **58**(Copyright 2007, The Institution of Engineering and Technology): 505-516.

Kwan, A. K. H., W. W. S. Fung, et al. (2010). "Reducing drying shrinkage of concrete by treatment of aggregate." Magazine of Concrete Research **62**(Copyright 2011, The Institution of Engineering and Technology): 435-442.

Lambert, P. (1998). "Reinforced Concrete–History, Properties & Durability." Corrosion Prevention Association.

Lamond, J. F. (2006). Significance of tests and properties of concrete and concrete-making materials, ASTM International.

Liu, Y. and R. E. Weyers (1998). "Modeling the time-to-corrosion cracking in chloride contaminated reinforced concrete structures." ACI Materials Journal **95**(Compendex): 675-681.

Liu, Y. and R. E. Weyers (2003). "Comparison of guarded and unguarded linear polarization CCD devices with weight loss measurements." Cement and Concrete Research **33**(7): 1093-1101.

Manning, D. G. (1996). "Corrosion performance of epoxy-coated reinforcing steel: North American experience." Construction and Building Materials **10**(5): 349-365.

Mehta, P. K. and P. J. M. Monteiro (2006). Concrete : microstructure, properties, and materials. New York, McGraw-Hill.

Nguyen, T., E. Byrd, et al. (1996). "In situ measurement of water at the organic coating/substrate interface." Progress in Organic Coatings **27**(1-4): 181-193.

Polder, R., C. Andrade, et al. (2000). "Test methods for on site measurement of resistivity of concrete." Materials and Structures **33**(10): 603-611.

Pyc, W. A. (1998). Field performance of epoxy-coated reinforcing steel in Virginia bridge decks, Virginia Polytechnic Institute and State University.

Pyc, W. A., R. E. Weyers, et al. (2000). Field Performance of Epoxy-Coated Reinforcing Steel in Virginia Bridge Decks. United States**:** 46p.

Sagüés, A. A. (1994). "Corrosion of epoxy coated rebar in Florida bridges." University of South Florida. Final Report to Florida DOT WPI.

Sagues, A. A. and R. G. Powers (1996). "Coating Disbondment in Epoxy-Coated Reinforcing Steel in Concrete? Field Observations." CORROSION 96.

Sagues, A. A. and A. M. Zayed (1989). Corrosion of Epoxy-Coated Reinforcing Steel in Concrete (Phase 1). United States**:** 58p.

Senthilkumar, S. R. R. and S. C. Natesan (2005). "Prediction of restrained plastic shrinkage cracking in plain cement concrete." Magazine of Concrete Research **57**(Compendex): 579-587.

Soroushian, P. and S. Ravanbakhsh (1998). "Control of plastic shrinkage cracking with specialty cellulose fibers." ACI Materials Journal **95**(Compendex): 429-435.

Weyers, R., W. Pyc, et al. (2003). "Bridge Deck Cover Specifications." Concrete international **25**(2): 61-64.

Weyers, R. E., B. D. Powell, et al. (1993). Concrete Bridge Protection, Repair and Rehabilitation Relative to Reinforcement Corrosion: A Methods Application Manual. United States**:** 280p.

APPENDIX A

Shrinkage Prediction Models

ACI 209R-92 Model

$$\varepsilon_{sh}(t, t_c) = \frac{(t - t_c)^{\alpha}}{f + (t - t_c)^{\alpha}} \varepsilon_{shu}$$

$$f = 26.0e^{\{0.36(V/S)\}}$$

$$\varepsilon_{shu} = 780\gamma_{sh} \times 10^{-6}$$

$$\gamma_{sh} = \gamma_{sh,tc}\gamma_{sh,RH}\gamma_{sh,vs}\gamma_{sh,s}\gamma_{sh,\Psi}\gamma_{sh,c}\gamma_{sh,\alpha}$$

$$\gamma_{sh,tc} = 1.202 - 0.2337 \log(t_c)$$

$$\gamma_{sh,RH} = \begin{cases} 1.40 - 1.02h & \text{for } 0.4 \leq h < 0.8 \\ 3.00 - 3.0h & \text{for } 0.8 \leq h < 1.0 \end{cases}$$

$$\gamma_{sh,vs} = 1.2e^{\{-0.12(V/S)\}}$$

$$\gamma_{sh,s} = 0.89 + 0.041s$$

$$\gamma_{sh,\Psi} = \begin{cases} 0.30 + 0.014\Psi & \text{for } \Psi \leq 50\% \\ 0.30 + 0.002\Psi & \text{for } \Psi > 50\% \end{cases}$$

$$\gamma_{sh,c} = 0.75 + 0.00036c$$

$$\gamma_{sh,\alpha} = 0.95 + 0.008\alpha \geq 1$$

where: $\varepsilon_{sh}(t,t_c)$ = shrinkage strain at time t (in./in.)

ε_{shu} = ultimate shrinkage strain (in./in.)

α = in $\varepsilon_{sh}(t,t_c)$ is a flatter hyperbolic form

V/S = volume-to-surface ratio (in.)

γ_{sh} = cumulative product of correction factors

$\gamma_{sh,tc}$ = moist curing factor, equal to 1for 7 days curing

$\gamma_{sh,RH}$ = relative humidity factor

$\gamma_{sh,vs}$ = volume-to-surface ratio factor

$\gamma_{sh,s}$ = slump factor

$\gamma_{sh,\Psi}$ = fine aggregate factor

$\gamma_{sh,c}$ = cement content factor

$\gamma_{sh,\alpha}$ = air content factor, α is air content in percent

t = time (days)

t_c = time (days)

Bazant-Baweja B3 Model

$$\varepsilon_{sh}(t,t_c) = -\varepsilon_{sh\infty} k_h \, S(t-t_c)^{\alpha}$$

$$\varepsilon_{sh\infty} = \varepsilon_{s\infty} \frac{E_{cm607}}{E_{cm(t_c+\tau_{sh})}}$$

$$\varepsilon_{s\infty} = -\alpha_1 \alpha_2 [0.02565 w^{2.1} f_{cm28}^{-0.28} + 270] \times 10^{-6}$$

$$E_{cmt} = E_{cm28} \left(\frac{t}{4 + 0.85t} \right)^{0.5}$$

$$S(t-t_c) = tanh\sqrt{\frac{(t-t_c)}{\tau_{sh}}}$$

$$\tau_{sh} = 190.8t_c^{-0.08}f_{cm}^{-0.25}[2k_s(V/S)]^2$$

$$E_{cm28} = 57{,}000\sqrt{f_{cm28}}$$

where:

$\varepsilon_{sh}(t,t_c)$	=	shrinkage strain at time t (in./in.)
$\varepsilon_{sh\infty}$	=	ultimate shrinkage strain (in./in.)
α_1	=	shrinkage constant related to concrete type
α_2	=	shrinkage constant related to curing conditions
w	=	water content (lb/yd^3)
f_{cm28}	=	concrete compressive strength at 28 days (psi)
E_{cm28}	=	modulus of elasticity of concrete at 28 days (psi)
E_{cmt}	=	factor to account for ultimate shrinkage, $E_{cm607}/ E_{cmt(tc-t)}$
k_s	=	member shape factor
k_h	=	relative humidity factor
τ_{sh}	=	shrinkage half time (days)
t	=	time (days)
t_c	=	time (days)
V/S	=	volume-to-surface ratio (in.)
$S(t-t_c)$	=	shrinkage time function

CEB MC90 Model

$$\varepsilon_{sh}(t, t_c) = \varepsilon_{cso}\, \beta_s(t - t_c)$$

$$\varepsilon_{cso} = \varepsilon_s\, (f_{cm28})\beta_{RH}(h)$$

$$\varepsilon_s(f_{cm28}) = [160 + 10\beta_{sc}\, (9 - f_{cm28}/f_{cm0})] \times 10^{-6}$$

$$\beta_{RH}(h) = -1.55\left[1 - \left(\frac{h}{h_o}\right)^3\right] \quad \text{for } 0.4 \le h < 0.99$$

$$\beta_{RH}(h) = 0.25 \quad \text{for } h \ge 0.99$$

$$\beta_s(t - t_c) = \left[\frac{(t - t_c)/t_1}{350[(V/S)/(V/S)_o]^2 + (t - t_c)/t_1}\right]^{0.5}$$

where:

$\varepsilon_{sh}(t,t_c)$	=	shrinkage strain at time t (in./in.)
ε_{cso}	=	notional shrinkage coefficient (in./in.)
β_{sc}	=	cement type factor coefficient
β_{RH}	=	relative humidity coefficient
f_{cm28}	=	concrete compressive strength at 28 days (psi)
f_{cmo}	=	equal to 1450 psi
h	=	relative humidity
t	=	time (days)
t_c	=	time (days)
t_o	=	equal to 1

V/S = volume-to-surface ratio (in.)

GL2000 Model

$$\varepsilon_{sh}(t, t_c) = \varepsilon_{shu}\, \beta(h)\beta(t - t_c)$$

$$\varepsilon_{shu} = 900k \left(\frac{4350}{f_{cm28}}\right)^{1/2} \times 10^{-6}$$

$$\beta(h) = (1 - 1.18h^4)$$

$$\beta(t - t_c) = \left[\frac{(t - t_c)}{(t - t_c) + 77(V/S)^2}\right]^{0.5}$$

where:

$\varepsilon_{sh}(t,t_c)$ = shrinkage strain at time t (in./in.)

ε_{shu} = ultimate shrinkage strain (in./in.)

$\beta(t - t_c)$ = cement type factor coefficient

$\beta(h)$ = relative humidity coefficient

f_{cm28} = concrete compressive strength at 28 days (psi)

h = relative humidity

t = time (days)

t_c = time (days)

k = cement type factor

AASHTO-LRFD Model

$$\varepsilon_{sh} = k_s k_{hs} k_{td} 0.48 \times 10^{-3}$$

$$k_s = 1.45 - 0.13(V/S) \geq 1.0$$

$$k_{hs} = 2 - 0.014H$$

$$k_f = \frac{5}{1 + f'_{ci}}$$

$$k_{td} = \frac{t}{61 - 4f'_{ci} + t}$$

where:

	ε_{sh}	=	shrinkage strain (in./in.)
	k_s	=	volume-to-surface ratio factor
	k_{hs}	=	relative humidity factor
	k_f	=	concrete strength factor
	k_{td}	=	time development factor
	H	=	relative humidity (%)
	V/S	=	volume-to-surface ratio (in.)
	t	=	time (days)
	f_{ci}'	=	compressive strength at time of initial loading, if unknown use $0.8f_c'$ (ksi)

APPENDIX B

Deck Slabs Sketches and Cut Locations

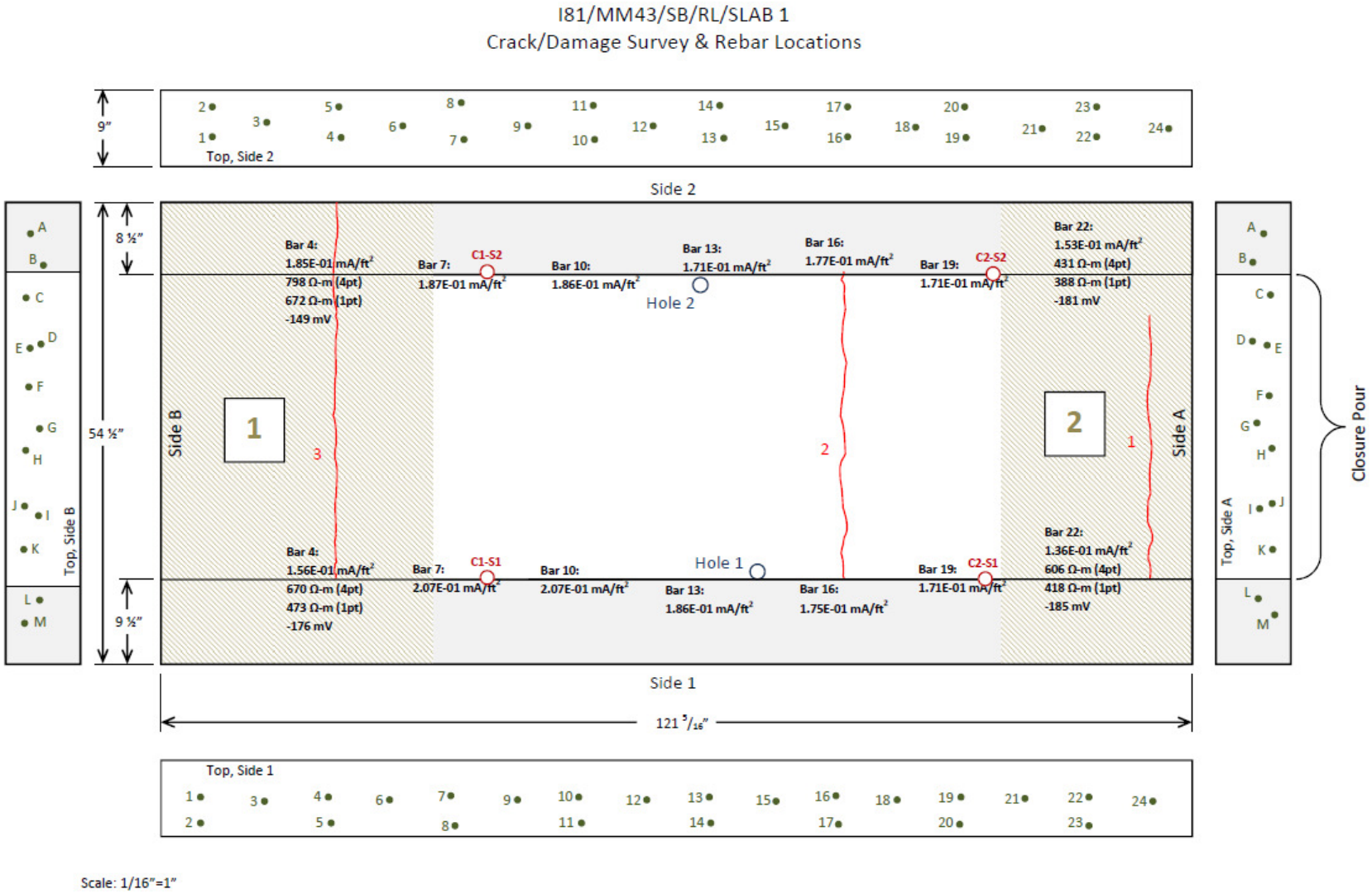

Figure B.1 Crack, Damage Survey and Rebar Locations for Slab 1

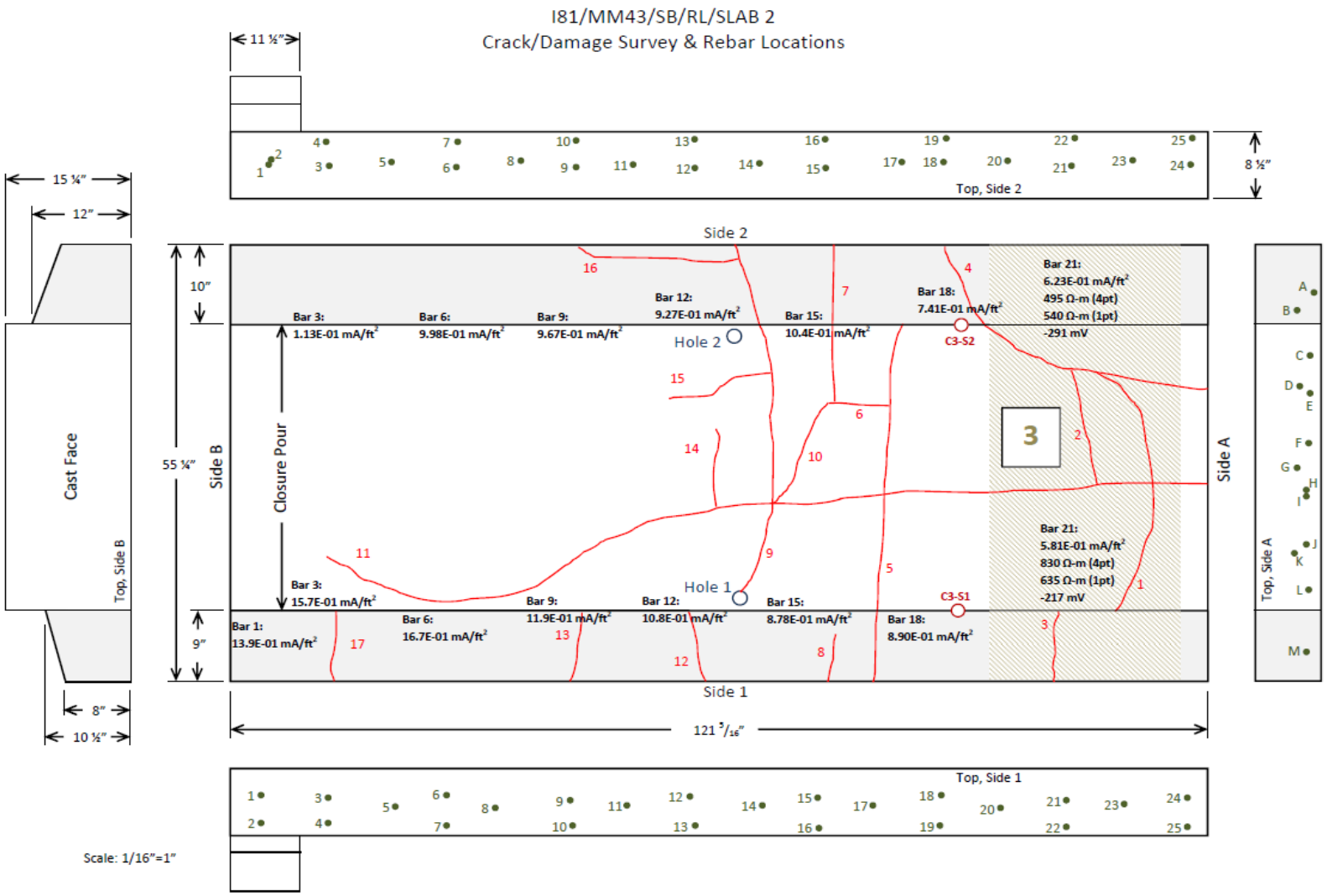

Figure B.2 Crack, Damage Survey and Rebar Locations for Slab 2

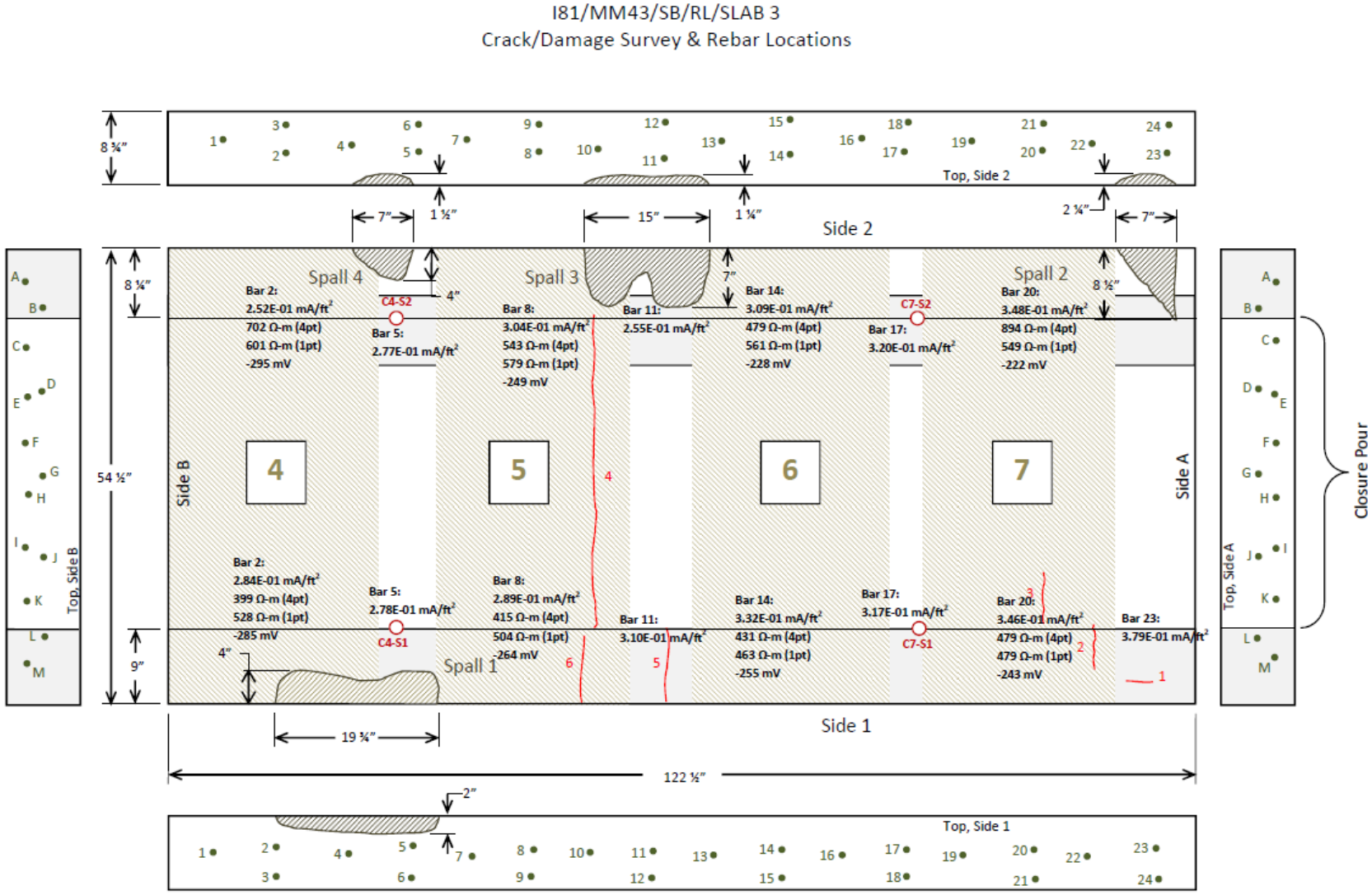

Figure B.3 Crack, Damage Survey and Rebar Locations for Slab 3

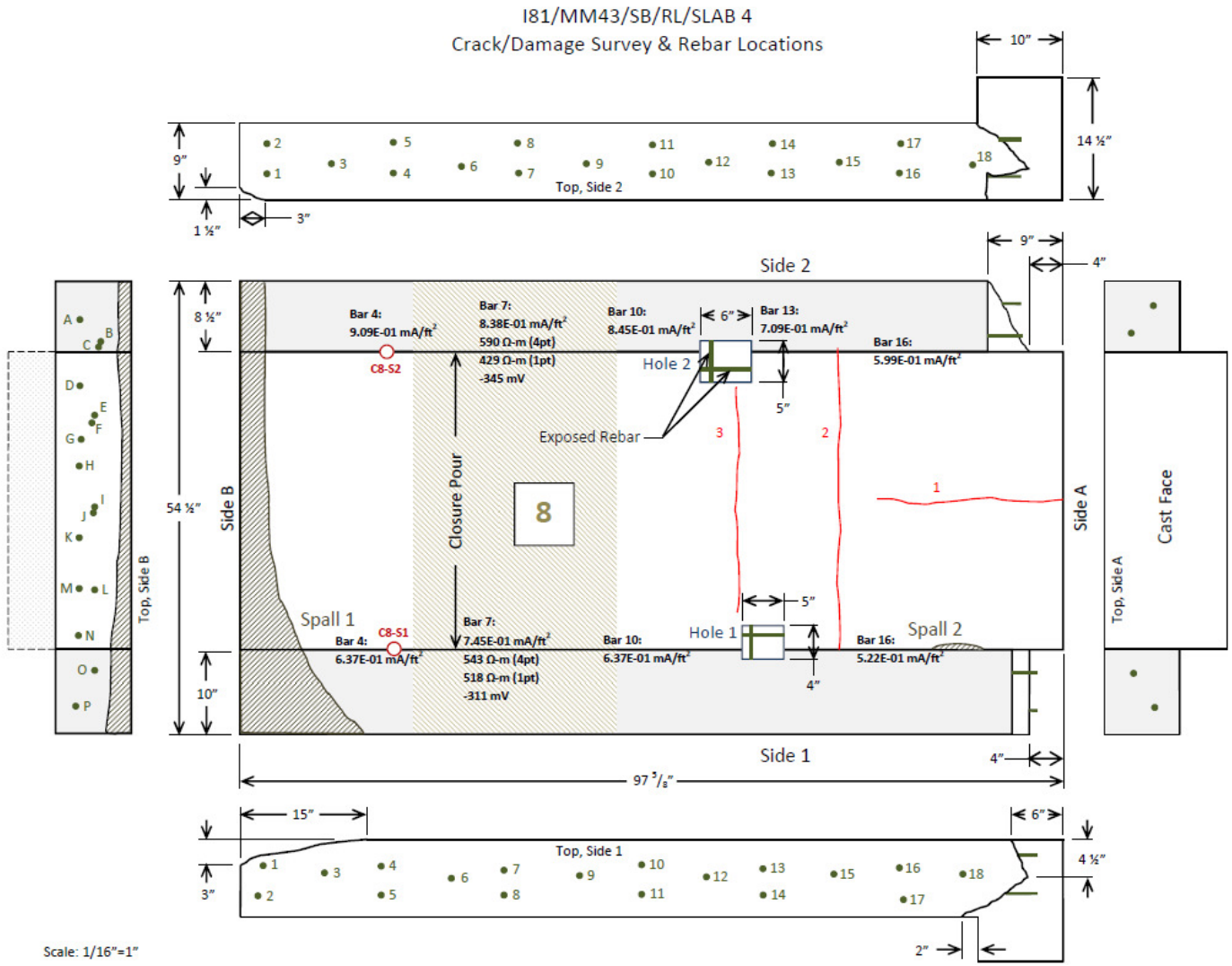

Figure B.4 Crack, Damage Survey and Rebar Locations for Slab 4

APPENDIX C

Specimens Dimensions and Cover Depths from Cut Deck Slabs

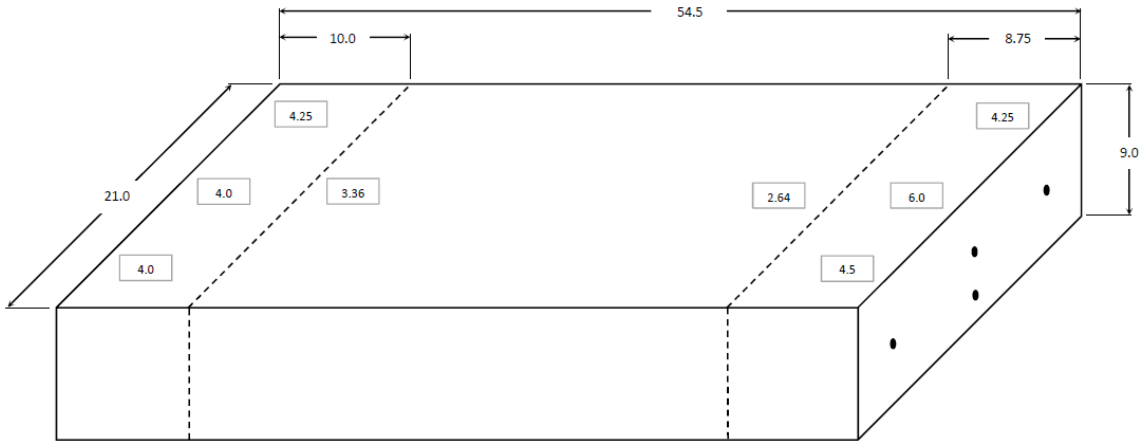

Figure C.1 Slab #1 Dimensions and Rebars Cover Depths

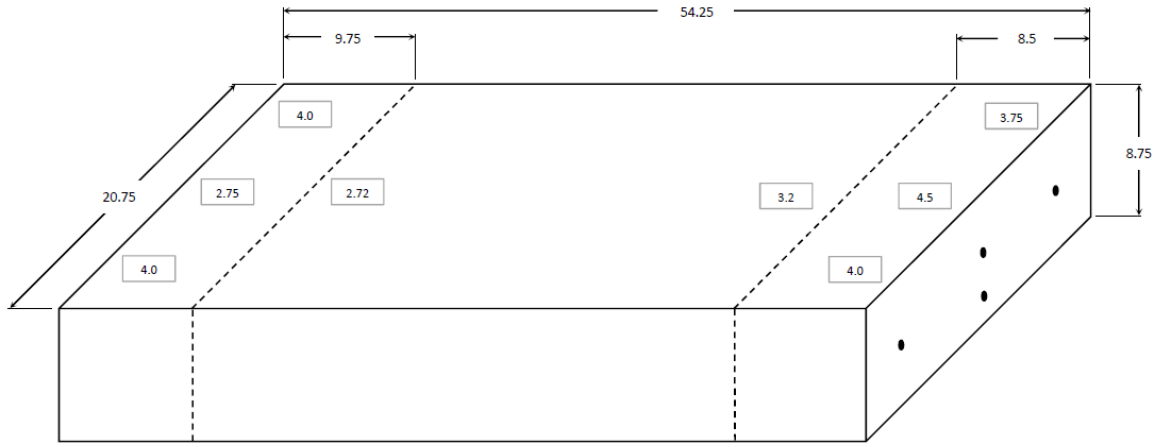

Figure C.2 Slab #2 Dimensions and Rebars Cover Depths

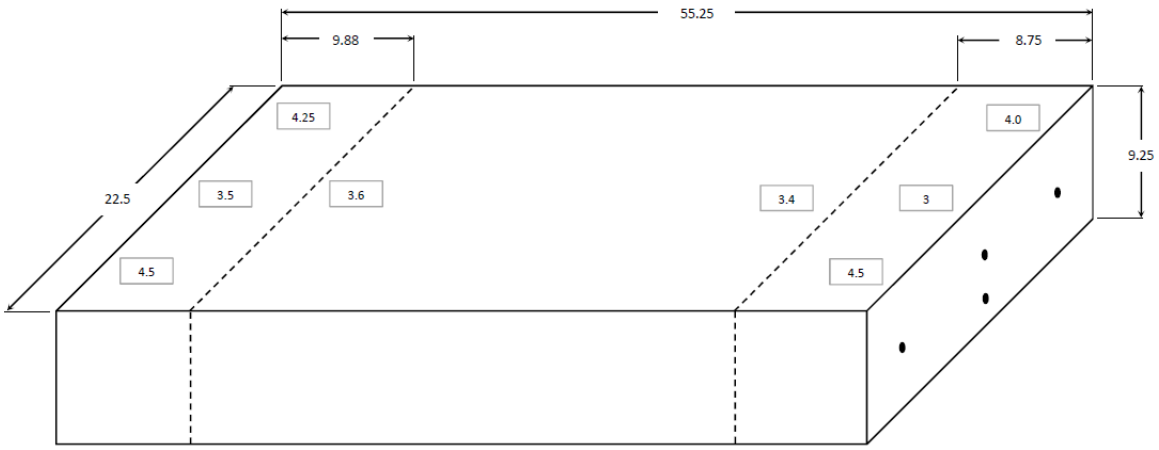

Figure C.3 Slab #3 Dimensions and Rebars Cover Depths

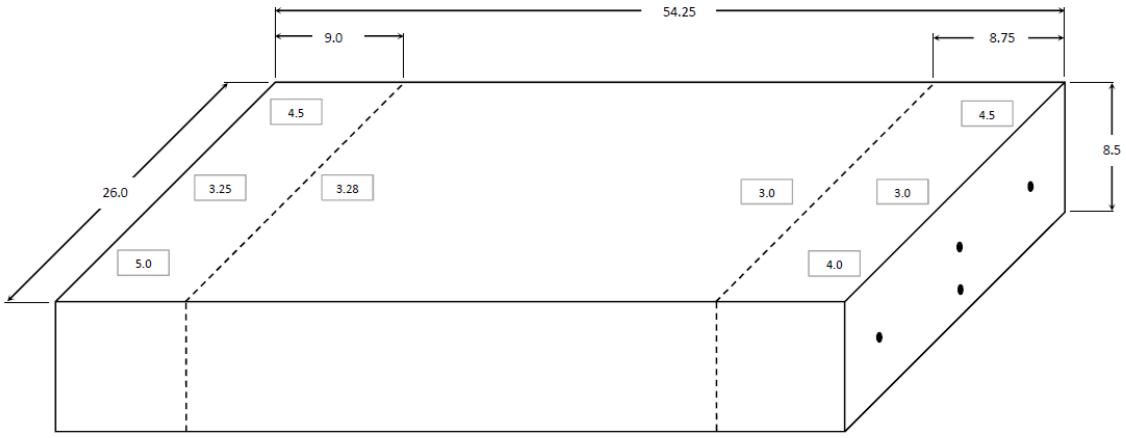

Figure C.4 Slab #4 Dimensions and Rebars Cover Depths

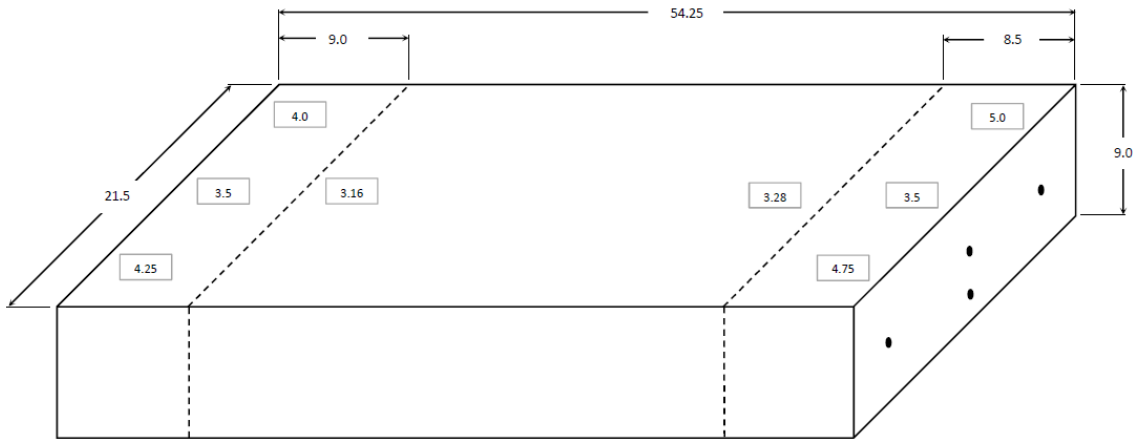

Figure C.5 Slab #5 Dimensions and Rebars Cover Depths

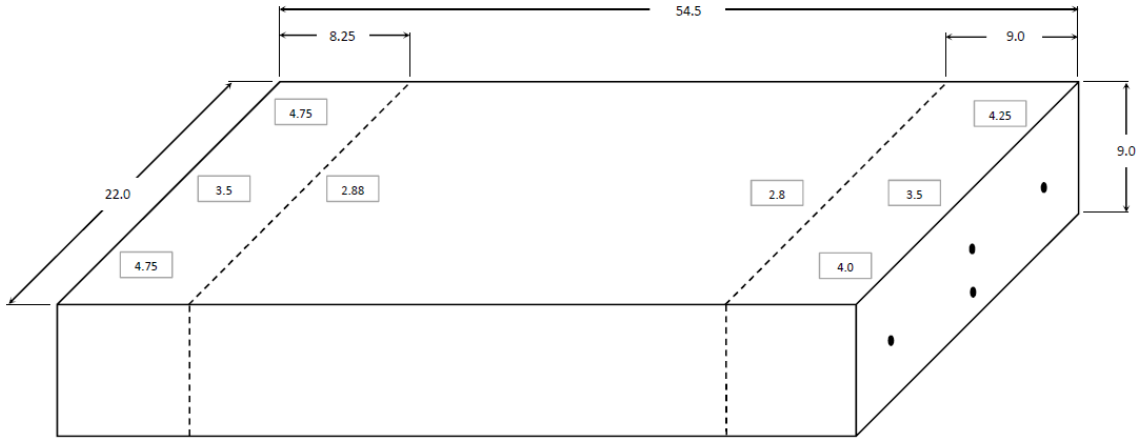

Figure C.6 Slab #6 Dimensions and Rebars Cover Depths

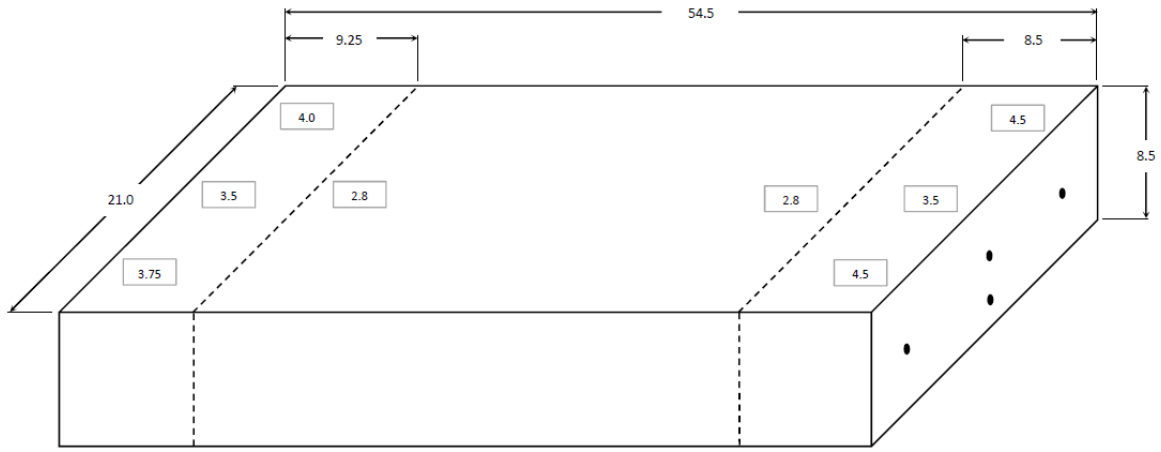

Figure C.7 Slab #7 Dimensions and Rebars Cover Depths

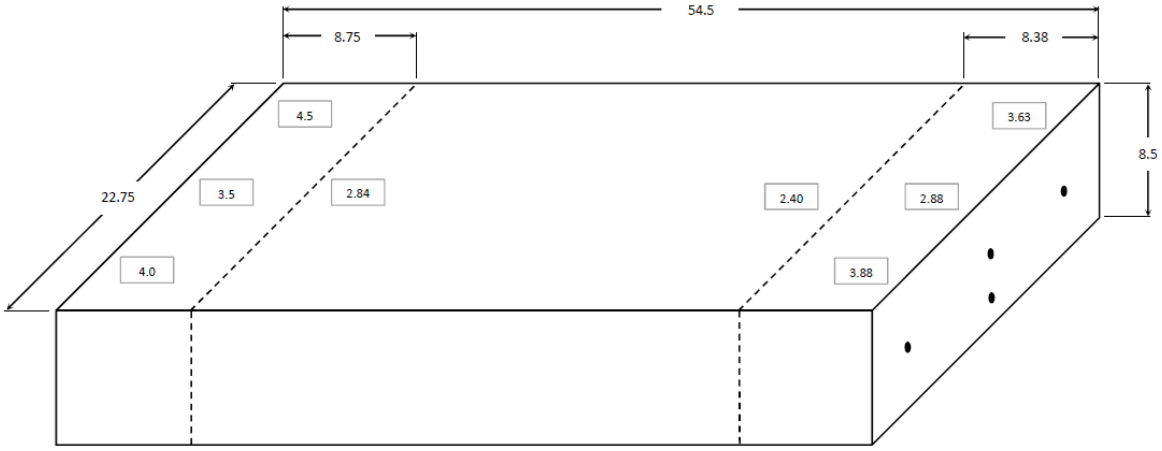

Figure C.8 Slab #8 Dimensions and Rebars Cover Depths